INVESTIGATION OF NONLINEAR DYNAMICS OF A SELF-EXCITED COMPLEX SYSTEM LIKE PLASMA

By

PANKAJ KUMAR SHAW

(Enrolment No.-PHYS05201204006)

Saha Institute of Nuclear Physics, Kolkata.

A thesis submitted to the

Board of Studies in Physical Sciences

In partial fulfillment of requirements

for the Degree of

DOCTOR OF PHILOSOPHY

of

HOMI BHABHA NATIONAL INSTITUTE

May 2017

Homi Bhabha National Institute

Recommendations of the Viva Voce Committee

As members of the Viva Voce Committee, we certify that we have read the dissertation prepared by Pankaj Kumar Shaw entitled "Investigation of nonlinear dynamics of a self-excited complex system like plasma" and recommend that it may be accepted as fulfilling the thesis requirement for the award of Degree of Doctor of Philosophy.

Supratik Mukhopadhyay 22/09/2017

Chairman – Prof. S. Mukhopadhyay **Date:**

M. S. Janaki 22.09.2017

Guide / Convener - Prof. M. S. Janaki **Date:**

Co-guide - (if any) **Date:**

Examiner – Prof. G. Ambika **Date:** 22.09.17

A. N. Sekar Iyengar 22-09-17

Member 1- Prof. A. N. S. Iyengar **Date:**

Member 2- Prof. Padmaja P. Mishra **Date:** 22/09/17

Final approval and acceptance of this thesis is contingent upon the candidate's submission of the final copies of the thesis to HBNI.

I/We hereby certify that I/we have read this thesis prepared under my/our direction and recommend that it may be accepted as fulfilling the thesis requirement.

Date: 22.09.2017

M. S. Janaki

Place: Kolkata

Co-guide (if applicable) **Guide**

STATEMENT BY AUTHOR

This dissertation has been submitted in partial fulfillment of requirements for an advanced degree at Homi Bhabha National Institute (HBNI) and is deposited in the Library to be made available to borrowers under rules of the HBNI.

Brief quotations from this dissertation are allowable without special permission, provided that accurate acknowledgement of source is made. Requests for permission for extended quotation from or reproduction of this manuscript in whole or in part may be granted by the Competent Authority of HBNI when in his or her judgment the proposed use of the material is in the interests of scholarship. In all other instances, however, permission must be obtained from the author.

Pankaj Kumar Shaw.

Pankaj Kumar Shaw

DECLARATION

I, hereby declare that the investigation presented in the thesis has been carried out by me. The work is original and has not been submitted earlier as a whole or in part for a degree/deploma at this or any other Institution/University.

Pankaj Kumar Shaw

Pankaj Kumar Shaw

List of Publications arising from the thesis

1. "Canard and mixed mode oscillations in an excitable glow discharge plasma in the presence of inhomogeneous magnetic field", Pankaj Kumar Shaw, A. N. Sekar Iyengar, and Md. Nurujjaman, Physics of Plasma, **2015**, 22, 122301.

2. "Intrinsic noise induced coherence resonance in a glow discharge plasma", Pankaj Kumar Shaw, D. Saha, S. Ghosh, M. S. Janaki, and A. N. Sekar Iyengar, Chaos, **2015**, 25, 043101.

3. "Investigation of coherent modes in the chaotic time series using empirical mode decomposition and discrete wavelet transform analysis", Pankaj Kumar Shaw, D. Saha, S. Ghosh, M. S. Janaki, and A. N. Sekar Iyengar, Chaos, Solitons & Fractals, **2015**, 78, 285-296.

4. "Investigation of coherent modes and their role in intermittent oscillations using empirical mode decomposition", Pankaj Kumar Shaw, S. Ghosh, D. Saha, M. S. Janaki, and A. N. Sekar Iyengar, Physics of Plasmas, **2016**, 23, 112103.

5. "Investigation of multifractal nature of floating potential fluctuations obtained from a dc glow discharge magnetized plasma", Pankaj Kumar Shaw, D. Saha, S. Ghosh, M. S. Janaki, and A. N. Sekar Iyengar, Physica A, **2017**, 469, 363-371.

6. "A localized cathode glow in the presence of a bar magnet and its associated nonlinear dynamics", Pankaj Kumar Shaw, S. Samanta,

D. Saha, S. Ghosh, M. S. Janaki, and A. N. Sekar Iyengar, Physics of Plasmas, **2017**, 24, 082105.

Pankaj Kumar Shaw.

Pankaj Kumar Shaw

To My Beloved Parents

Acknowledgements

It is my immense pleasure to express my gratitude and sincere thanks to all those people who have made this thesis work possible by contributed in numerous ways.

Firstly, I would like to express my heartfelt thanks to my supervisor, Prof. A. N. Sekar Iyengar and Prof. M. S. Janaki, whose encouragement and direction from the initial to the final level enabled me to develop an understanding about my research problems. Their invaluable suggestions, teaching, guidance and never-ending encouragement, without which, I would not have been able to complete my work. Their availability and regular discussion helped me to develop a scientific approach to tackle my research problem. They always gave me freedom to work independently which helps me to grow like an independent researcher. Prof. A. N. S. Iyenger created a friendly environment in the lab, which allowed me to discuss whatever I felt regarding my research work whether it is meaningful substance or childish.

I would like to thank my doctoral committee members, Prof. S. Mukhopadhaya and Prof. P. Mishra, in making a yearly evaluation of my progress report and giving valuable suggestions.

I would like to take an opportunity to thank Prof. Awadhesh Prasad, Delhi University, for his valuable suggestions and discussions regarding the theoretical study of nonlinear dynamics. I would like to thank Prof. Punit Parmananda for his suggestions during the work of antiperiodic oscillation in a Duffing's oscillator circuit. I sincerely thank to Dr. S. Mahapatra who provided me an opportunity to work on magnetron sputtering device in BIT Mesra. I would like to thank Dr. Nurujjaman, NIT Sikkim, without whom one of my research associated problem, i.e, investigation of mixed mode and canard oscillations was impossible. I express my thanks to Prof. B. Dasgupta who allowed me to carry out a research problem, energization of a charge particle in chaotic magnetic field, indipendent of my thesis work.

I would like to thank Prof. I. Das, Experimental Condense Matter Physics (ECMP) Division, for giving me their Hall Probe for the magnetic field measurement. I want to thank Prof. S. Sarkar, for giving me their computation support for the simulation of electronic circuit. I would also like to thank Prof. Dhananjay Bhattacharyya, Computational Science Division, for their computation support regarding the CUDA programming.

I want to thank Prof. N. Chakraborty whose teaching helped me to me understand the basic plasma physics and motivated me to learn plasma physics. I would also like to thank Prof. Sujit Saha, Prof. R. Pal, Prof. S. Raychaudhuri and Mr. S. Chowdhuri for their valuable discussions and suggestions regarding various aspects of my research work.

Carrying out an experiment in glow discharge plasma device, always involves many technical knowledge. It is my immense pleasure to acknowledge Dipankar Da and Asoke Da for technical helps during experiments. I would like to acknowledge Partha Da, Subhasis Da, Monobir Da and all other staffs of the Plasma Physics Division of Saha Institute of Nuclear Physics.

I would like to acknowledge my lab-mates Sabuj and Debajyoti for their discussions and suggestions regarding the research problems. They are more like my research collaborators. We shared many research articles together. I would also like to thank my other lab-mates Satyajit and Sayanee with whom I have spent very cheering time specially with Satyajit during lunch time.

It is my pleasure to acknowledge all my seniors and juniors (research fellows) of the Plasma Physics Division with whom I have experienced joyful company. I am thankful to Subir Da, Avik Da, Debu Da, Sudip Da, Anwesha Di, Sourav Da and Abhijit Da for their helps and suggestions. I spent very cheerful moments with my juniors Mithun and Subha in the division. It is my great pleasure to have joyful company with batch-mates and other friends. I have spent very cheering time with them specially during the year ending tour that enabled me to have a relaxing time and allowed me to work freshly.

I would remain forever grateful towards my parents and all members of my family for their continued encouragement, blessings and emotional supports throughout my research work.

I would like to thank my wife Mrs. Annu Shaw, for her continuous emotional support, encouragement and cooperation, without which this journey would be a lot more difficult. I recall the moments when she relieved me of many of my responsibilities, by taking the trouble herself.

Finally, I would like to thanks all my well wishers for their help and words of encouragement.

SINP, Kolkata

May, 2017 Pankaj Kumar Shaw

Contents

Synopsis

The contents of this thesis are mainly centred around the experimental studies and investigations of nonlinear dynamical phenomena observed in a self excited complex system like plasma. Complex systems are composed of many small components that interact nonlinearly. They exhibit spatial structures and dynamical behavior ranging from simple ordering to chaotic states through complex structures, both in space as well as time. Complex systems encompass a wide range of fields such as fluids, plasmas, condensed matter systems, biological systems, social, traffic and financial systems [1]. Physical world, thus can be considered to mainly consist of complex systems which exhibit nonlinear dynamical behavior such as multiscale avalanche, self-organized criticality, chaos, turbulence, and stochastic and coherent resonances to name a few. In the last three decades or so, with the development of nonlinear dynamics based on large scale numerical simulations, complex systems have become a very important interdisciplinary research subject with enormous potential of practical applications. Dynamics of a complex system can be understood by investigating its time evolution, i.e, change of state as a function of time. In real life, the information about the time evolution is recorded as a time series, a sequence of measurement taken at successive equally spaced points in time. These time series data may have growing, decaying, constant or oscillatory behavior. Since oscillatory behaviour is mainly due to nonlinear interaction between the components of complex system, the study of such behaviour forms a major area of interest. The origin of these oscillations may be due to: 1) interplay of internal complex system parameters, called self excited oscillation, 2) external forcing, called forced oscillation. These two types of oscillatory behaviour form the basis of study in self excited and forced complex systems respectively.

Plasma is a common example of complex system consisting of electrons, ions and neutral particles. Plasma has numerous sources of free energy like energetic electrons (having energy greater than the thermal energy of electrons in the system) and gradients in density and temperature, that are dissipated by giving rise to several instabilities like beam plasma and drift wave instabilities [2, 3]. Therefore, the dynamics of plasma is highly nonlinear and complex. In general, an understanding of the various plasma processes can be obtained by investigating the plasma equilibrium parameters like density, electron temperature, plasma potential as well as features related to plasma waves such as frequency and dispersion relation. However, to explain certain phenomena like plasma transport and to achieve features like chaos control in plasma, one requires information about the underlying dynamics of plasma which can be extracted from the plasma oscillations. As these oscillations are nonlinear, one needs nonlinear analysis tools to investigate the plasma dynamics. Plasma fluctuation investigation is also important from a practical point of view since plasma systems are used to develop thin film/nanoparticle growth and there are few reported works which indicate the correlation between plasma fluctuation and fluctuations of nanoparticle growth [4]. Thus, investigation of nonlinear plasma fluctuations in order to extract the underlying nonlinear dynamics of plasma is a very important area of research.

In 1984, Boswell et al. reported the experimental evidence of deterministic chaos and showed that the natural oscillations on an electron beam propagating parallel to a magnetic field, undergoes a period doubling route to chaos with an increase in the beam current [5]. First experimental observation of chaotic behavior and period doubling in a pulsed plasma discharge was reported by Cheung et al. [6] whereas first observation on deterministic chaos in dc excited glow discharge plasma was made by Braun et al. in 1987 [7]. After that, a large number of nonlinear phenomena like mode locking, period pulling, frequency entrainments, synchronization, homoclinic bifurcation, period doubling and intermittency route to chaos were observed [8, 9, 10, 11]. Nurujjaman et al. studied nonlinear phenomena like chaos to order transition, stochastic and coherence resonance in a dc glow discharge unmagnetized plasma with cylindrical geometry [3, 12].

Due to the practical importance and industrial applications of glow discharge plasma for surface treatment [13], etching, thin film deposition, the nonlinear dynamical behaviour of glow discharge plasma are being diagnosed extensively in recent years [3, 12, 14, 15, 16] to achieve better performance. In these works, a number of parameters (e.g., discharge voltage, pressure, homogeneous magnetic fields, external sinusoidal forcing, external noise forcing, etc.) are identified to control the plasma dynamics of the system. Although many experiments based on various control parameters have been carried out to study the nonlinear behaviour, the role of intrinsic noise and inhomogeneous magnetic field have not yet been explored much. In this thesis, efforts are focussed to study how the presence of external inhomogeneous magnetic field produced by a bar magnet, external homogeneous magnetic fields and intrinsic plasma noise affect the plasma dynamics. For this purpose, we have carried out several experiments in an argon glow discharge plasma, performed analysis of plasma oscillations using various nonlinear time series analysis tools and developed dynamical models to explain the observations. In this thesis, we mainly focus on the self excited oscillations of the plasma, i.e., self induced due to interplay of internal plasma parameters, for the study of plasma dynamics.

To begin with, we have explored the behaviour of an excitable glow discharge plasma in the presence of an external magnetic field perturbation using a bar magnet. Using the magnetic field strength as a control parameter, experimental observations of a canard orbit and mixed mode oscillations [17] (MMOs) have been made. At low values of magnetic field, small amplitude quasiperiodic oscillations were excited, and with the increase in the magnetic field large amplitude oscillations were observed. Analyzing the experimental results it seems that the magnetic field could be playing the role of intrinsic noise for the observation of such nonlinear phenomena. It is observed that the noise level increases with the increase in magnetic field strength. The experimental results have also been corroborated by a numerical simulation using a FitzHugh-Nagumo [18] (FHN) like macroscopic model derived from the basic plasma equations and phenomenology, where the noise has been included to represent the internal plasma noise. This macroscopic model shows MMO in the vicinity of the canard point when external noise is added.

Next, we change the behaviour of system from excitable state to normal oscillatory state. In the presence of a bar magnet placed outside the plasma chamber, an additional effect apart from the generation of intrinsic noise like appearance of a localized glow (fireball like structure) is observed near the cathode surface. Since the bar magnet is placed near the cathode, it is likely that it can modify the oscillations in a localized region near the cathode surface that can in turn affect the bulk plasma oscillations. Floating potential fluctuations showed that emergence of such localized structure leads the system towards chaotic state. It is seen that the plasma density in the localized glow region and the intensity of this structure increases with the increase of the magnetic field strength. Increasing the magnetic field strength reveals a transition from order to chaos via period doubling bifurcation. This transition is analyzed by using bifurcation diagram, phase space plots, power spectrum plots, Hilbert Huang transform and by estimating the largest Lyapunov exponent. In addition to this, evidence of normal homoclinic as well as inverse homoclinic bifurcation is seen.

Further we have carried out an experiment in the presence of an axial homogeneous magnetic field and in which chaotic oscillations have been observed and analyzed using multifractal detrended fluctuation [19] analysis (MF-DFA). The generalized Hurst exponents (h(q)), local fluctuation function (Fq (s)), the R$\acute{e}$nyi exponents (τ(q)) and the multifractal spectrum $F(\alpha_h)$ have been calculated by applying the MF-DFA method. The result of the MF-DFA shows the multifractal nature of these fluctuations. An investigation of the effect of the magnetic field strength on the multifractal nature of the fluctuations was carried out and it is seen that degree of multifractality is reduced with the increase in the field strength. Obtained results suggested the existence of long-range correlations in the fluctuations. Comparing the MF-DFA results for the data set with those for shuffled and surrogate series, we found that its multifractal nature is due to the existence of significant long-term correlation.

Motivated by the fact that some times the intrinsic noise can induce complicated nonlinear phenomena like mmo, we next investigated thoroughly the effect of intrinsic noise on excitable dynamics of the plasma in the absence of magnetic field. For the first time, experimental evidence of intrinsic noise induced coherence resonance [20] in a glow discharge plasma was observed. Initially the system was started at a discharge voltage (DV) where it exhibited fixed point dynamics, and then with the subsequent increase in the DV, the few spikes were excited and with further increase of DV the number of spikes as well as their regularity increased. The regularity in the interspike interval of the spikes is estimated using normalized variance (NV). Coherence resonance was determined using normalized variance curve and also corroborated by Hurst exponent and power spectrum plots. We showed that the regularity of the excitable spikes in the floating potential fluctuations increases with the increase in the DV, upto a particular value of DV. Using a Wiener filter, we separated the noise component which was observed to increase with DV and hence conjectured that noise can play an important role in the generation of the coherence resonance. From an anharmonic oscillator equation describing ion acoustic oscillations, we have been able to obtain a FitzHugh-Nagumo [18] (FHN) like model which has been used to understand the excitable dynamics in our earlier experiment. The numerical results agree quite well with the experimental observations.

It is well known that experimental time series are always contaminated by noise. Therefore, we have also attempted to extract coherent modes of the noise contaminated experimental signals. In view of this, for the first time, we proposed an empirical mode decomposition (EMD) [21] based method for coherent mode detection of a chaotic or turbulent time series data. To establish our method, we carried out a comparative study on the investigation of coherent modes in chaotic time series data based on two techniques: the empirical mode decomposition and the discrete wavelet transform. We have applied these techniques to the different types of chaotic time series data obtained from a glow discharge plasma. The discrete wavelet transform and EMD analysis of the chaotic time series, combined with some simple statistical estimates like variance and correlation coefficient, help in identification of coherent modes. Our studies clearly showed the efficiency of EMD based coherent mode detection technique and its advantage over traditional coherent mode detection technique like discrete wavelet transform based.

To further consolidate our method, we have analyzed intermittent chaotic fluctuation [22] data from a glow discharge plasma using empirical mode decomposition. Here the nature of the oscillations changes from an initial relaxation oscillation to a final chaotic oscillatory state via intermittent chaos. The time series data has been decomposed into several intrinsic mode functions (IMFs) using EMD. Furthermore, the estimation of the variance of the IMFs and the correlation of these IMFs with the original time series helps us to identify the presence of coherent modes in the fluctuations. Through this analysis, we could clearly observe that initially during the relaxation oscillations the system was dominated by one type of coherent mode, whereas in the final chaotic state it was dominated by another coherent mode. In the intermediate case, i.e. intermittent chaotic state, both the coherent modes were seen to be present. Hilbert Huang spectrum [21] of the fluctuations clearly suggests the intermittent change in the frequency with time.

With the advent of plasma based imaging techniques, surface treatment, therapeutics, etc., an understanding and control of the complex behaviour of plasma is emerging as a challenging problem. Many of these processes have much in common with the characteristics of glow discharge plasmas. As an application of our work, we can suggest consideration of nonlinear dynamical features of plasma and the effect of intrinsic noise on these dynamics while operating glow discharge plasma devices for practical applications. Shiratani et al. proposed a simple theoretical model that describes the correlation between plasma fluctuation and fluctuation of nanoparticle growth in reactive plasmas [4]. Thus our studies can be used for experimental investigation of correlation between plasma fluctuations and thin film growth in plasma based systems. Our nonlinear dynamical experiments in the presence of a bar magnet and their results can be useful in magnetron sputtering devices [23] that are based on bar magnet and cross field discharges. Investigation of multifractal dynamics presented in this thesis can be useful to understand the multifractal behaviour and transport related problem in magnetized plasma device like tokamak [24]. The concept of multifractality is of great importance for space plasmas [25] because it allows us to look at intermittent turbulence in the solar wind [26]. Our proposed method for the detection of coherent mode is a very efficient tool. The method can be very useful for extracting better results and information from a noise contaminated time series data.

In summary, the results and conclusions presented in this thesis would enrich the understanding of complex and nonlinear dynamics of magnetized as well as unmagnetized plasma.

---

[1] Y. Bar-Yam, *Dynamics of Complex Systems*, Addison Wesley, Reading, Massachusetts, (1997).

[2] G. Murtaza, M. Nadeem, and P. K. Shukla, Phys. Fluids B **3**, 1507 (1991).

[3] Md. Nurujjaman, R.Narayanan, and A. N. Sekar Iyengar, Chaos **17**, 043121 (2007).

[4] M. Shiratani et al., Japanese Journal of Applied Physics **53**, 010201 (2014).

[5] R. W. Boswell, Plasma Physics and Controlled Fusion **27**, 405 (1985).

[6] P. Y. Cheung, and A. Y. Wong, Phys. Rev. Lett. **59**, 551 (1987).

[7] T. Braun, Jorge A. Lisboa, R. E. Francke, and J. A. C. Gallas, Phys. Rev. Lett. **59**, 613 (1987).

[8] T. Klinger, F. Greiner, A. Rohde, A. Piel, and M. E. Koepke, Phys. Rev. E **52**, 4316 (1995).

[9] E. Rosa, W. Pardo, C. M. Ticos, J. A. Walkenstein, and M. Monti, Int. J. Bifurcation Chaos **10**, 2551 (2000).

[10] T. Braun, J. A. Lisboa, and J. A. C. Gallas, Phys. Rev. Lett. **68**, 2770 (1992).

[11] J. Qin, L. Wang, D. P. Yuan, P. Gao, and B. Z. Zhang, Phys. Rev. Lett. **63**, 163 (1989).

[12] Md. Nurujjaman, A. N. Sekar Iyengar, and P. Parmananda, Phys. Rev. E **78**, 026406 (2008).

[13] P. P. Tsai, L. C. Wadsworth, and J. R. Roth, Textile Research Journal **67**, 359 (1997).

[14] E. Pugliese, R. Meucci, S. Euzzor, J. G. Freire, and J. A. C. Gallas, Scientific Reports **5**, article 8447 (2015).

[15] P. Alex, S. Arumugam, K. Jayaprakash, and K. S. Suraj, Results in Physics **5**, 235 (2015).

[16] D. G. Dimitriu, M. Aflori, L. M. Ivan, C Ionita, and R. W. Schrittwieser, Plasma Phys. Control. Fusion **49**, 237 (2007).

[17] P. Borowski, R. Kuske, Y.-X. Li, and J. L. Cabrera, Chaos 20, 043117 (2010).

[18] E. M. Izhikevich, and R. FitzHugh, Scholarpedia **1**, 1349 (2006).

[19] J. W. Kantelhardt et al., Physica A **316**, 87 (2002).

[20] A. S. Pikovsky, and J. Kurths, Phys. Rev. Lett. **78**, 775 (1997).

[21] N. E. Huang et al., Proc. R. Soc. Lond. A **454**, 903(1998).

[22] S. Ghosh et al., Physics of Plasmas **21**, 032303 (2014).

[23] P. K. Song, Y. Shigesato, I. Yasui, C. W. Ow-Yang, and D. C. Paine, The Japan Society of Applied Physics **37**, 1870 (1998).

[24] B. A. Carreras et al., Physics of Plasmas **7**, 3278 (2000).

[25] W.M. Macek, Nonlinear Processes in Geophysics **14**, 695 (2007).

[26] E. Marsch, and C. Y. Tu, Nonlinear Processes in Geophysics, **4**, 101 (1997).

List of Figures

List of Tables

Chapter 1

Introduction

The main objective of this thesis is to contribute to the knowledge of nonlinear dynamical phenomena in unmagnetized and magnetized glow discharge argon plasmas through systematic experimental studies of plasma fluctuations. We have also carried out theoretical modeling to understand the experimental results wherever possible. For an experimentalist, the main component of nonlinear dynamical characterisation is through different types of time series analysis like estimation of largest Lyapunov exponent, power spectrum, Hurst exponent, etc. In addition to these analysis techniques we have used empirical mode decomposition to not only explore the spectral components, but also in the detection of coherent modes in the chaotic systems. In this chapter, we present a brief overview on complex systems, nonlinear dynamics, plasma physics and our motivation for investigation of nonlinear dynamics in plasma systems.

1.1 Complex System and Nonlinear Dynamics: an Overview

A system composed of many small nonlinearly interacting units is usually referred to as a complex system. The field of complex systems cuts across all traditional disciplines of science as well as engineering, management and medicine. Social, traffic, financial, biological and plasma systems are also examples of a complex system which despite of their wide diversity exhibit similar universal laws and phenomena [1]. Due to this ubiquitous nature, the study of complex systems has emerged as a new scientific discipline and has been recognized as a interdisciplinary research subject.

The change of state of a physical system as a function of time is in general called dynamics. Changes take place due to the interplay of forces acting on the system which may lead to classification as linear or nonlinear dynamics. The subject of dynamics began when Newton discovered the laws of motion and universal gravitation [2] and applied the differential equations [3] to solve two body problem in order to deal with the problem of calculating the motion of the earth around the sun. Newton started to introduce the differential computations and method was extended to the three-body problem by the physicists. However, it was found that three body problems being nonlinear and non-integrable are impossible to solve. In late 1800s, Poincaré developed a geometric approach, which emphasized qualitative rather than quantitative questions, to analyze such problems [4]. This technique of Poincaré approach has blossomed into the modern subject of dynamics. In his research on the three-body problem, Poincaré became the first person to discover deterministic chaos which laid the foundations of modern chaos theory.

In the beginning of 1900s, scientists were largely concerned with nonlinear oscillators as they played a vital role in the development of such technologies as radio, radar, phase-locked loops and lasers. Theoretical study of nonlinear oscillators stimulates the discovery of new mathematical techniques [5]. In the year 1963, Lorenz discovered chaotic motion on a strange attractor while solving a simplified system of three coupled first-order nonlinear equations of the fluid convection model describing the atmospheric weather conditions [6]. He found that the solutions to his equations never settled down to an equilibrium or to a periodic state instead they continued to oscillate in an irregular, aperiodic fashion and the bounded non-periodic trajectories of the equations started from two nearby initial states would soon become completely uncorrelated resulting in unpredictability of the future state in a fully deterministic dynamical system. Such a solution became known as chaotic and with this discovery, the field of chaotic dynamics was born. The study of nonlinear dynamical systems experienced an explosive growth when Ruelle and Takens proposed a new theory for the onset of turbulence in fluids in 1971 [7]. In the late 70s, Feigenbaum discovered the constant called the Feigenbaum constant to characterize the universal features of period doubling bifurcation [8]. Later, bifurcation diagrams, Lyapunov exponent, correlation dimension, etc., derived on the basis of chaos theory, have been used to characterize chaos and to understand the nonlinear dynamics of a system [9, 10, 11].

Nonlinearity is everywhere and it is a characteristic of a complex system. Complex systems exhibit nonlinear dynamical behavior like chaos, multiscale avalanche, self-organized criticality, turbulence, stochastic resonances, etc. [12, 13]. In the last three decades and so, with the developments of nonlinear dynamics and large scale numerical simulations, complex systems have become a very important interdisciplinary research subject with the enormous potential of practical applications. In recent times, increasing attention has been focussed on exploring real technological applications of nonlinear dynamics: controlling of chaos [14, 15], synchronization of chaos [16], secure communication [17], laser [18], etc. Applications of nonlinear dynamics have been found very significant in plasma which is an example of a complex system. Nonlinear dynamics found its application during explanation of plasma instabilities, understanding of plasma transport, characterization of plasma turbulence, etc. [13, 19].

1.2 Definition of Some Standard Oscillations

1.2.1 Periodic Oscillation

Any back and forth motion about a mean position is termed as an oscillatory motion and if it repeat itself about after equal intervals of time such oscillation is called periodic oscillation. Periodic oscillation is possible only for the system having phase space dimension ≥ 2.

1.2.2 Quasiperiodic Oscillation

In addition to periodic behaviour, there exists another type of regular motion, exhibited by a dynamical system containing two or more incommensurate frequencies, known as quasiperiodic oscillation. For instance, if a system has two distinct frequencies ω_1 and ω_2 then ratio of these two frequencies (ω_1/ω_2) should be irrational for the quasiperiodic motion.

1.2.3 Chaotic Oscillation

Chaos is a long term aperiodic behaviour in a deterministic system, and shows sensitive dependence on initial conditions. Chaotic dynamics are neither recurring nor settles down to a particular fixed point but behaves rather strangely. Chaotic dynamics are possible only for the system having phase space dimension ≥ 3.

1.2.4 Canard Solution

Canard explosion is a behaviour of transition from small amplitude oscillatory state to relaxation oscillatory states within an exponential range of control parameters, and transition occurs through a sequence of canard cycles. Canard phenomena occur in a system having one slow and one fast variable. It is hard to observe it experimentally due to extreme sensitivity to control parameter.

1.2.5 Mixed Mode Oscillation

Mixed mode oscillation (MMO) is the oscillatory behavior of the system characterized by an alternation of large amplitude and small amplitude oscillations. A pattern in an MMO is described by a symbol L^s where L and s denotes the number of large and small oscillations respectively. Regular MMO consists of a recursive L^s pattern, whereas L^s pattern is not recursive in the irregular mixed mode oscillation.

1.2.6 Intermittency

For any dynamical system, intermittent behaviour is characterized by an irregular alternation between the periodic and chaotic phases or different types of chaotic phases. In fluid dynamics, intermittency appears when long term laminar phases are interrupted by irregular bursts.

1.3 Plasma Physics: an Introduction

The universe consists of four fundamental constituents: solid, liquid, gas and plasma. As temperature is increased, the state of matter changes from solid to liquid. With further increase in temperature, the liquid turns into gas. Further increase in temperature, the outermost electrons of the gaseous atoms can overcome the nuclear attraction and escape thereby the gas becomes ionized. In this process, a partially or fully ionized gas of negative electrons and positive ions and/or neutrals may be formed. This state of the matter was called a plasma by Irving Langmuir in 1928 [20]. The Plasma state is known to be the fourth state of matter. Plasma is defined as a quasineutral gas of charged and neutral particles which exhibits collective behavior [21]. Due to these features of plasma, it can be considered as a complex system. A system involving plasma is subjected to long range electromagnetic forces. It is very difficult to predict the dynamics of a system involving such a huge number of particles interacting over a large scale. Since the electric field of an individual electron is shielded by the presence of neighbouring particles, on a scale larger than shielding distance, the collective effect dominates over individual particle interaction and individual particle need not to be considered. The first observation of the collective motion was made by Tonks and Langmuir in a gas discharge, showing that the gas of charged particles behaves differently as compared to gases [22].

Plasma can be broadly characterized by the following basic parameters:

1. density of the electrons and ions, $n_{e,i}$. In the quasi-neutral state of plasma, the density of the electrons and the ions is almost equal, $n_i \approx n_e \equiv n$ and n is usually called the plasma density;

2. energy distributions of the particles, $f_{n,e,i}$.

Here, suffices n, e and i are stand for neutral, electron and ion respectively.

For any ionized gas to be termed as plasma, the following conditions must be fulfilled

$$\lambda_D << L \tag{1.1}$$

$$N_D >>> 1 \tag{1.2}$$

$$\omega\tau >> 1 \tag{1.3}$$

where $\lambda_D = \sqrt{(\epsilon_0 K T_e / n e^2)}$ is the Debye screening length, i.e., the characteristic length over which any small electrostatic perturbation may be neutralized. L is the dimension of the plasma. $N_D = n\frac{4}{3}\pi{\lambda_D}^3$ is the total number of plasma particles in a Debye sphere, τ is the collision time and ω is the characteristic frequency of standing oscillations of the electrons. The first two conditions, given above, are actually implications of each other whereas the third condition guarantees that the dynamics of the plasma particles are governed by long range Coulomb interactions rather than Newtonian collisions.

1.4 Plasma Dynamics: Oscillations and Waves

It is known that a plasma is a quasineutral medium. So, any small deviation in the neutrality gives rise to self-generated electric fields in order to limit the charge build up. The electric field limits the charge accumulation in a region via restoring force which forces the electrons to exhibit oscillations. Plasma has a number of natural modes of oscillations. The most fundamental mode is the electron plasma frequency which is given by:

$$\omega_{pe}^2 = \frac{e^2 n_e}{\epsilon_0 m_e} \tag{1.4}$$

where, ϵ_0 and m_e are the permittivity of free space and electron mass. The ions can also oscillate at their own natural frequency called the ion plasma frequency, and is given by,

$$\omega_{pi}^2 = \frac{e^2 n_i}{\epsilon_0 m_i} \tag{1.5}$$

where, m_i is the ion mass.

Plasma is very rich in wave phenomena [23]. In presence of warm plasma effects, a low frequency wave with the electrons providing the restoring force and the ions contributing to the inertia is usually observed in plasma systems and is known as the ion acoustic wave. Dispersion relation governing this wave in the long wavelength approximation is given by

$$\omega = k\sqrt{\frac{k_B T_e}{m_i}} \tag{1.6}$$

Here, k and k_B are wave number and Boltzmann constant respectively. In presence of ionization and recombination effects, the mode exhibits itself in the form of ionization instabilities.

A magnetized plasma supports a large number of electrostatic and electromagnetic modes [24, 25]. If an equilibrium state of a plasma is perturbed then plasma responds with wave-like behavior. In general, plasma not often exists in an equilibrium state in the laboratory as well as in nature [23]. In plasma, various free energy sources in the form of energetic electrons (having energy greater than the thermal energy of electrons in the system), density gradient and spatial gradient provides the energy to excited plasma wave as a result of which amplitude of these wave grows unbound. These phenomena are commonly known as instability. In a general sense, an instability represents the ability of a plasma to relax from a non-thermal state through a collective process in a time much less than the binary collision time. These excited plasma instabilities mostly propagate as waves. Commonly, unmagnetized plasma supports the following three natural modes:

1. electromagnetic wave with dispersion relation $\omega^2 = \omega_{pe}^2 + c^2k^2$;
2. high frequency electrostatic wave with dispersion relation $\omega^2 = \omega_{pe}^2 + \frac{3}{2}v_{th_e}^2 k^2$;
3. low frequency electrostatic ion-acoustic wave with dispersion relation $\omega = kc_s$.

Here, ω, v_{th} and c_s are the frequency of modes, electron thermal velocity and ion acoustic velocity respectively.

However, in the presence of a magnetic field, the plasma supports a larger variety of natural modes. If the driving force of the wave is strong enough, instead of a single wave, fluctuations of continuous power spectra are observed. This feature develops a turbulent or chaotic fluctuation.

1.5 Plasma Physics as a Complex System and its Contribution to Nonlinear Dynamics

Plasma is a highly nonlinear and complex medium. As discussed in section 1.4, there are many sources of free energy in the plasma which drives the plasma instabilities so that the dynamics of plasma becomes highly nonlinear and complex.

Due to the collective behaviour of plasma (because of the electric and magnetic fields) waves can also be developed in them. The linear conventional tools and linear model are not sufficient to understand these nonlinear plasma processes. In the late 60s and later, nonlinear oscillator based models like Van der Pol oscillator were used to explain the growth and saturation of the plasma instabilities [19]. A first experimental observation of nonlinear phenomena like periodic pulling in periodically forced self oscillatory plasmas, made by Abrams et al. in 1969, that has been proposed to explain the transition to turbulence in a bounded plasma characterized by weakly unstable modes [26]. This result is also supported using Van der Pol model. Starting from a two fluid model of plasma, Keen et al. showed that an ion acoustic instability can be described by the sinusoidally forced Van der Pol oscillator [19]. Experimental evidence of deterministic chaos in the electron beam plasma system was reported by Boswell et al. [27] in 1984 wherein they found that the natural oscillations on an electron beam propagating parallel to a magnetic field, undergoes a period doubling route to chaos state with an increase in the beam current. Cheung et al. reported the first experimental observation of chaotic behavior and period doubling in a pulsed plasma discharge [28]. First observation was made on deterministic chaos in a dc excited glow discharge plasma by Braun et al. [29] in 1987. Afterwards various observations were made on deterministic chaos in various plasma systems via an intermittent route to chaos, period doubling route to chaos, quasiperiodic route to chaos and period adding route to chaos [30, 31, 32]. In 1992, an evidence of homoclinic chaos was reported in the electrical discharge plasma system by T. Braun, et al. [33]. Many other nonlinear phenomena like mode locking, period pulling, frequency entrainments, etc., had been observed by Klinger et al. [34, 35] whereas the gradual transition from the nonchaotic to chaotic regime had been observed by S. Ghorui, et al. [36, 37]. Nurujjaman et al. showed various nonlinear phenomena like chaos to order transition, stochastic and coherence resonance in a glow discharge unmagnetized plasma with cylindrical geometry [30, 38]. In many other experiments almost similar phenomena had been observed where different types of gases, geometric configurations and parametric regimes were explored.

Most of the time oscillations in the plasma are self excited, i.e., self originating due to interplay of internal plasma parameters. So, by forcing the plasma system one can have nonlinear phenomena which had been observed in a forced oscillator system. Various nonlinear phenomena like homoclinic chaos, intermittency, period doubling route to chaos have been observed in the forced plasma system. Forcing may be sinusoidal or noise. General thinking is that the system behavior in the presence of noise forcing will be random but there are many studies which have revealed that noise can play a constructive role like noise induced order in chaotic dynamics, synchronization of chaotic systems, stochastic and coherence resonances. Lin et al. and Dinklage, et al. observed stochastic resonance in plasma [39, 40]. Another complex nonlinear phenomena: mixed mode oscillation (MMO), which is often encountered in a chemical system, has also been reported in discharge plasma by Braun et al. [33]. Mikikian et al. [41] also reported MMO in a dusty plasma system. Thus, one can say that plasma is a highly complex system and exhibits various nonlinear dynamical phenomena.

1.6 Motivation

Modern life-style is immensely dependent on plasma technologies. Plasma processing of material, plasma laser, plasma torch, food packaging, plasma display, solar photo-voltaic lighting, protective coatings, creation of exotic new materials, biomedical application are to name a few. There is another major role of plasma for producing fusion energy that can fulfill the energy requirement for our growing future needs. In Section 1.5, it is seen that the dynamics of plasma are highly nonlinear and complex. In general, an understanding of the various plasma processes can be obtained by investigating the plasma equilibrium parameters like density, electron temperature, plasma potential. Apart from these, features related to plasma waves such as frequency and dispersion relation also give information about the plasma process. However, to explain certain phenomena like plasma transport, which is very important in case of fusion experiment, and to achieve features like chaos control in plasma, one requires information about the underlying dynamics of plasma which can be extracted from the plasma oscillations. Consideration of plasma fluctuations is also important during development of plasma based thin film/nanoparticle growth due to the correlation between plasma fluctuation and fluctuations of nanoparticle growth.

Conventional plasma physicist would be interested in oscillations from a spectral point of view like identification of frequencies and their power etc., but a nonlinear dynamist would tend to explore every small details in the oscillations e.g. plasma physics in general does not have the word mixed mode oscillation, but it is an important phenomena in nonlinear dynamics. In conventional plasma analysis, a plasma with no oscillations would be considered to be stable, which may not really be true since a small perturbation may lead the system to an unstable state. Even in the variation of a control parameter, a conventional plasma physicist may vary it in large steps without really going into the details of the oscillations whereas to study nonlinear dynamics, one would vary the control parameter in the smallest step possible. Smaller details like the various types of bifurcations and how the system went from order to chaos or vice versa, whether features like intermittency or crisis occur would greatly interest a nonlinear dynamist. Thus, investigation of nonlinear plasma fluctuations in order to extract the underlying nonlinear dynamics of plasma has emerged out as an important area of research.

All the above discussion motivates us to investigate and explore the interesting physical phenomena related to nonlinearity of plasma. As the glow discharge plasma device is very common and versatile in plasma technology and also very easy to operate in a large parametric window of discharge voltage and neutral pressure. As a result the dynamical behaviour of glow discharge plasma are being diagnosed extensively in recent years [30, 42, 43, 44]. Although many experiments based on various control parameters have been carried out to study the nonlinear behaviour in glow discharge plasma, the role of intrinsic noise and inhomogeneous magnetic field (dipolar magnetic field) have not yet been explored much. The noise may come into the plasma system by two ways. First, externally applied sources like noise and function generators generates the extrinsic noise. Second, various plasma mode interactions, and experimental devices like power supply generate the intrinsic noise. Within the scope of the present thesis a glow discharge plasma devise was used to produce argon discharge plasma for studying various non-linear behavior of both unmagnetized as well as magnetized plasma. Research work carried out in this thesis are focussed to study how the presence of external inhomogeneous magnetic field produced by a bar magnet, external homogeneous magnetic fields (axial magnetic field) and intrinsic plasma noise affects the plasma dynamics.

During the investigation of plasma dynamics in the presence of dipolar magnetic field, various interesting nonlinear dynamical phenomena like mixed mode oscillation, canard oscillation and period doubling have been seen. A role of intrinsic noise is seen in the observation of canard and mixed mode oscillations. Can a homogeneous magnetic field perturbation also lead to such nonlinear behavior? This question motivates us to carry out an experiment in the presence of axial homogeneous magnetic field, and in this experiment we have seen the multifractal behaviour of the plasma dynamics. Understanding the multifractal behaviour is very important phenomena in magnetized plasma devices like tokamak and is of great importance for space plasmas. Motivated by the fact that sometimes intrinsic noise can induce complicated nonlinear phenomena as observed in our experiments in magnetized plasma, we next inspected thoroughly the effect of intrinsic noise on excitable dynamics of unmagnetized plasma. In general an experimental time series is always contaminated by noisy signals as also seen in our experiments. It has been realized that the accuracy of results can be improved by eliminating the coherent part of a time series data from its incoherent part. This motivates us to develop a method for coherent mode detection of a chaotic or turbulent time series data.

1.7 Scope and Organization of the Thesis

The scope of this thesis is to explore the effect of axial, dipolar magnetic fields and intrinsic noise on the plasma dynamics. To achieve our goal, we have done several experiments in a glow discharge magnetized as well as unmagnetized plasma. Apart from the experiments, we have carried out a few numerical simulations to understand nonlinear dynamical response of plasma in connection with the above experiment. In addition to this, an empirical mode decomposition based coherent mode detection technique is developed which turns out to be very efficient to filter out the coherent part of a chaotic or turbulence data from its incoherent part.

The thesis contents are distributed through nine different chapters. It is organized as follows: chapter 1 starts with introduction of complex systems, nonlinear dynamics, and plasma physics. It also provides a glimpse of the contribution of plasma in the fields of nonlinear dynamics. Details about the glow discharge plasma experimental system and the diagnostics used for plasma characterization are described in chapter 2. It also describes the tools used for the analysis of plasma fluctuations. Experimental results on the mixed mode oscillation and canard oscillation in the excited glow discharge plasma in the presence of an inhomogeneous magnetic field are given in chapter 3. Role of intrinsic noise in the generation of such plasma oscillation is shown, and a numerical simulation, to understand the dynamical origin of these plasma oscillations and to verify the role of intrinsic noise, is carried out in this chapter. Chapter 4 extended the work of chapter 3, where glow discharge plasma system kept in a normal oscillatory state instead of an excited one and a localized glow region of excess ionization and its associated nonlinear dynamics is shown. Chapter 5 presents the experimental studies of multifractal dynamics of plasma in the presence of axial magnetic field. Multifractal dynamics of plasma are confirmed using multifractal detrended fluctuation analysis technique. Effect of intrinsic noise on the plasma dynamics in the unmagnetized case is demonstrated in the chapter 6. For the first time, an experimental evidence of intrinsic noise induced coherence resonance in a plasma system is shown and verified using numerical simulations. FitzHugh-Nagumo like model, derived from the ion density perturbation equation, is obtained to explain the intrinsic noise induced coherence resonance. An experimental signal is always contaminated with the noise and an incoherent part. To address this problem, in chapter 7 we have developed a method to extract the coherent mode in a chaotic or turbulent time series data. This method is based upon the empirical mode decomposition technique and its efficiency is shown by applying this method on three different fluctuations obtained from the glow discharge plasma device. Chapter 8 presents the applicability of empirical mode decomposition based coherent mode detection method on the intermittent data. Intermittent chaotic fluctuations of plasma are analyzed using this method and the obtained results further consolidate its efficiency and its applicability on various chaotic and turbulent data. Finally, in chapter 9, works presented in this thesis are summarized and the future scope of work has been presented.

Chapter 2

Experimental Setup: Glow Discharge Plasma Device, Plasma Diagnostics and Plasma Fluctuations Analysis Techniques

In this chapter, detailed description of experimental setup, diagnostics and data analysis techniques have been presented. Experiments have been carried out in a dc glow discharge plasma device. Langmuir probe is used as a diagnostic tool for the plasma characteristics and plasma floating potential fluctuations. A detailed methodology of various linear, nonlinear and statistical time series analysis tools, used for the analysis of floating potential fluctuations is presented.

In the laboratories, plasmas are created by supplying energy to the neutral gas. There are various ways to supply the necessary energy to the neutral gas for plasma production like exothermic chemical reaction, adiabatic compression of the gas, etc. Supply of energy to the gas reservoir via energetic beams is also an option. However, the electrical breakdown of the gas is the most widely used method for the production of plasma in the laboratory. There are always some electrons and ions in any volume of the neutral gas formed due to the interaction of the cosmic rays and radioactive radiations. With application of external electric field, these electrons get accelerated and collide with the atoms and molecules of the neutral gas with sufficient energy as a result of which ionization of the neutral gas occurs. The avalanche of charged particles, formed during this process, is balanced by the charge carrier losses like recombination, losses to the wall of the container, etc., so that a steady state plasma is formed. According to the temporal behaviour of the applied electric field, discharges are classified as direct current (dc) discharges, radio frequency (rf) discharges, microwave discharges, etc. In the present experiments, dc discharge has been used for the plasma production.

2.1 Experimental System: Glow Discharge Plasma

In a glow discharge plasma device, plasma is created by the direct current discharge. Glow discharge plasmas are low temperature plasmas and very useful in various applications like plasma based discharge cleaning, plasma sputtering processes, etc. In dc glow discharge, the electrons are energized by applying an electric field between the electrodes containing the neutral gas.

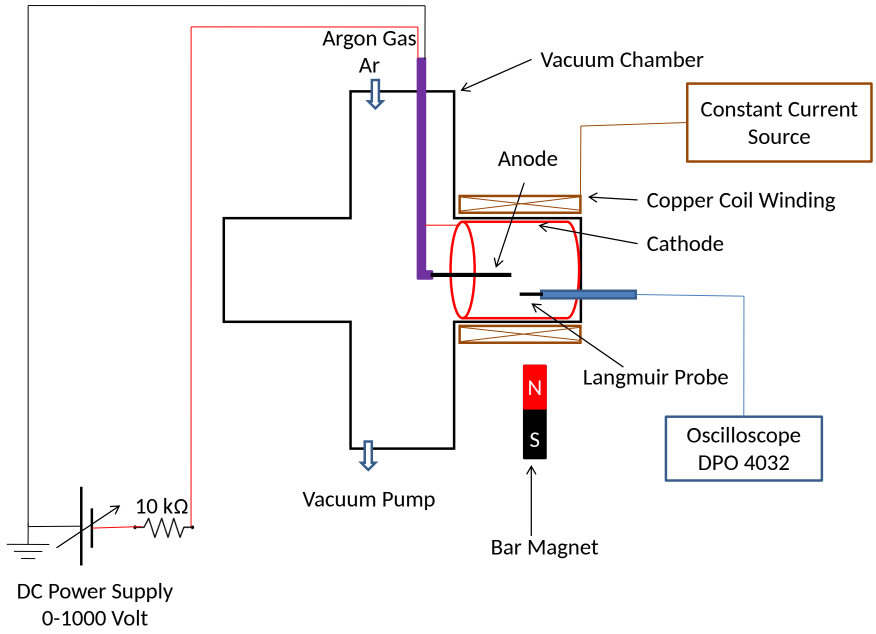

Figure 2.1: Schematic diagram of the dc glow discharge plasma device.

The experiments were carried out in a cylindrical hollow cathode dc glow discharge plasma device. The schematic diagram of the experimental setup is shown in the figure 2.1 whereas side and top views of the setup are shown in the figures 2.2 and 2.3 respectively. The setup consists of a cylindrical cathode of diameter $\sim$10 cm and length $\sim$20 cm, and a central anode rod of diameter $\sim$ 3 mm and length $\sim$ 3 cm. The whole setup was mounted inside a vacuum chamber which was evacuated to a base pressure $\sim$ 0.01 $mbar$ using oil rotary pump. The neutral pressure inside the vacuum chamber was controlled by a needle valve and the range of the gas pressure in experiments was between $\sim$ 0.03$-$0.5 $mbar$. Argon (Ar) plasma was produced inside the system at working pressure by applying a discharge voltage (DV) between anode and cathode which could be varied in the range of 0$-$1000 V. A copper coil, connected to a constant current source, is wound over the cylindrical vessel to produce a uniform axial magnetic field (B). There was also

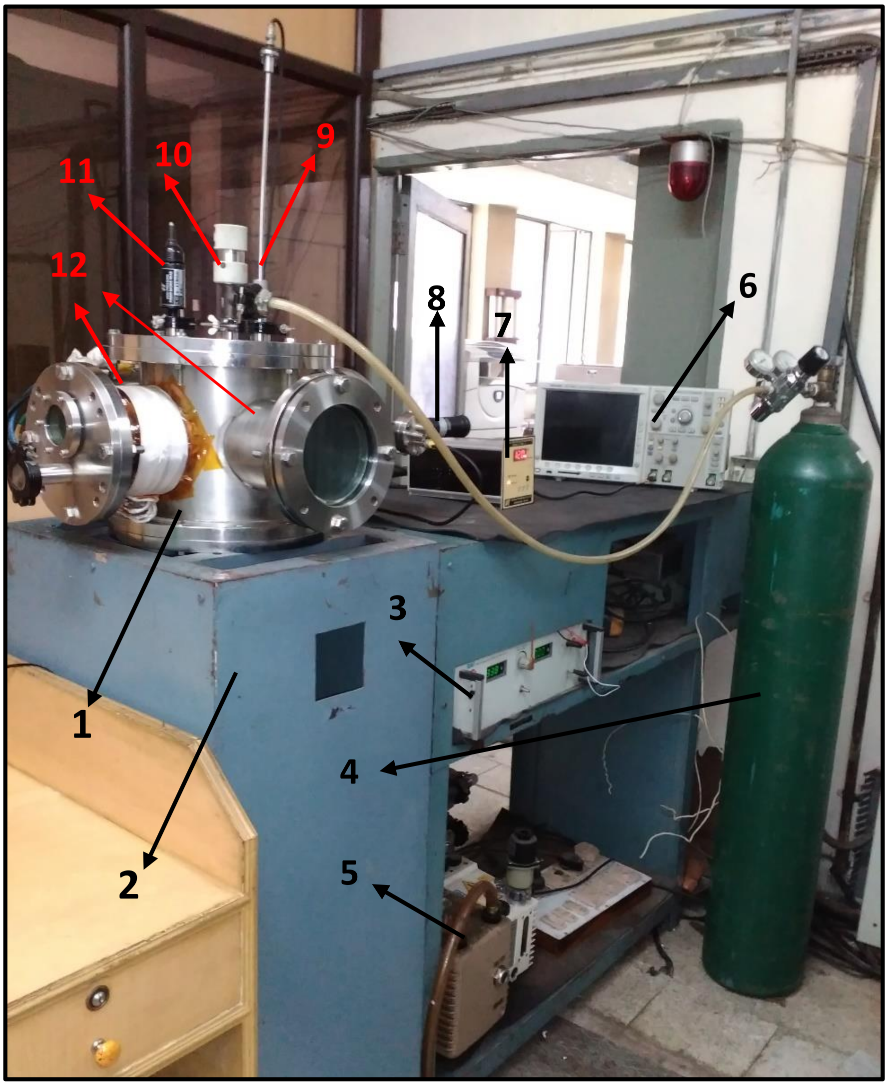

Figure 2.2: Picture of the dc glow discharge plasma device: 1) vacuum chamber, 2) stand, 3) high voltage power supply, 4) argon gas cylinder, 5) rotary pump, 6) digital oscilloscope, 7) pressure reading meter, 8) Langmuir probe, 9) power supply connection, 10) pressure control unit: needle valve, 11) Pirani gauge, and 12) side cylindrical chambers attached with main vacuum chamber.

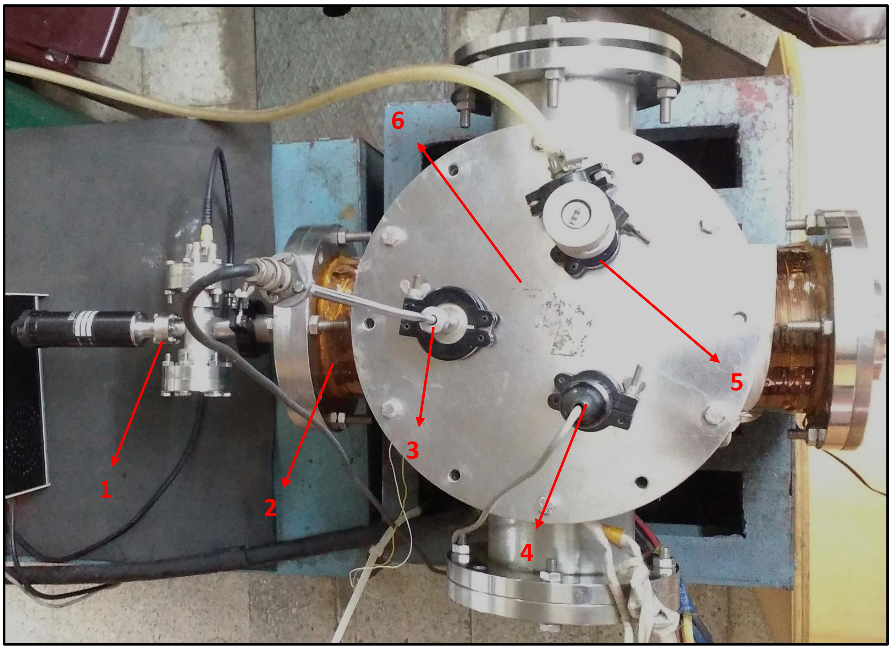

Figure 2.3: Top view of the dc glow discharge plasma device: 1) probe holder, 2) copper coil winding on side cylindrical body having cylindrical cathode chamber, 3) power supply connection, 4) Pirani gauge, 5) pressure control unit: needle valve, and 6) upper flange.

a provision to produce an inhomogeneous magnetic field by keeping a bar magnet near to the cathode surface. Detail of various parts of the device is given below:

- **Vacuum Chamber and Vacuum System:** The vacuum chamber is made up of stainless steel and mainly consists of three parts: cylindrical body, bottom flange and upper flange. Upper and bottom flanges, have diameter 30 cm and, are separated by a distance of 30 cm. Upper flange consists of three opening ports allowing us to connect the gas inlet valve, a Pirani gauge and power connection for the electrode system, whereas bottom flange consists of one opening port to which pumping system is connected. Main cylindrical body of chamber is attached to four side cylindrical bodies each of length $\sim$ 20 cm. One of these four side cylindrical bodies has been used to mount the cylindrical cathode chamber. These side cylinders also have flanges attached to them with opening ports allowing for insertion of Langmuir probes. The whole vacuum chamber is supported on a stand.

The vacuum chamber is connected to oil rotary pump with pumping speed of 250 l/s through an opening port in bottom flange. A gate valve, placed in between the pump and opening port, provides the isolation of the vacuum vessel from rotary pump. The gate valve is kept open during the pumping, and closed when the system is not under operation. A Pirani gauge head is connected to an opening in the upper flange for the measurement of the pressure in the chamber.

- **Electrode System:** A cylindrical stainless steel chamber having diameter of $\sim$10 cm and $\sim$20 cm long is placed in the one of the side cylindrical body attached with the vacuum vessel. The cathode chamber is attached with negative polarity of the power supply and also covered with teflon tape to avoid the contact between cathode chamber and vacuum vessel. A copper rod of length ~ 3 cm and diameter ~ 3 mm is placed along the axial direction of the cylindrical cathode with the help of a hanging rod and kept grounded. Hence, copper rod acts as an anode for the system. Picture of the electrode system is shown in figure 2.4.

- **Power Supply:** Power to the electrodes to initiate the discharge process has been supplied by a high voltage dc power supply (Aplab H1010). It is a variable power supply of range 0-1000 V and maximum output current is 1 amp.

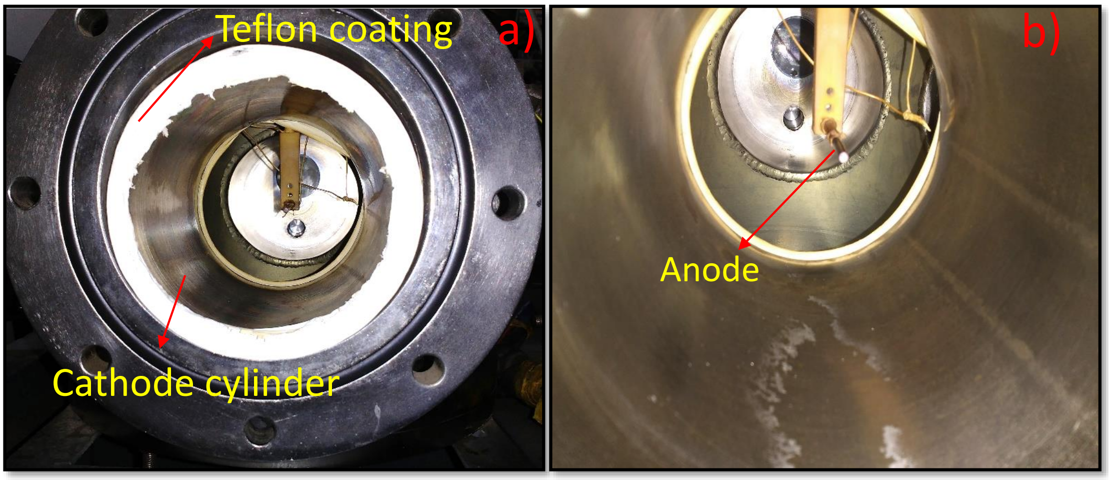

Figure 2.4: Picture of the electrode system.

- **Magnetic Field System:** A copper coil is wound over the cylindrical body containing the cathode chamber with proper isolation to form a solenoid like structure. Two ends of the copper coil are connected with a contact current power supply source to produce an axial homogeneous magnetic field inside the cathode chamber containing plasma. Apart from this, we have also provision for applying inhomogeneous magnetic field by placing a bar magnet out side the cathode chamber.

2.2 Plasma Diagnostic

One requires knowledge about the plasma parameters like density, temperature, distribution function to understand the nature of plasma, its properties and various phenomena in it. Thus, measurement of these plasma parameters experimentally as completely and as accurately as possible is needed. Because of this, an experimental plasma physicist devotes huge effort to planning, developing and providing techniques for diagnosing the properties of plasmas. Various diagnostic tools have been used in plasma experiments [45, 46, 47], for measurement of plasma parameters, like Langmuir probe, emissive prove.

Suitable diagnostics are needed for the characterization of plasma fluctuations and the waves, instabilities occurring in it. The measurements require adequate temporal as well as spatial resolution. Langmuir probe (also called electrostatic probe) is one of the suitable and widely used diagnostic for this purpose. To serve our purpose, i.e., investigation of nonlinear dynamics in plasma, we have used Langmuir probe.

2.2.1 Langmuir Probe

Langmuir probe technique, developed by Irving Langmuir in 1924, is one of the most widely used and the earliest technique in plasma diagnostics for measuring the properties of laboratory plasma. Langmuir probe is nothing but a metallic electrode inserted into the plasma. The greatest advantage of Langmuir probe is that it is the simplest and cheapest diagnostic that allows the local measurement of plasma parameters with high temporal as well as spatial resolution. It can be used to measure various plasma parameters like electron temperature (T_e), electron density (n_e), plasma potential (V_P), etc. over a wide range of plasma parameters. However, the accuracy of the Langmuir probe measurement is not very good. In spite of this discrepancy, it is often used for the advantages mentioned above.

The information about the plasma is obtained from the probe for measuring the current drawn by it at various applied biased voltages. Figure 2.5 shows a typical I-V characteristic of a cylindrical shaped Langmuir probe. Here V and I are the applied bias voltage to the probe and the current drawn by the probe respectively. The I-V curve has three distinct regions: i) electron saturation region, ii) transition

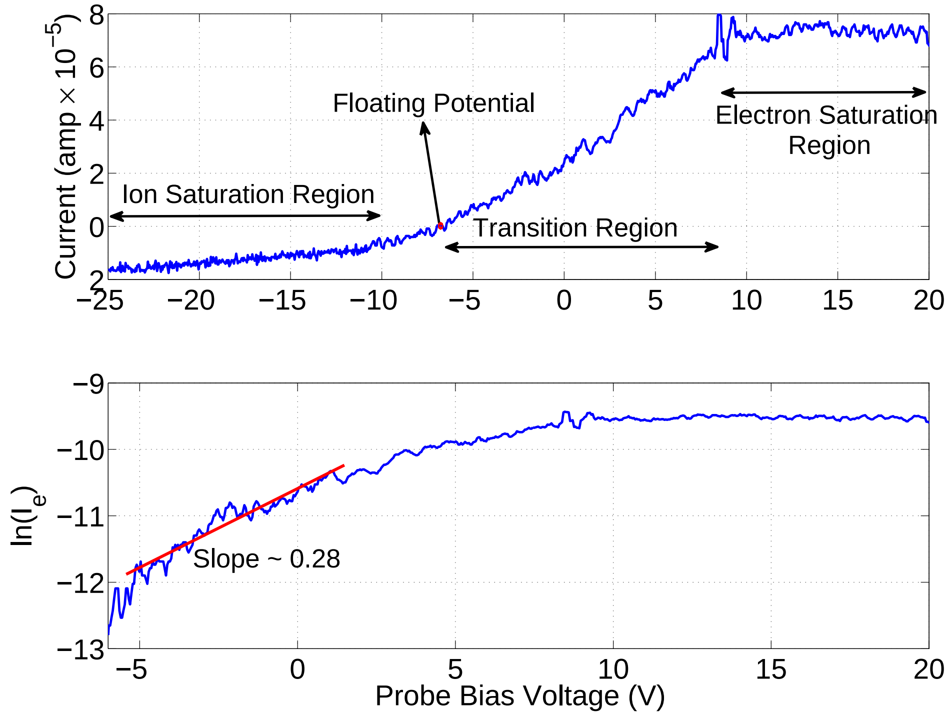

Figure 2.5: A typical Langmuir probe's I-V characteristic curve.

region and iii) ion saturation region.

- **Electron Saturation Region:** when the bias voltage V is equal to the plasma potential (V_P) then electric field will vanish and perturbation to the plasma is minimum. Thus, the current drawn by the probe at this point is mainly due to the charge particles which reach the probe because of their thermal velocity. Since the thermal velocity of electrons is much higher than ions due to their lighter mass, we can neglect the effect of ions. Therefore, at this point, current collected by the probe is mainly the electron current. If V is increased above V_P, electron current does not increase further since all the electrons arriving at the probe are collected. This region is called the electron saturation region and the corresponding electron saturation current is given by

$$I_{e,sat} = neA\sqrt{\frac{T_e}{2\pi m_e}} \tag{2.1}$$

where n, e, A, T_e and m_e are plasma density, electronic charge, area of Langmuir probe, electron temperature and electron mass respectively.

- **Transition Region:** when V is made negative with respect to the V_P, probe starts to repel electrons and accelerate ions resulting in decrease of electron current and increase of ion current. Hence, total probe current decreases. Finally, at sufficiently negative value of V electron current reduces to very small fraction of $I_{e,sat}$ and overall current becomes equal to the ion current. At this potential total current drawn by the probe is zero and the potential is called floating potential (V_f). An insulated probe placed inside the plasma would assume this potential. This is because of that an insulated probe inside the plasma is rapidly charged up negatively until the electrons are repelled and net electrical current brought to zero. This region of the I-V characteristics is called the transition region or retarded-field region. If the electron distribution is Maxwellian, the shape of the curve in this region after subtracting the ion contribution would be exponential. Electron current in the transition region is given by

$$I_e = I_{e,sat} \exp\frac{e(V - V_P)}{T_e} \tag{2.2}$$

- **Ion Saturation Region:** when V is negative enough to repel all the electrons then the total current collected by the probe is ion current. Probe current remains constant with the further decrease of V resulting in a saturation region. This region is called an ion saturation region. Ion saturation

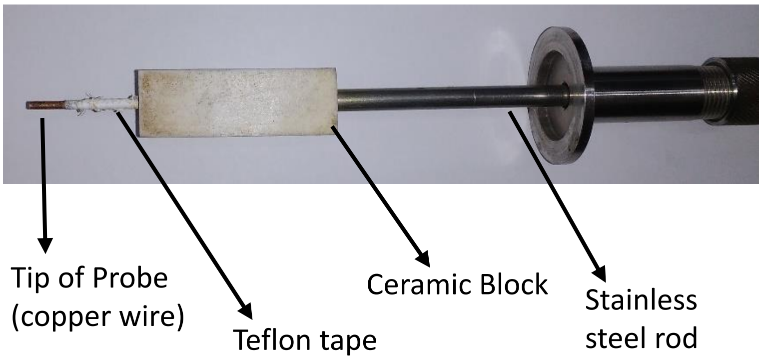

Figure 2.6: Picture of the Langmuir probe used in the experiments.

current is obtained from the Bohm sheath criterion and is given by

$$I_{i,sat} = 0.61neA\sqrt{\frac{T_e}{m_i}} \tag{2.3}$$

where m_i denotes ion mass.

By measuring the probe current and applied voltage to probe, we can estimate the electron temperature as a slope of $\ln(I_e)$ vs V curve, and can estimate plasma density from Eq. (2.3).

Langmuir probes used in the glow discharge plasma device for the characterization of its plasma are cylindrical, and made from copper wire of diameter ~ 1.5 mm and length ~ 1 cm. A teflon coated stainless steel wire has been soldered to the probe, and it has been fitted inside a ceramic block. Ceramic block is then fitted with a stainless steel (ss) tube for the support of the probe in such a way that the portion which will be inserted into the plasma are keeping out of the of ss tube. Picture of a Langmuir probe used in the experiments is shown in figure 2.6. In the present experiments, the floating potential and its fluctuations have been measured and recorded using a tektronix digital oscilloscope (DPO 4034).

2.3 Data Analysis Techniques: Time Series Analysis Tools

To understand the changing behaviour of the things in the universe, observations are made sequentially over time. A time series is a collection of such observations made sequentially and typically equally spaced in time. These time series contain the information about the measured physical quantities of a system. Useful information about the underlying dynamics of the processes and other characteristics of the data can be obtained by careful analysis of these times series. The special feature of time series analysis is the fact that the analysis must take into account the time order because the successive observations are usually not independent observations, whereas most other statistical theory is concerned with random samples of independent observations. The main objective of the time series analysis is to reveal the underlying dynamics governing by the system. Hence, time series analysis is an important area of research in many branches of science like econophysics, plasma, geophysics, neuroscience.

In order to explore the plasma dynamics, plasma fluctuation data have been analyzed. These fluctuations are generally oscillatory in nature. Since oscillatory behaviour is mainly due to nonlinear interaction between the various plasma components. The origin of these oscillations may be due to: 1) interplay of internal complex system parameters, called self excited oscillation, 2) external forcing, called forced oscillation. These two types of oscillatory behaviour form the basis of study in self excited and forced plasma systems respectively. In this thesis, we mainly focused on the self excited oscillations of the plasma.

In this thesis, we have made sequential observation of floating potential and recorded its time series. These time series are analyzed using various linear and nonlinear time series analysis tools along with some statistical tools in both time as well as frequency domain. In linear analysis tools, power spectrum and discrete wavelet transform have been used, whereas in nonlinear analysis tools, multifractal detrended fluctuation analysis, Lyapunov exponent, Hurst exponent, etc., have been used. Few statistical tools like normal variance, correlation coefficient have also been used to characterize regularity in the fluctuations. The methodology of the time series analysis tools used in this thesis is given bellow:

2.3.1 Power Spectrum

Any time series data can be considered as a superposition of various sine and cosine functions with different frequencies. Presence of frequency components in a signal is a useful information to extract physical information about a system. A time series can be analyzed in the frequency domain by using Fourier transform. The Fourier transform, of a function $x(t)$ in given by

$$\tilde{x}(f) = \frac{1}{\sqrt{N}} \sum_{n=1}^{N} x_n e^{2\pi ikn/N} \tag{2.4}$$

where $f_k = k/(N\Delta t)$, $k = -N/2, ..., N/2$ and Δt is the sampling interval. N is the total number of data points in the time series. A periodic or quasi periodic signal shows sharp spectral line in power spectrum plot, whereas for a chaotic signal it will show a broadband.

The Power spectrum method has been used extensively in order to find the characteristic modes, and the dominant mode present in the plasma fluctuations.

2.3.2 Phase Space Reconstruction

The observation of single variable, a scalar time series, of real process usually does not provide all possible states and cannot represent the multidimensional phase space of the dynamical system. Hence, it is necessary to extract the information of the multidimensional structure from the available scalar time series. Since the system variable are coupled to each other, it is possible to reconstruct the multidimensional phase space trajectory from observed time series by a time delay reconstruction.

According to Taken's theorem [48], for a given time series data: $x_0, x_1, ..., x_n$ where x_i denotes the output of variable at time i, the reconstructed attractor (phase space vector) of the original system is given by

$$X_i = [x_i, x_{i+\tau}, x_{i+2\tau}, ...x_{i+(m-1)\tau}] \tag{2.5}$$

where τ and m are embedding delay and embedding dimension respectively. m can be estimated using false nearest neighbour method [49] whereas τ can be estimated using mutual information method [50]. Using this phase space vector, one can draw a trajectory in the phase space.

2.3.3 Lyapunov Exponent

The Lyapunov exponent describes the rate of divergence or convergence of nearby trajectory onto the attractor in phase space. As the chaotic dynamical systems are sensitive to initial conditions, two nearby trajectories diverge exponentially in the phase space. Hence estimation of Lyapunov exponent (LLE) is one of the classic and standard test for chaoticity in a dynamical system. There are various methods to estimate the Lyapunov exponent. In this thesis, we have used Rosenstein method [11] and Wolf method [9]. Rosenstein method has been employed using TISEAN software package [51] whereas Wolf method has been employed using package downloaded from webpage [52].

- **Rosenstein Method:** If $d(0)$ is the initial distance between two points on the nearby trajectories and after time t distance between them is $d(t)$, then for a chaotic signal they are related by a relation:

  $$d(t) = d(0)\exp(\lambda t) \tag{2.6}$$

  where λ is called Lyapunov exponent.

  A practical time series is basically a scalar measurement. So in order to estimate the Lyapunov exponent, reconstruction of time series into phase space is necessary. Let X_j and $X_{\hat{j}}$ are the jth pair of the nearest neighbour on the reconstructed trajectory of that time series in the phase space and $d_j(0) = \parallel X_j - X_{\hat{j}} \parallel$ is the distance between them. Here, $\parallel \quad \parallel$ denotes the Euclidian norm. The separation after time $t = i\Delta t$, where Δt is the sampling time, can be written as

  $$d_j(t) = d_j(0)\exp(\lambda_L t) \tag{2.7}$$

  where λ_L is the rate of separation. The above equation can be written as

  $$\ln d_j(t) = \ln d_j(0) + \lambda_L t \tag{2.8}$$

  There is another additional constraint, nearest neighbors have a temporal separation greater than the mean period of the time series, imposed. This allows us to consider each pair of neighbors as nearby initial conditions for different trajectories. The largest Lyapunov exponent is then estimated as the mean rate of separation of the nearest neighbors.

- **Wolf Method:** Let, the initial Euclidean distance between the two neighbouring points in the phase space reconstruction trajectory is d_0 and the final distance after time t_{evolve} between the evolved points is d_{evolve}. After each t_{evolve}, we replace evolved point by a new point in the embedding space whose distance to the evolved initial point is as small as possible, under the constraint that the angular separation between the evolved and replacement element is small. This procedure is repeated until the initial point reaches the end of the time series [53]. Finally, Lyapunov exponent (λ_L) is calculated according to the equation

$$\lambda_L = \frac{1}{Mt_{evolve}} \sum_{i=0}^{M} \ln \frac{d_{evolve}^{(i)}}{d_0} \tag{2.9}$$

where M is the total number of replacement steps.

2.3.4 Multifractal Detrended Fluctuation Analysis

The MF-DFA method is the modified version of detrended fluctuation analysis (DFA) used to detect multifractal properties of time series. The multifractal detrended fluctuation analysis (MF-DFA) consists of five steps. For a given time series x_k of length N, steps for MF-DFA are given below [54]:

1. Determine the profile of underline time series

$$Y(i) \equiv \sum_{k=1}^{i} [x_k - < x >] \qquad i = 1, 2, ..., N. \tag{2.10}$$

2. Divide the profile $Y(i)$ into $N_s \equiv \mathrm{int}(N/s)$ non-overlapping segments of equal lengths s.

3. Compute the local trend for each of the $2N_s$ segments by a least squares fit of the series. Then determine the variance

$$F^2(s,\nu) \equiv \frac{1}{s}\sum_{i=1}^{s}\{Y[(\nu-1)s+i]-y_\nu(i)\}^2, \qquad \nu = 1,2,....,N_s \qquad (2.11)$$

and

$$F^2(s,\nu) \equiv \frac{1}{s}\sum_{i=1}^{s}\{Y[N-(\nu-N_s)s+i]-y_\nu(i)\}^2, \qquad \nu = N_s+1, N_s+2, ..., 2N_s \qquad (2.12)$$

where $y_\nu(i)$ is a fitting polynomial in segment ν. Linear, quadratic, cubic or higher order polynomials can be used in the fitting procedure. Usually, a linear function is selected for fitting the function [55].

4. Average over all segments to obtain the qth-order fluctuation function, given by

$$F_q(s) \equiv \{\frac{1}{2N_s}\sum_{\nu=1}^{2N_s}[F^2(s,\nu)]^{q/2}\}^{1/q}. \qquad (2.13)$$

5. Determine the scaling behaviour of the fluctuation functions by analyzing log-log plots of $F_q(s)$ versus s for each value of q. If the series x_k is long range power law correlated, $F_q(s)$ increases as a power law for large values of s,

$$F_q(s) \sim s^{h(q)} \qquad (2.14)$$

In general, the exponent $h(q)$, known as the generalized Hurst exponent, may depend on q. For stationary time series, $h(2)$ is identical to the well-known Hurst exponent (H).

$h(q)$ is independent of q for monofractal time series, since the scaling behaviour of the variances $F^2(s,\nu)$ is identical for all segments ν. For the multifractal time series, there will be a significant dependence of h(q) on q. If we consider positive values of q, the segments ν with large variance $F^2(s, \nu)$ will dominate the average $F_q(s)$. Thus, for positive values of q, h(q) describes the scaling behaviour of the segments with large fluctuations. Usually the large fluctuations are characterized by a smaller scaling exponent $h(q)$ for multifractal series. On the other hand, for negative values of q, the segments ν with small variance $F^2(s, \nu)$ will dominate the average $F_q(s)$. Hence, for negative values of q, $h(q)$ describes the scaling behaviour of the segments with small fluctuations, which are usually characterized by a larger scaling exponent.

A multifractal description can also be obtained by considering partition functions [56] :

$$Z_q(s) = s^{\tau(q)} \tag{2.15}$$

The relation between classical multifractal scaling exponents $\tau(q)$ (Rényi exponent) obtained from standard partition function-based multifractal formalism and generalized Hurst exponent $h(q)$ is given by:

$$\tau(q) = qh(q) - 1; \tag{2.16}$$

The generalized multifractal dimension is given by:

$$D(q) \equiv \frac{\tau(q)}{q-1} = \frac{qh(q) - 1}{q-1}; \tag{2.17}$$

There is another way to characterize multifractal properties of a time series by using singularity spectrum $f(\alpha)$ which is related to $\tau(q)$ via a Legendre transform:

$$f(\alpha) = q\alpha - \tau(q) = q(\alpha - h(q)) + 1; \tag{2.18}$$

where $\alpha = \tau'(q)$.

The width and shape of the multifractal spectrum reflect the temporal variation of the local scale invariant structure of the time series. The width of the singularity spectrum denotes the degree of multifractality of a time series.

2.3.5 Empirical Mode Decomposition (EMD)

Empirical mode decomposition (EMD), proposed by Huang et al. [57], has emerged as a very efficient tool for the analysis of a nonlinear and non-stationary time series data. It is a method to decompose a signal into its inherent signals which usually refer as intrinsic mode functions (IMFs). An IMF is just a simple oscillatory mode satisfying the following conditions: 1) envelopes of maxima and minima must have zero mean 2) the difference between the number of local extrema and the number of zero-crossings must be zero or one. The first condition assures that the IMF is symmetric, and the second condition assures that no riding waves of multiple frequency exist in an IMF. These two conditions ensure that the IMF is monocomponent in frequency [57]. Most of the experimental signals are multicomponent in nature, i.e., there exist different scales simultaneously. These signals can be considered as a superposition of fast oscillation with a slow one at the local level. Therefore, we need to decompose these signals into their inherent modes for the study of their basic structure. This EMD approach is based on the local time scales, i.e., the detection of the local maxima and minima.

The algorithm to extract IMF from a signal $x(t)$ involves the following steps:

1. Identify all the local maxima/minima and connect them using cubic spline to form an envelope of maxima/minima, $E_{max}(t)/E_{min}(t)$.

2. Compute the mean between these two envelopes $m(t) = \frac{E_{max}(t)+E_{min}(t)}{2}$.

3. Extract the residue $h_{11}(t) = x(t) - m(t)$. Ideally, $h_{11}(t)$ should be an IMF as expected, However it may not satisfy the condition to be an IMF in reality.

4. Iterate step (1-3) on residue, i.e., repeat the sifting process n times, until $h_{1n}(t)$ is an IMF and $h_{1n}(t) = C_1(t)$ is designated as the first IMF.

5. Compute the residue $R_1(t) = x(t) - C_1(t)$.

6. Iterate step (1-5) on $R_1(t)$ to compute the second IMF $C_2(t)$ and the residue $R_2(t)$.

7. The sifting procedure is then repeated on residuals $R_{n-1}(t)$ until $R_n(t)$ becomes a monotonic function or at most has one local extreme point.

The above algorithm removes the high frequency oscillation from the data with each repetition, resulting in higher IMFs containing a lower frequency oscillation than the earlier one. The sifting procedure mentioned above is continued till a particular stopping criteria is met, ideally when the two conditions for a signal to be an IMF are fulfilled. But imposing a too low threshold for terminating the process may lead to the generation of spurious IMFs. There are many stopping criteria discussed in literature [57, 58]. Here, we have adopted a stopping criteria proposed by Rilling et al. [58], based on two thresholds δ_1 and δ_2, the ratio of mean to the amplitude of the envelopes i.e. on $S(t) = \left|\frac{M(t)}{A(t)}\right|$. The two threshold conditions δ_1 and δ_2 are imposed to guarantee globally small fluctuations in the mean while taking large excursions. For a given fraction of time $(1-\alpha)$, $S(t)$ should be less than δ_1 and for the rest of the time $S(t)$ should be less than δ_2. Here, α is a constant. In our later analysis, δ_1, δ_2 and α are set at same values as used by Rilling et al. [58], i.e., at 0.05, 0.5 and 0.05 respectively.

2.3.6 Correlation Coefficient

The correlation coefficient (CC) of a time series Y(t) with another time series X(t) is given by:

$$CC = \left| \frac{\sum_{i=1}^{N}(Y(t_i) \cdot X(t_i))}{\sqrt{\sum_{i=1}^{N} Y(t_i) \cdot Y(t_i)}\sqrt{\sum_{i=1}^{N} X(t_i) \cdot X(t_i)}} \right| \tag{2.19}$$

where N is the data length of the signal. The value of CC is normalized to lies between 0 and 1.

In our works, we have used this statistical quantities to find out the correlation between an IMF with its original signal. The CC of an IMF, gives an idea about its contribution to the original signal, and is calculated using the following relation:

$$CC = \left| \frac{\sum_{i=1}^{N}(IMF(t_i) \cdot X(t_i))}{\sqrt{\sum_{i=1}^{N} IMF(t_i) \cdot IMF(t_i)}\sqrt{\sum_{i=1}^{N} X(t_i) \cdot X(t_i)}} \right| \tag{2.20}$$

where $X(t)$ is a signal and N is the data length of the signal. The IMFs, whose CC is more than 10% are considered as relevant (physically significant mode) and the rest are considered as redundant.

2.3.7 Hilbert Huang Transform

The Hilbert Huang transform (HHT) was proposed by Huang et al. [57]. The HHT represents the signal being analyzed in the time-frequency domain by combining the empirical mode decomposition (EMD) and the Hilbert transform.

Hilbert transform of a time series $X(t)$ is written as:

$$Y(t) = \frac{1}{\pi} P \int_{-\infty}^{+\infty} \frac{X(t')}{t - t'} dt' \tag{2.21}$$

where P is the Cauchy principal value. From this we can construct an analytical signal $Z(t)$ defined as $Z(t) = X(t) + jY(t) = A(t)e^{j\phi(t)t}$, where $A(t) = \sqrt{X^2 + Y^2}$

and $\phi(t) = \arctan(Y/X)$ are the instantaneous amplitude and phase angle respectively. Hence the corresponding instantaneous frequency can be defined as: $\omega(t) = \frac{d\phi(t)}{dt}$.

In order to get information about the instantaneous frequency, we need to have a monocomponent signal, whereas almost all experimental signals are multicomponent in nature. So, first we have to convert the signal into monocomponent signals which can be achieved using empirical mode decomposition. Empirical mode decomposition decomposes a signal into some individual monocomponent signals which are termed as IMF for which the concept of instantaneous frequency is valid. The Hilbert transformation of the IMF is termed as a Hilbert Huang transform. The instantaneous amplitude and instantaneous frequency can be organized in the form of a time-frequency spectrum $H(\omega, t)$, also known as the Hilbert-Huang spectrum which is given by the relation

$$H(\omega, t) = Re \sum_i A_i(t) \exp\left[j \int \omega_i(t) dt\right] \tag{2.22}$$

2.3.8 EMD Based Bicoherency

In the section 2.3.7, we have seen that the IMFs can be represented in the form of $Z_i(t) = A_i(t)e^{j\phi_i(t)t}$ using Hilbert transform. The interaction amongst them can be studied by estimating the Bicoherency factor [59]

$$\gamma = \frac{< Z_i^* Z_{i+1} Z_{i+2} >}{< A_i A_{i+1} A_{i+2} >} \tag{2.23}$$

where the angular bracket represents the time average.

The value $< Z_i^* Z_{i+1} Z_{i+2} >$ is nearly 0 for random values of ϕ_i, ϕ_{i+1} and ϕ_{i+2} and equal to $< A_i A_{i+1} A_{i+2} >$ when $\phi_i = \phi_{i+1} + \phi_{i+2}$. Hence, γ is bounded between 0 and 1. First, we calculated the largest number of 2π phases in each of the triplets [59]. Since N (number of 2π phases) is an ensemble of independent wave periods, the error in the bicoherency factor is given by $\sigma = \frac{1}{\sqrt{N}}$. If bicoherency factor for a particular IMF is larger than the error value, then there is an existence of triplet interaction between that particular IMF and two successive modes.

2.3.9 Discrete Wavelet Transform

Wavelet transform [60, 61], a tool for analysis of non-stationary time series data, decomposes a time series $x(t)$ into a superposition of the elementary functions $\psi_{a,b}(t)$ derived from a mother wavelet $\psi(t)$ by dilation and translation, i.e.,

$$\psi_{a,b}(t) = \frac{1}{\sqrt{a}}\psi\left(\frac{t-b}{a}\right), \tag{2.24}$$

where a (> 0) is a dilation parameter and b is a translation parameter. Both a and b are real parameters.

Wavelet transform are of two types: continuous wavelet transform (CWT) and discrete wavelet transform (DWT). If the data are confined to a discrete set, it is important to consider a discrete version of wavelet transform. In this case, the wavelet transform is performed only on a discrete grid of the parameters of dilation and translation, i.e., a and b can take only integral values. The orthonormal wavelet basis function can be obtained from Eq. (2.24) by setting $a = 2^{-m}$ and $b = n/2^m$.

The DWT is defined as,

$$x_m^n = \int_{-\infty}^{+\infty} x(t)\psi_{m,n}(t)dt, \tag{2.25}$$

where the orthonormal basis function is given by

$$\psi_{m,n}(t) = 2^{m/2}\psi\left(2^m t - n\right). \tag{2.26}$$

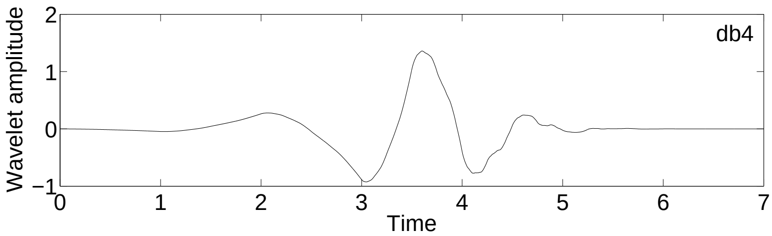

Figure 2.7: Fourth order Daubechies wavelet.

The transform is simply a linear combination of basis functions. The contribution of the signal at particular scale m is given by,

$$x_m(t) = \sum_n x_m^n \psi_{m,n}(t)dt. \tag{2.27}$$

One can obtain the original time series using inverse transform for the orthogonal decomposition

$$x(t) = \sum_{m,n} x_m^n \psi_{m,n}(t)dt. \tag{2.28}$$

In this thesis, we have employed the Daubechies wavelet $\psi_r(t)$ which are in the form of Eq. (2.24) and has the following properties [62]:

1. $\psi_r(t)$ is supported in the interval of [0, 2r+1].

2. $\psi_r(t)$ has r vanishing moment, i.e.,

$$\int_{-\infty}^{+\infty} t^r \psi_r(t)dt = 0. \tag{2.29}$$

3. The continuous derivative of $\psi_r(t)$ is δr, where $\delta \simeq 0.2$.

For $r = 1$, this orthogonal basis function reduces to Haar wavelet. The Daubechies wavelets are determined recursively from its scaling function. Fourth order Daubechies wavelet, shown in figure 2.7, is used during wavelet analysis in this thesis.

2.3.10 Hurst Exponent

The Hurst exponent (H) was first introduced by Hurst to study the long term memory stored in a time series data. It quantifies the relative tendency of a time series either to regress strongly to the mean or to cluster in a direction. The value of H is bounded between 0 and 1. A value of $H = 0.5$ corresponds to a completely uncorrelated series. Motion corresponding to $H > 0.5$ have tendency to persist in its progression in the direction of motion, whereas for $H < 0.5$, motions have a tendency to turn back upon themselves. The value of $H < 0.5, > 0.5$ and 1 indicate the anti-persistence (anti correlated), persistence (correlated) and periodic nature of the time series signal. A number of estimators of long-range dependence such as rescaled range (R/S) analysis, detrended fluctuation analysis, aggregated variances, etc. have been proposed in the literature. The oldest and best-known is the so-called rescaled range (R/S) analysis popularized by Mandelbrot et al. [63, 64] and based on previous hydrological findings of Hurst [65].

For any time series signal X_i, the R/S is defined as the ratio of the maximal range of the integrated signal normalized to the standard deviation:

$$\frac{R(m)}{S(m)} = \frac{max(Z_1, Z_2, ..., Z_m) - min(Z_1, Z_2, ..., Z_m)}{\sqrt{S^2(m)}}, \tag{2.30}$$

where Z_m is the cumulative-summed (integrated) time series. For a time series of length i, $X = \{X_t : t = 1, 2, .., i\}$, Z_m is given by

$$Z_m = X_1 + X_2 + ... + X_m - m\bar{X}, \tag{2.31}$$

where $\bar{X}$, $S^2(m)$ and m are respectively the mean, variance, and time lag of the signal. The expected value of R/S scales like cm^H as $m \to \infty$. Here, c and H are a constant and Hurst exponent respectively. To estimate the value of the Hurst exponent, $log_{10}(R/S)$ is plotted against $log_{10}(m)$. The slope of linear regression gives the value of Hurst exponent.

Presence of coherent oscillations can also be identified as a linear regime in the plot of $log_{10}(R/S)$ versus $log_{10}(m)$ and the value where bending begins in the curve correspond to the time period of the oscillation. It is possible to have more than one linear regime in the plot which indicates the presence of multiple coherent modes/oscillations [13] as well as multiple centres of rotation [66].

2.3.11 Normalized Variance

The normalized variance (NV) is a measure of the regularity of occurrence of spikes in a time series signal. It is defined as $NV = \sigma_{ISI}/m_{ISI}$, where ISI is the time elapsed between successive spikes, σ_{ISI} and m_{ISI} are standard deviation of ISI and mean of ISI respectively. It is evident that the value of the computed NV will be lower for the more regular induced dynamics. For purely periodic dynamics, the NV will be zero.

All the above methods and their algorithms have been implemented using MATLAB code language, and used in this thesis for the analysis of plasma fluctuations.

Chapter 3

Canard and Mixed Mode Oscillations in an Excitable Glow Discharge Plasma in the Presence of a Bar Magnet

In this chapter, the effect of an inhomogeneous magnetic field produced by a bar magnet on the excitable dynamical state of a glow discharge plasma system is investigated. The possible physical process behind the generation of nonlinear dynamical phenomena: canard and mixed mode oscillations in the plasma is discussed. The obtained results are explained in the light of magnetization of ions and presence of intrinsic noise. Starting from a FitzHugh-Nagumo like macroscopic model derived from the basic plasma equations and phenomenology, dynamical origin of such nonlinear phenomena is identified and corroborated with possible physics.

3.1 Introduction

An excitable system is a nonlinear dynamical system having a single stable attractor, but it has two modes of returning to the equilibrium state. For small perturbations away from the equilibrium, it returns to equilibrium in monotonic fashion; however, for perturbations beyond a threshold value, it undergoes a large excursion before settling down. It is well known that a change in the control parameter or external perturbation of an excitable complex system near the threshold produces various nonlinear phenomena such as noise induced resonances, canard oscillations and mixed mode oscillations, which have been observed experimentally as well as numerically in many physical, chemical, biological and electronics systems [41, 67, 68, 69, 70, 71, 72, 73, 74, 75, 76, 77, 78, 79, 80, 81, 82]. However, these kind of phenomena have been observed in a very few plasma experiments [38, 39, 40, 83, 84]. This is mainly because, it is not easy to achieve excitability condition in a plasma system. So far, most of the nonlinear dynamical experiments, which depend on the excitability of plasma were performed in the glow discharge plasmas. In these experiments the excitability has been achieved through Hopf bifurcation [39, 40] or homoclinic bifurcation [38]. When plasma is perturbed at its excitable state by using noise or a periodic signal or both types of signal, the system shows coherence resonance, stochastic resonance, frequency entertainments, period pulling and other perturbation-enhanced nonlinear phenomena [38, 39, 40, 83, 84, 85]. It is observed that if the change in the system control parameter near the threshold is very small or systems are perturbed by noise, then such systems may also show canard-enhanced phenomena. For example, the FitzHugh-Nagumo (FHN) model or some real experiments generate canard and various canard-enhanced phenomena due to small change in the control parameter and noise perturbation [67, 71, 81, 86, 87, 88, 89, 90, 91, 92].

The canard phenomena in an excitable system means the generation of small amplitude quasiperiodic oscillations that has been observed through numerical simulation as well as in a few experiments for a small change in the control parameter near the threshold of excitability [67, 71, 79, 80]. Though a small change in the control parameter is easily realizable in numerical simulations to get canard phenomena, it is difficult to achieve such tiny change in the case of real experiments. In the case of a glow discharge plasma [83, 84, 38, 85], where the discharge voltage or current acts as a control parameter, canard induced phenomena have not yet been observed by changing the discharge voltage or current. This may be due to the fact that discharge voltage or current acts as a coarse control parameter due to the limitation of our present experimental setup. Small changes in the parameters can be achieved by changing other external parameter like magnetic field or by changing the intrinsic noise level of the system. It is also observed that very small amount of noise perturbation excites canard orbit and MMO (oscillatory dynamics involving oscillations with greatly different amplitudes). Various mechanisms are responsible for MMOs in a deterministic system, such as the existence of a Shilnikov type homoclinic orbit or subcritical Hopf bifurcation [93, 94]. A stochastic process can also generate MMOs [80, 91]. As small amount of intrinsic/internal noise is always present in a plasma system, it can generate various noise induced phenomena under suitable parametric conditions. As the level of internal noise can be changed easily by changing certain experimental parameter like discharge voltage or external magnetic field, such changes in the noise level can generate noise induced phenomena like MMOs in a plasma system.

3.2 Canard and Mixed Mode Oscillations

To carry out an experiment, initially the chamber was filled with argon gas at pressure ~ 0.36 $mbar$ and a discharge was initiated by increasing the discharge voltage (DV). At this pressure, system showed an excitable fixed point dynamics at DV ~ 401 V. An inhomogeneous magnetic field was applied to the plasma by using a bar magnet as shown in the schematic diagram of experimental setup (figure 2.1) in the chapter 2. When the magnet is kept far away, the field experienced at the cathode boundary is almost negligible and on bringing it nearer to the system, the field strength increases. The variation in the magnetic field with distance is shown in figure 3.1 (a). Figure 3.1 (b) shows the ion cyclotron frequency (f_{ci}) corresponding to magnetic field strengths derived using the relation $f_{ci} = 1.52 \times 10^3 Z\mu^{-1}B\ Hz$, where, $\mu = \frac{m_i}{m_p}$; Z is charge state and B is the magnetic field in Gauss (G). m_i and m_p is the argon mass and proton mass respectively. Once the excitability is achieved through change of the DV, it was kept fixed through out the experiment and the magnetic field, act as a control parameter, was varied to get the desired dynamics.

Figure 3.2 shows the plasma floating potential fluctuations for different values of magnetic fields. Figure 3.2(a) shows the quasiperiodic small amplitude oscillations at a magnetic field of ~ 2 G (i.e., just after the introduction of the magnetic field). Figures 3.2(b) and 3.2(c) show the plasma fluctuations at $B \sim 6$ G and $B \sim 14$ G respectively. It is seen from these plots that the large but bounded periodic limit cycle oscillations appears between the small quasiperiodic oscillations confirming

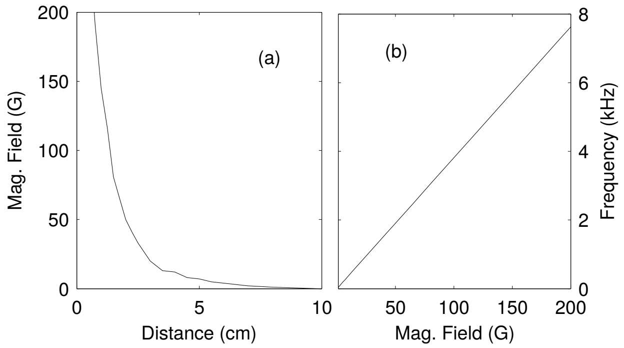

Figure 3.1: a) Variation of the applied magnetic field as a function of distance from the cathode chamber. b) Estimated values of ion cyclotron frequency at different values magnetic field strength.

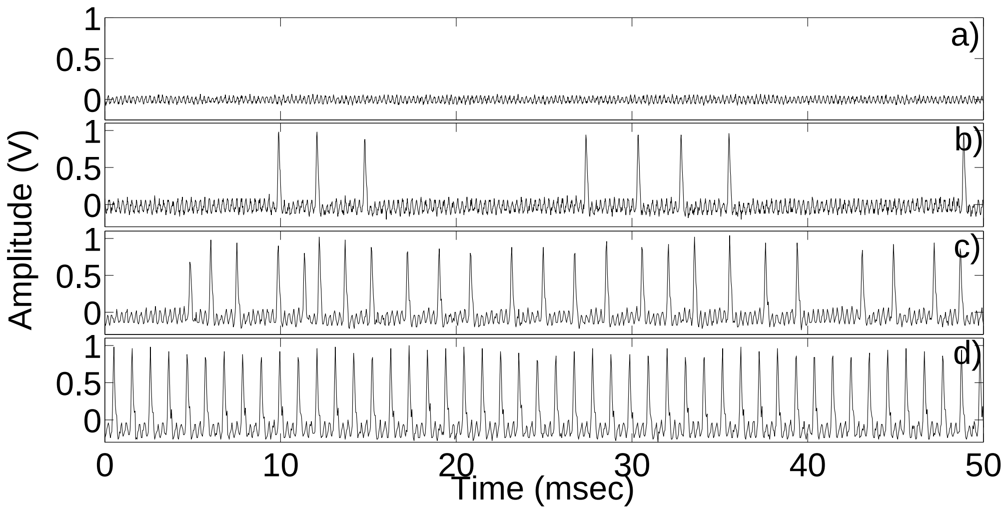

Figure 3.2: Plasma floating potential fluctuations at different values of magnetic field: a) 2 G: small amplitude quasiperiodic oscillation, b) 6 G: emergence of canard trajectory and spiky oscillations, c) 14 G: appearance of the irregular mixed mode oscillation, and d) 25 G: appearance of the regular mixed mode oscillation. DV and pressure are kept fixed at 401 V and 0.36 $mbar$ respectively.

the occurrence of canard orbit and spiky oscillation. In figures 3.2(b) and 3.2(c) the appearance of sporadic long quasiperiodic sequence may be due to parametric drifts of the system from the mean fixed point. These oscillations were observed for wide range of magnetic field values ($\sim 6\ G$ to $\sim 20\ G$). When the magnetic field became $\sim 25\ G$, large oscillations were observed after every two small oscillations [Figure 3.2(d)] and this has been observed till 100 G. As the magnetic field was applied from outside the vacuum vessel, it was not possible to go beyond the 100 G limit with the present configuration of the experimental setup.

The observed oscillations in the figures 3.2(c) and 3.2(d) show the characteristics of MMO. In order to characterize these oscillations, a symbolic notation m^n is assigned to the MMO states, where m gives the number of large-amplitude oscillations and n the number of small-amplitude oscillations in a single pattern. A combination of 1^6, 1^5 and 1^4 is seen in the figure 3.2(c), but the combination is not in a periodic fashion. This type of MMOs are generally termed as a compound and irregular MMOs. The nature of oscillation became regular MMO of 1^2 type for the higher values of magnetic field as seen in figure 3.2(d).

Figure 3.3 shows the power spectrum corresponding to the data shown in the figure 3.2. In the figure 3.3(a), distinct peaks approximately around $\sim 4205\ Hz$ and $\sim 4155\ Hz$ are seen in the case of quasiperiodic oscillation which is lying in the range of ion acoustic oscillations. These two frequencies are incommensurate in the nature justifying the quasiperiodic characteristic of the oscillation. In the figure 3.3(b), a broadband is observed with dominant power around $\sim 4\ kHz$ for the quasiperiodic oscillation with few large amplitude spikes. For the irregular MMOs, dominant peaks in the power spectrum [figure 3.3(c)] are observed around 600 Hz

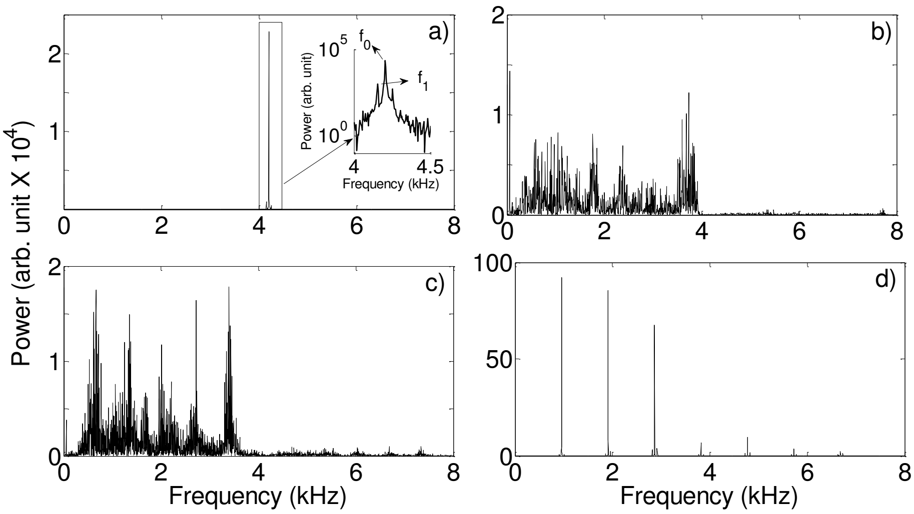

Figure 3.3: Power spectrum plots for: a) 2 G: quasiperiodic oscillation shown in figure 3.2(a). Here $f_0(4205Hz)$ and $f_1(4155Hz)$ are two incommensurate frequencies. b) 6 G: quasiperiod oscillation with few large amplitude spikes shown in the figure 3.2(b), c) 14 G: irregular MMO, and d) 25 G: regular MMO shown in the figure 3.2(c) and figure 3.2(d) respectively.

and its harmonics which is broadband in the nature. This broadband may due to the interaction of ion acoustic and ion cyclotron modes, and the frequencies in the broadband are lying in the range of ion cyclotron and ion acoustic frequencies. A clear distinct peaks are seen around $\sim 960\ Hz$ and its harmonics in the case of regular MMO which might correspond to ion cyclotron frequency ($\sim 950\ Hz$ at 25 G) and its higher harmonics. It is also seen that the observed power for the dominant frequency is approximately 100 times as compared to irregular MMOs. The distinct peaks in the power spectrum plot for regular MMO confirm the periodic nature of oscillation. In case of irregular MMOs power is distributed all over the modes whereas for the regular MMO it is concentrated in the ion cyclotron mode.

Figure 3.4 shows the reconstructed phase space projection corresponding to the experimental data shown in figure 3.2. The phase space projections show all

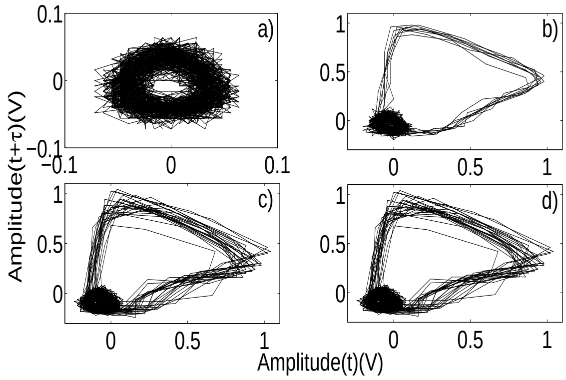

Figure 3.4: Reconstructed phase space plots for the fluctuations shown in figure 3.2. First plot (a) clearly shows the small amplitude quasiperiodic oscillation whereas other three are showing the occurrence of spikes and canard trajectories. In these plots the time delay, estimated using mutual information technique, $\tau = 0.04\ ms$ has been used.

the expected noisy version of canards. The phase space projection also show the features of MMOs, i.e., small quasi periodic oscillations followed by a number of large amplitude limit cycle oscillation.

The main feature of a system which shows MMO is that it must be nonlinear with multiple timescales [87, 88, 91]. Occurrence of the multiscale dynamics in an excitable plasma system has already been confirmed [38], where multiscale dynamics has already been exploited to demonstrate noise induced coherence and stochastic resonances [38, 85]. MMO driven by deterministic process display a strong trend in increasing amplitude of small amplitude quasiperiodic subthreshold oscillation, while those driven by stochastic process have a weaker trend or no trend at all, for average amplitude of small amplitude quasiperiodic oscillation [80]. In the present experiment, we have not observed any increasing trend in the small amplitude quasiperiodic oscillations which suggests that the observed MMOs may be noise driven. We feel that the internal plasma noise is responsible for the generation of MMOs. In order to understand the role of internal plasma noise, we have investigated variation in the noise level with magnetic field which is presented in the section 3.3.

3.3 Role of Magnetic Field in the Generation of Internal Plasma Noise

Magnetic field can affect the plasma system by helping in increasing the confinement of charged particles [95, 96]. The application of an inhomogeneous magnetic field in the plasma leads to the generation of ion cyclotron oscillations with different frequencies and polarization characteristics which interact nonlinearly with the different plasma modes for example ion acoustic modes [97]. This may be responsible for the broadband spectrum, which we term as an internal plasma noise. Since electron cyclotron frequencies are very high as compared to the frequencies of interest in the experiment we can ignore such effects. The electrons can participate in increasing the collisions with neutrals and hence change the ionization content in the present experiment.

Figure 3.5 shows a sketch of the magnetic field lines in the presence of the bar magnet. The magnetic lines of force nearer to the cathode surface (-ve potential surface) traps the electrons, clearly visualized from the figure 3.5, which gyrate around magnetic field and move back and forth (e.g. between point A and B) along these lines of force. Thus magnetic field leads to confinement of electrons, causing an enhancement in the ionization due to increase in the number of collisions. An enhancement in the ionization increases the strength of the oscillations. When the bar magnet is close to the cathode surface, the number of trapped electrons will be higher due to the higher density of magnetic lines of force leading to a

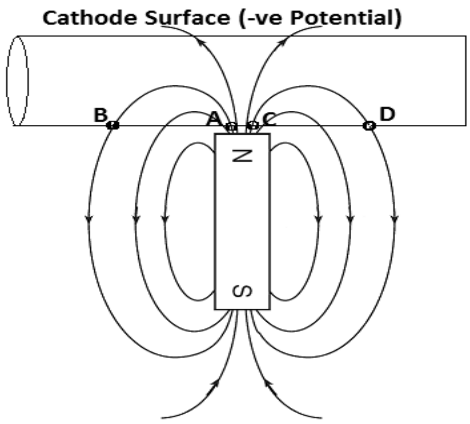

Figure 3.5: Magnetic lines of force in the presence of the bar magnet when it is close to the cathode surface. The electrons originating at point A will get reflected at point B and vice versa.

further enhancement in the ionization and hence the amplitude of the oscillations. This effect indicates that internal plasma noise strength will increase with the increase in the magnetic field strength. Figure 3.6 shows the variation in the noise level, estimated directly from the time series data using the Wiener filter matlab subroutine, with the change in magnetic field strength. Wiener filter [98], proposed by N. Wiener, is a class of optimum linear filter which involve linear estimation of a desired signal sequence from another related sequence. The Wiener filter minimizes the average squared distance between the filter output and a desired signal [99]. It shows that noise level increases with the increase in magnetic field. As the noise level increases with the increase in magnetic field, we may conclude that internal plasma noise has a role in the excitation of canard orbit and MMO. The role of magnetization is also important especially that of ions. When the magnetic field was < 25 Gauss, the Larmor radius of ions was greater than the system dimension (> 10 cm) which indicates that the ions were unmagnetized. A plasma system is said to be magnetized if its characteristic length-scale is comparable to the Larmor

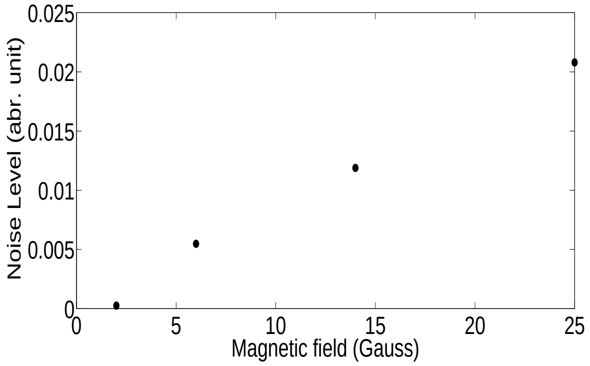

Figure 3.6: Internal noise level as a function of magnetic field. It shows noise level increases with magnetic field strength

radius [100]. So for B $<$ 25 G, the only effect on the system may be due to the internal noise generated by the magnetic field, whereas for B $>$ 25 G, the ions become magnetized (Larmor radius $\sim$ 8 cm). Hence it is quite likely that the internal noise plays a less significant role in the system dynamics since the ion cyclotron oscillations begin to dominate. However, we cannot neglect the minor effect of internal noise which is always present in the system. The estimates of ion cyclotron frequency and Larmor radius for different values of magnetic field is shown in table 3.1. The ion cyclotron frequency at 25 G is 950 Hz, which is approximately equal to the experimental observed frequency (960 Hz). We have observed that the power of the mode for regular MMO is $\sim$ 100 times larger than that of the irregular MMO indicating the dominance of ion cyclotron mode over the internal noise effect in the case regular MMO.

Internal noise and magnetization of ions are always present in a plasma in a magnetic field. Depending on the magnetization of the ions, the dynamics are different. Presence of internal plasma noise leads to irregular MMOs (for $B < 25\,G$) wherein there is no increase in the amplitude of the subthreshold oscillations. In the case of regular MMOs (for $B > 25$ G), the internal plasma noise is still present in

Table 3.1: Estimation of ion cyclotron frequency (f_{ci}) and ion Larmor radius (L_i) for different values of applied magnetic field; q, B, m_i and v_{th} are charge, magnetic field, ion mass and ion thermal velocity respectively.

Magnetic Field (B)	$f_{ci} = (\frac{qB}{m_i})$	$L_i = (\frac{m_i v_{th}}{qB})$	Magnetization
2 G	76 Hz	102 cm	Unmagnetized
6 G	228 Hz	34 cm	Unmagnetized
14 G	532 Hz	14.5 cm	Unmagnetized
25 G	950 Hz	8.2 cm	Magnetized

addition to the ion cyclotron modes. While the ion cyclotron modes lead to regular MMOs, the presence of the internal plasma noise probably does not allow the increase of the amplitude of the subthreshold oscillations. When the magnetization was low the internal noise dominates and we observed irregular MMOs whereas when the magnetization was higher the ion cyclotron mode dominates and we observe regular MMO.

3.4 Dynamical Model for Canard and Mixed Mode Oscillations

Keen et al. [19] had derived an anharmonic oscillator equation for ion acoustic instabilities treating plasma as a two fluid model with source terms to contribute to the nonlinear effects. In an effort to understand the dynamical origin of the canards and MMOs in an excitable system, we obtained an excitable FHN like model from the anharmonic oscillator equation for ion acoustic instabilities [19, 101]. The anharmonic oscillator for the ion density perturbation is given by [19]

$$\frac{d^2 n_1}{dt^2} - (\alpha - 2\lambda n_1 - 3\mu n_1^2)\frac{dn_1}{dt} + \omega_0^2 n_1 = 0 \tag{3.1}$$

where n_1, α, λ, μ and ω_0 are the perturbed plasma density, ionization term, coefficient of two body recombination, coefficient of three body recombination and ion acoustic frequency respectively.

By normalizing the above equation using $\tau = \omega t$; $x = n_1/n_0$; $p = \alpha/\omega$; $q = 2\lambda n_0/\omega$; $r = 3\mu n_0^2/\omega$; $s = \omega_0^2/\omega^2$ we obtain

$$\ddot{x} - (p - qx - rx^2)\dot{x} + sx = 0 \tag{3.2}$$

By using a Liénard-like coordinate, Eq. (3.2) can be decomposed into the following system of two first order equation:

$$\dot{x} = (px - \frac{qx^2}{2} - \frac{rx^3}{3}) - sy \tag{3.3}$$

$$\dot{y} = x \tag{3.4}$$

We have obtained a FHN like model, by rearranging the parameters, given by

$$\epsilon\dot{x} = (ax - \frac{bx^2}{2} - \frac{cx^3}{3}) - y \tag{3.5}$$

$$\dot{y} = x \tag{3.6}$$

where ϵ, a, b and c are $1/s, p/s, q/s$ and r/s respectively and represent system parameters. The difference between the original FHN model and our present equation is the presence of the quadratic term.

Though we have not applied external noise in the experiment, it is observed that internal plasma noise level increases with magnetic field strength [figure 3.6]. So a Gaussian noise term ($D\xi(t)$) and a constant biasing term (K) are introduced in right hand side of Eq. (3.6) that represent the internal plasma noise and the discharge voltage respectively. Hence we obtain

$$\epsilon\dot{x} = (ax - \frac{bx^2}{2} - \frac{cx^3}{3}) - y \tag{3.7}$$

$$\dot{y} = x + K + D\xi(t) \tag{3.8}$$

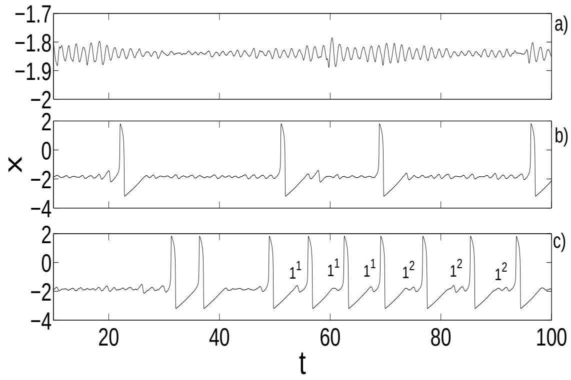

Figure 3.7: Oscillations obtained from numerical model. a) small amplitude quasiperiodic oscillation at $D = 0.01$, b) emergence of canard oscillation and large amplitude spikes at $D = 0.1$, and c) irregular MMO at $D = 0.3$.

where D is strength of noise and $\xi(t)$ is Gaussian noise.

The value of K is chosen such that system shows a fixed point excitable behavior. As a change in the magnetic field leads to a change in the internal noise strength, so we have used the noise strength (D) as our control parameter. Fourth order Runge Kutta method has been used to solve the above Eqns. (3.7) and (3.8). The parameters a, b, c, K and ϵ are fixed at 1, 0.9, 0.8 1.84 and 0.05 respectively. For the given choice of a, b, c and ϵ, the dynamics corresponds to a fixed point solution for $K > 1.83$, whereas for $K < 1.83$ a limit cycle solution exists. Athough this model is not an exact representation of the experimental system on microscopic level but this model is sufficient to explore the dynamical origin of the canards and mixed mode oscillations.

Figure 3.7 shows the simulated time series of x at different D as mentioned in the caption of the figure. Figure 3.7(a) shows the quasiperiodic behaviour just after application of the noise in the system. When the value of D is increased the time series shows coexistence of quasiperiodic oscillation and large amplitude limit cycle oscillation [as seen in figure 3.7(b)]. Further increase in the value of D leads the system toward MMO. It is clearly seen from the figure 3.7(c) that the time series has the characteristic behaviour of irregular MMO. A combination 1^1 and 1^2 MMO states are seen in the figure. An irregular MMO similar to the experimental results has been observed in the numerical simulation by changing noise strength. However regular MMO has not been observed by changing the noise strength in the present simulation. It indicates that the origin of regular MMO might not be a stochastic process. This fact is also observed in the experiment. For higher values of the magnetic field, the system dynamics is driven by ion cyclotron mode rather that stochastic process. We have obtained similar results for different combination of system parameters: $a = 0.9, b = 0.8, c = 0.7, K = 1.86$ and $\epsilon = 20$ with D used as control parameter. Thus, irregular MMOs are probably dominated by stochastic process, whereas regular MMOs are probably dominated by ion cyclotron mode.

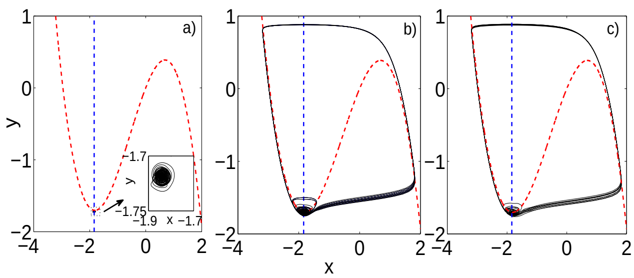

Figure 3.8: Phase space plots corresponding to the numerically simulated oscillations shown in the figure 3.7. It is clearly showing the occurrence of canard oscillation and spikes. The dotted lines represent the nullclines.

In figure 3.8, we have plotted a phase-space trajectory corresponding to time series shown in figure 3.7. These phase space plots clearly show the occurrence of canard oscillation and spikes in our numerical model. In these plots the main large trajectory in phase space corresponds to the large amplitude variation during spikes, and smaller loop corresponds to small amplitude oscillations.

Since this model is developed using basic phenomenology without considering the microscopic facts of the plasma, so exact reproduction of the experimental signal is not possible. However, the results obtained from numerical simulation show qualitative agreement with experimental results and its revealed that the noise plays a significant role in the generation of canard and irregular MMO.

3.5 Summary and Conclusions

The effect of the magnetic field near the threshold of an excitable plasma system has been studied in this chapter. As the dynamics of the system under present experimental conditions is multiscale in nature, and when the system is perturbed by a magnetic field, it shows canard and mixed mode oscillations. The applied magnetic field was inhomogeneous in nature, and it generates internal plasma noise. Strength of the plasma noise increases with the increase in the magnetic field. Internal plasma noise triggers quasiperiodic small amplitude oscillation. When the internal noise strength increases, the dynamics of the system goes from the small amplitude quasiperiodic oscillations to small-amplitude oscillations with sporadic single spikes, then to irregular MMOs. Regular MMO has been also observed for the higher magnetic field strength. It is seen that ions were magnetized for higher values of magnetic field whereas for lower magnetic field ions were unmagnetized. So, the observation of regular MMO might be due to the dominance of ion cyclotron mode over internal plasma noise. A numerical model, resembling an FHN model obtained from anharmonic oscillator for ion acoustic instabilities, has been used to understand the dynamics of the observed experimental results. Simulation shows that an excitable system in the presence of noise can also produce irregular MMO and canard oscillation in place of coherence resonance phenomenon.

Beyond the interest in the study of these nonlinear phenomena from experimental and dynamic point of view, their characterization is also very important for experiments involving real applications in glow discharge plasma. Such studies may be useful for various applications of discharge plasma like plasma coating, plasma sputtering and other plasma application.

Chapter 4

A Localized Cathode Glow in the Presence of a Bar Magnet and its Associated Nonlinear Dynamics

Under conditions when the plasma is displaying normal oscillatory dynamics, subjecting it to a dipolar magnetic field using a bar magnet reveals formation of localized regions of intense ionization known as cathode spots. The size and intensity of such region is seen to vary with a change in the magnetic field strength, following which the dynamics of the region also undergoes various transitions. The bulk plasma oscillations reflect these changes and are investigated for different values of magnetic field.

4.1 Introduction

Whenever a localized region of plasma is subjected to constraints like localized electric field, or any disturbance that affects the local thermodynamic equilibrium, appearance of complex space charge structures are reported [102]. Fireball, sheath, double layer and plasma bubble are various manifestations of complex space charge configurations that have been well studied [16, 103, 104, 105]. These structures give rise to various plasma instabilities that make plasma oscillations complex and nonlinear. In the current experiment, a localized glow region like a fireball is formed near the cathode surface of a glow discharge plasma device when a bar magnet is placed outside the plasma chamber close to the cathode surface. Appearance of this structure leads to complex and nonlinear oscillations of the floating potential. As we studied in the chapter 1, the investigation of nonlinear dynamics of plasma in the presence of a magnetic field is a subject of great interest due to its usefulness in various areas like plasma fusion processes, plasma processing, space plasma, magnetron discharges, glow discharge plasma, etc. [106, 107, 108]. Lots of theoretical as well as experimental investigations have been done in plasma systems where the magnetic field is unidirectional [105, 109, 110]. A dipole magnetic field is known to bring about several interesting features in the dynamics of a single charged particle. A magnetized particle undergoes cyclotron motion around the field lines, bounce motion between the poles as well as curvature and gradient drifts across the magnetic field. Most of the astronomical bodies like stars as well as planets are known to possess strong magnetic fields, and the confinement of plasmas embedded in such fields poses many challenging questions. Magnetospheric plasmas are self-organized structures of plasmas in magnetic dipoles [111] that provide natural confinement of charged particles. The mapping of plasma sheath in a magnetic dipole field has been done experimentally [112] to understand the implications to the solar wind interaction with lunar magnetic anomalies. Earth's magnetic field has a significant role in the oscillations of the ionospheric plasma and flow of the plasma around the Earth [113]. In the context of laboratory plasmas, magnetron sputtering devices use plasma discharges based on bar magnet [114, 115].

Many works exist in literature reporting studies on fireball structure and its associated nonlinear dynamics in magnetized as well as unmagnetized plasma. Although there are investigations on plasma subject to a dipole type of magnetic field in magnetic dipole discharge experiments [116], literature does not show enough evidence of investigations of fireball like structure and its associated nonlinear dynamics where the magnetic field strength of a bar magnet is used as a control parameter.

The present work aims to study the dynamics of nonlinear oscillations associated with the localized cathode glow in a glow discharge plasma in presence of a bar magnet placed external to the device. The analysis of recorded floating potential fluctuations reveal order to chaos transition with the increase of magnetic field strength. We observed a transition from order to chaos via period doubling route which is associated with the cathode glow in the presence of a bar magnet. The presence of a magnetic field is known to bring about significant modification in the behaviour of the sheath that is formed in the vicinity of a solid surface that is in contact with a plasma. The introduction of inhomogeneous magnetic fields of dipole nature is capable of generating complex sheath structures with a potential minima due to the magnetic mirror like effects leading to back and forth oscillations of electrons, and increased collision rates. In addition to influencing the potentials structure near cathode surface, the dynamics of charged particles undergoing trapping oscillations also can be expected to be reflected in the plasma fluctuations measured in the bulk region. Hence we have also carried out a numerical simulation [117] for the study of ion dynamics by considering that ions are trapped inside a potential structure near the cathode surface.

4.2 Appearance of Localized Glow Near Cathode Surface

In the pervious chapter, we have seen the effect of a dipolar magnetic field on the excitable dynamics of the plasma. Here, we are concerned with a normal oscillatory state that is subject to a magnetic field from a bar magnet. It is known that excitable dynamics is sensitive to any small or large perturbation. However, the stable oscillatory states, i.e, attractors are generally not sensitive to small amount of perturbations. Thus, in all the following results we have neglected the effect of intrinsic noise produced due to the application of dipolar magnetic field. Generation of intrinsic noise due to application of magnetic field is discussed in previous chapter. The strength of the field is varied by changing the distance of the bar magnet from the cathode surface and its variation with distance is shown in the figure 4.1.

In the present experiment, DV and pressure are kept fixed at $\sim 597\ V$ and $\sim 0.130\ mbar$ respectively. The application of the magnetic field produces a localized glow, a fireball like structure, near the cathode surface. As we have discussed in chapter 3, due to the presence of a bar magnet placed near the cathode surface,

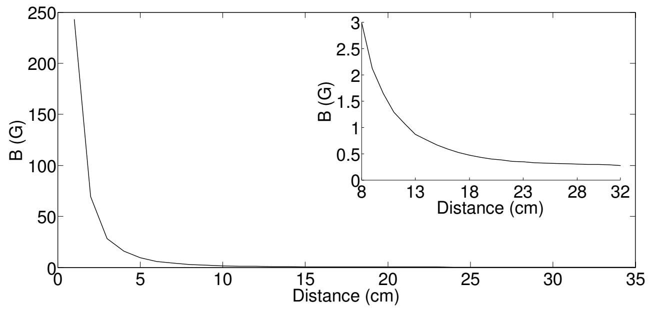

Figure 4.1: Magnetic field strength (B) as a function of distance between the bar magnet and the nearest cathode surface. Inset figure shows the range 8-32 cm.

the secondary electrons produced from the cathode surface travel along the dipolar field lines (shown in the figure 3.5), get reflected by sheath near cathode surface, ionize neutrals, and produce a dense plasma compared to the bulk plasma near the cathode surface. Secondary emitted electrons from the cathode surface gain energy when they traverse the cathode sheath across the magnetic field. The energized electrons ionize the gas. The increased ionization in the present experiment leads to the formation of a cathode glow region. From the figure 4.2, it is clearly seen that a localized glow region appears at the cathode surface whose intensity increases with the increase in the strength of the magnetic field. This appearance of a strong glow at the cathode suggests additional ionization in that region. Plasma density, measured in the glow region, increases with the magnetic field strength as depicted in the figure 4.3. This observation also confirms the enhancement of the ionization in the glow region.

4.3 Analysis of Order to Chaos Behaviour

In figure 4.4, we have shown the time series of floating potential fluctuations with increasing magnetic field strength, at a constant DV $\sim 597\ V$ and pressure ~ 0.130

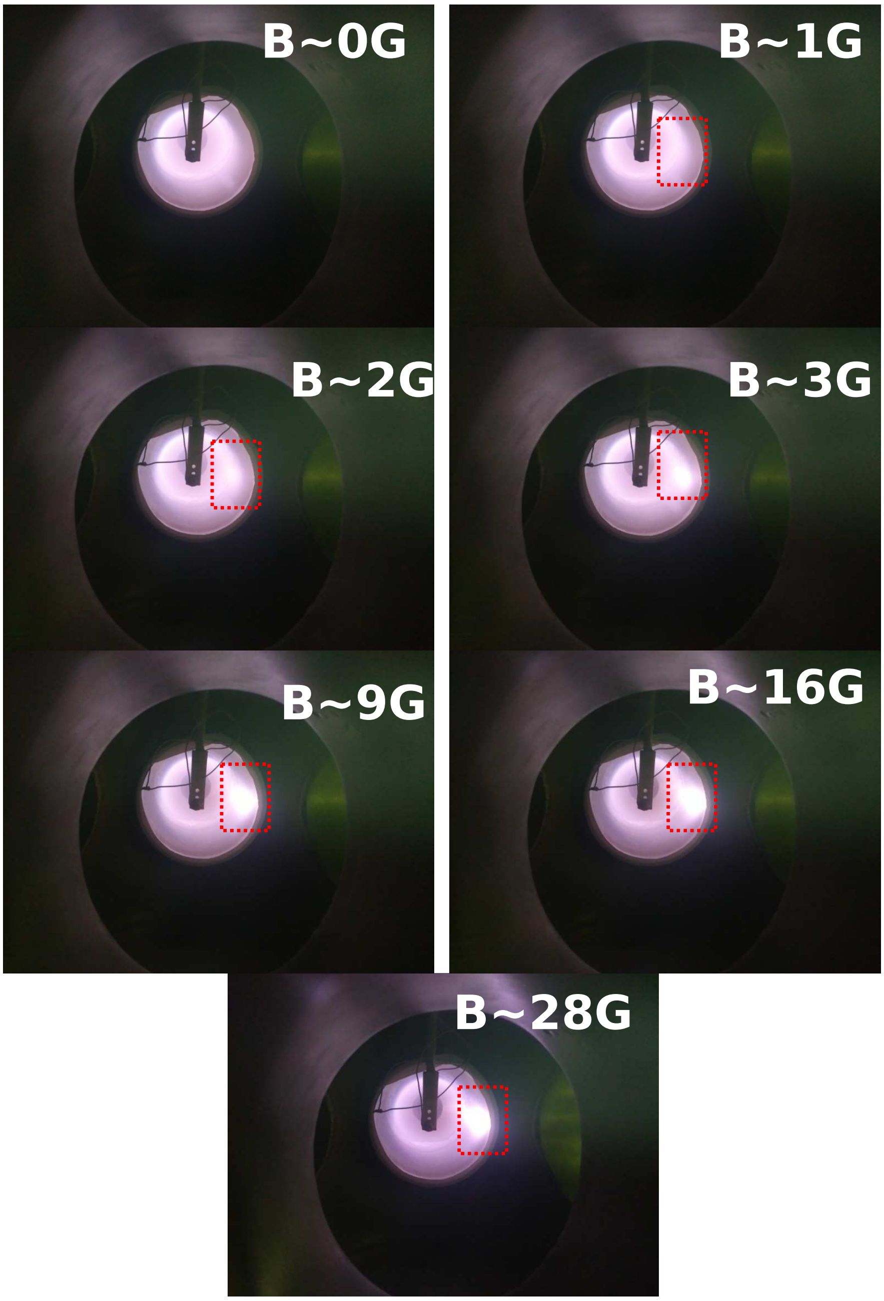

Figure 4.2: Localized glow region, the complex space charge configuration, near cathode surface with application of magnetic field.

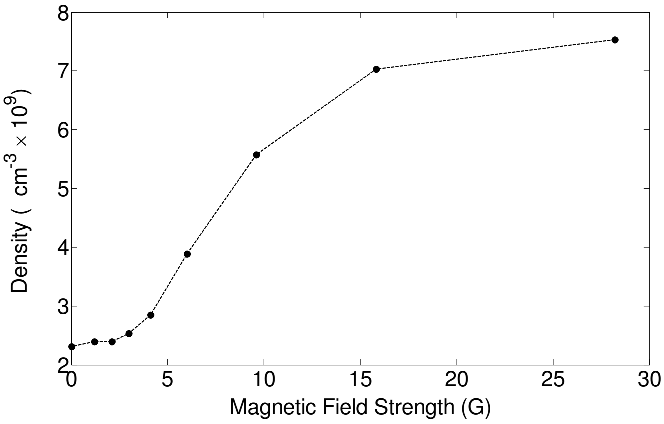

Figure 4.3: Variation of plasma density near localized glow region with the magnetic field strength.

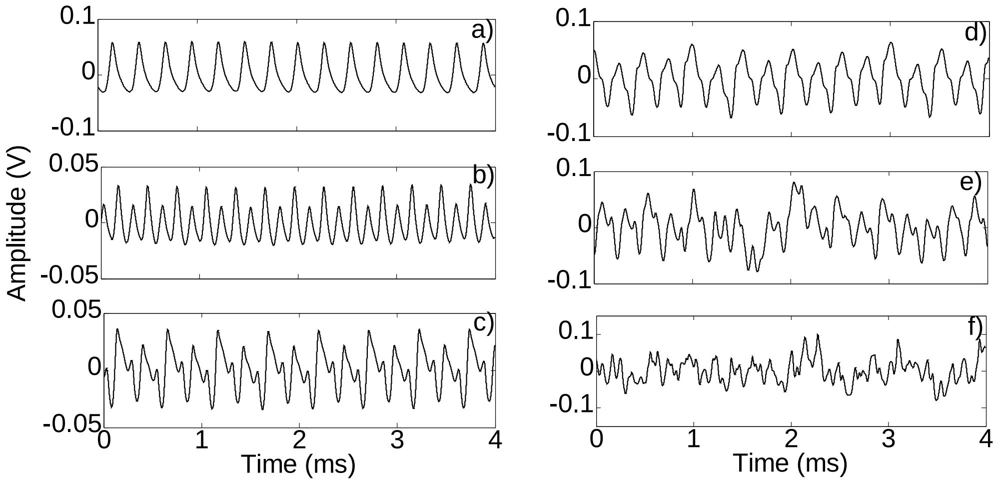

Figure 4.4: Time series plots of floating potential fluctuations, showing period doubling bifurcation, at different values of magnetic field strength: a) 0.520 G, b) 0.665 G, c) 1.292 G, d) 2.122 G, e) 2.992 G, and f) 9.610 G. During the experiment, discharge voltage and pressure are kept fixed at $\sim 597\ V$ and ~ 0.130 $mbar$ respectively.

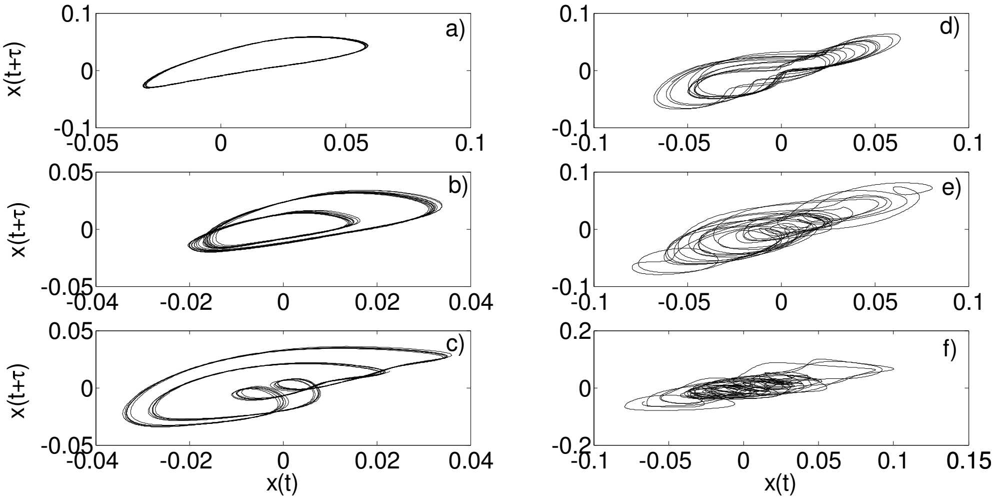

Figure 4.5: Reconstructed phase space plots corresponding to the time series shown in the figure 4.4. In these plots, the time delay $\tau = 0.02\ ms$ has been used. a) 0.520 G, b) 0.665 G, c) 1.292 G, d) 2.122 G, e) 2.992 G, and f) 9.610 G.

mbar, as mentioned in the figure caption. It is clearly seen from the figure that the system gradually changes from periodic to chaotic state with the increase in the magnetic field strength. The time series of the floating potential fluctuations suggests that appearance of glow region changes the dynamics of the system. This additional ionized region (glow region) may have different plasma characteristics as compared to the bulk plasma region. The nonlinear interaction between the oscillations in the two regions is probably responsible for the observations of such nonlinear dynamics. Before appearance of the localized glow structure ($< 2\ G$), dynamics were in the periodic state whereas after the appearance of the structure, dynamics becomes chaotic.

Figure 4.5 shows the reconstructed phase space projection corresponding to the time series shown in the figure 4.4. At 0.587 G, one loop in the phase space plot is noticed [figure 4.5(a)] whereas with the increase in the magnetic field strength two and four loops are seen in figures 4.5(b) and 4.5(c) respectively. Further increase

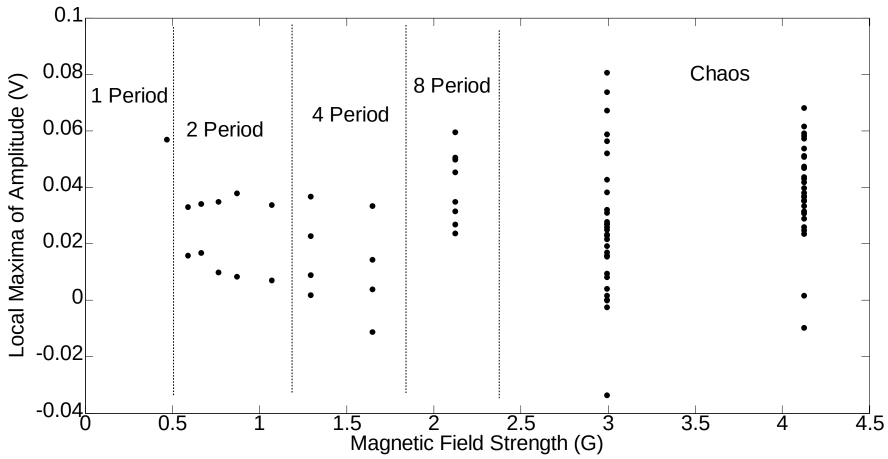

Figure 4.6: Bifurcation diagram: Plot of the local maxima of the time series as function of magnetic field strength.

in the magnetic field strength leads to several loops in phase space plot as depicted in figures 4.5(d)-4.5(f) indicating the chaotic nature.

The amplitude bifurcation diagram, i.e., plot of the local maxima of the fluctuations as a function of the applied magnetic field is shown in figure 4.6 where one can see a single period followed by two periods. This diagram shows a well known period doubling bifurcation feature and offers a good insight into the mechanism of system dynamics going from order to chaos. It would be ideal to verify the period doubling phenomena with small variation in the control parameter. However, small variations in the applied magnetic field are quite complicated to manage in the experimental situation. As a result of which identifying the exact point of bifurcation is very difficult. Hence, verification of the Feigenbaum constant for period doubling bifurcation is not possible.

Fast Fourier transform (FFT) corresponding to the time series data [figure 4.4] is shown in figure 4.7. It is noticed that for the periodic oscillations, distinct peaks are observed whereas in the case of chaotic oscillations, broadband in the power spectrum are observed. The dominant frequencies are lying in the range of $2-15$

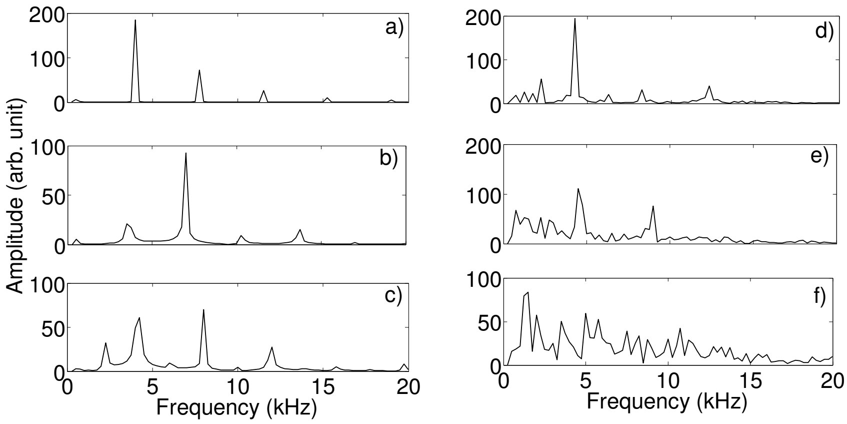

Figure 4.7: Power spectrum plots corresponding to the time series shown in the figure 4.4. a) 0.520 G, b) 0.665 G, c) 1.292 G, d) 2.122 G, e) 2.992 G, and f) 9.610 G.

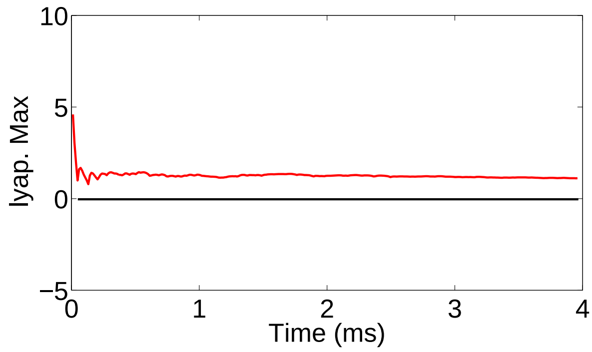

Figure 4.8: Typical Lyapunov exponent spectrum obtained for a chaotic signal corresponding to B = 2.992 G.

kHz.

The largest Lyapunov exponent (LLE), shown in figure 4.9, is estimated for the experimental time series signals of the floating potential fluctuations using the Wolf et al.[9] method. Typical Lyapunov spectrum with convergence of the maximal Lyapunov exponent as a function of the sampling time for a chaotic signal (B=2.992 G) is shown in figure 4.8. It is seen from figure 4.9 that the LLE is oscillating around a value ~ 0 in case of periodic oscillations whereas a sudden jump is observed in the LLE as the oscillations change its nature from periodic

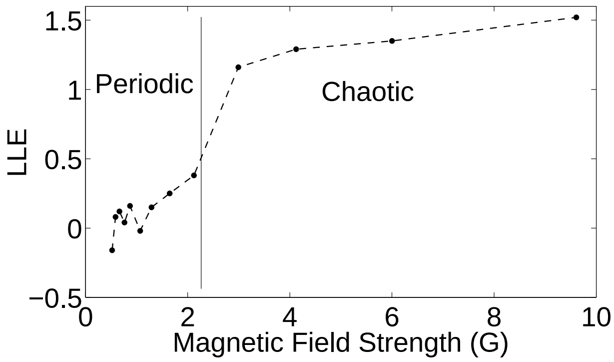

Figure 4.9: Plot of largest Lyapunov exponent (LLE) as a function of magnetic field strength. The error bar in the LLE is 2-4% from several estimates.

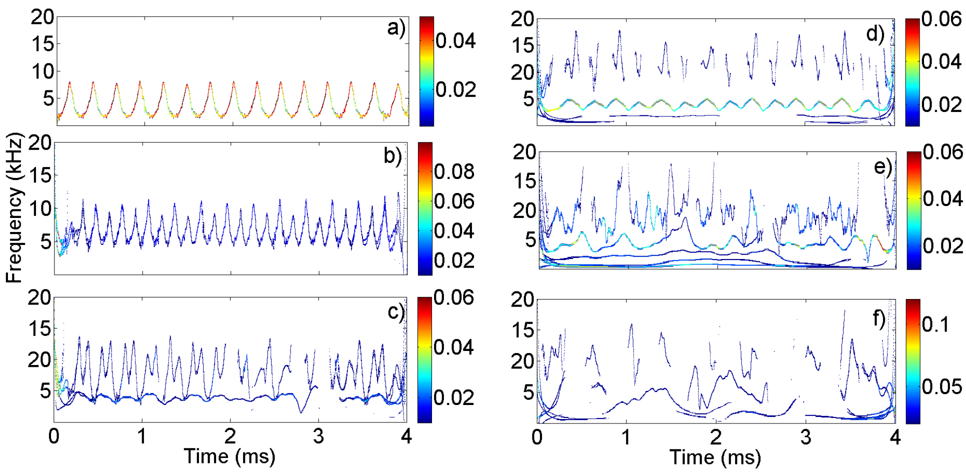

Figure 4.10: Time-frequency-energy representation corresponding to the floating potential fluctuations shown in the figure 4.4.

to chaotic. The jump in the LLE indicates the transition point from periodic to chaotic.

Figure 4.10 shows the time-frequency-energy plot of the floating potential fluctuations shown in the figure 4.4. The frequency band centred around $\sim 5\ kHz$ for the one period oscillation is seen in the figure 4.10(a) with an intrawave frequency modulation of a magnitude range $\sim$ 2-8 kHz. A similar frequency modulation is seen in figure 4.10(b) with the centre band frequency around $\sim 7.5\ kHz$. In the figure 4.10(c), $\sim$ 4 kHz frequency is appearing at all times whereas the higher frequency shows a discontinuity and frequency modulation indicating the transition from periodic to chaotic states [118]. The discontinuity in the lower and higher frequency contours were seen along with a frequency modulation with centre band frequency around $\sim 4.5\ kHz$ in figure 4.10(d). As system changes from order to chaos, the discontinuity starts to appear in the contours. Finally a clear discontinuity in the contour plots, for the chaotic signals, is observed in figures 4.10(e)-4.10(f). Frequency bifurcation is also seen in the plots as the dynamics changes from single period to chaos. A single frequency band, two frequency bands, four frequency bands and so on are observed in the figures 4.10(a)-4.10(b), 4.10(c), 4.10(d) and 4.10(e)-4.10(f) respectively.

4.4 Model for the Ion Oscillations Trapped Within a Potential Well

In the presence of the curved magnetic field lines, the electrons, while gyrating around the field lines, also undergo back and forth oscillations, being reflected from the cathode surface. This results in increased collisions with the neutrals as well as ionization events that manifest as an unstable localized spot (as seen in the figure 4.2) in the proximity of the cathode surface. In this scenario, the usual monotonic potential structure near the cathode surface is modified to a potential structure with a minima [112] resembling a virtual cathode and can be represented analytically as $\phi(y) = \phi_0(1 - \exp(-\alpha(y-a))^2$ where a is the position of minima of the potential structure and α is a constant. The typical potential profile is shown in the figure 4.11 which can facilitate the trapping of ions in the potential well. As

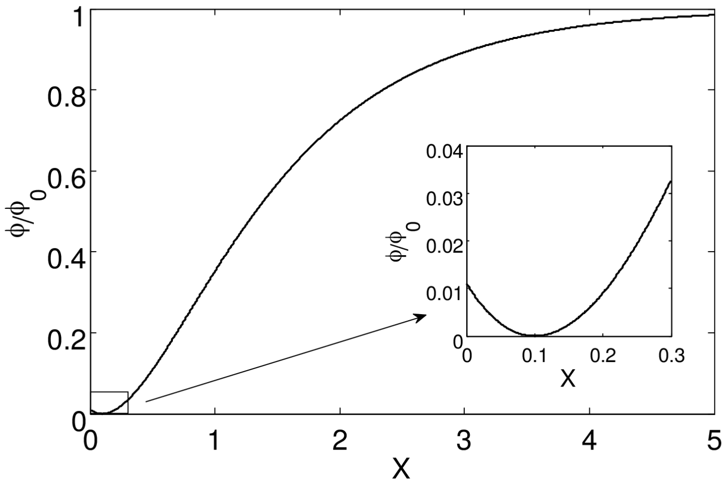

Figure 4.11: A typical normalized potential structure with minima.

ions are trapped in this potential, they oscillate in the potential structure. Thus, it is quite likely that the floating potential fluctuations measured in the bulk plasma reflect these oscillations.

Assuming the variation of the potential in one dimension only, the dynamics of ions can be described by the following equation of motion

$$\frac{d^2y}{dt^2} = \frac{e}{m}E(y) - \nu\frac{dy}{dt} + fcos(\omega t) \tag{4.1}$$

where m, e, ν, f and ω are the mass of the ion, the charge of the ion, damping coefficient, force per unit mass and forcing frequency respectively. The first term in the right hand side is the electrostatic force on the ions whereas the second term represents the dissipative term which indicates the presence of collisional effects in the plasma. The last term in Eq. (4.1) represents a forcing term which arises due to unstable cathode spot resulting from trapping of ions, increase of local ionization as well as back and forth movement of electrons. With the increase in the magnetic field, intensity of the cathode spot is seen to increase, thus forcing strength can be considered to be a control parameter. Using $E = -d\phi/dy$, the above equation becomes:

$$\frac{d^2y}{dt^2} + \frac{2e\phi_0\alpha}{m}\exp(-\alpha(y-a))(1-\exp(-\alpha(y-a)) + \nu\frac{dy}{dt} \quad = \quad fcos(\omega t) \tag{4.2}$$

The following normalization of variables is carried out by considering $X = y/y_0$ and $\tau = \omega_p t$, where y_0 is a characteristic length scale and ω_p is ion plasma frequency. Thus, Eq. (4.2) can be written as

$$\ddot{X} + A\dot{X} + B\exp(-(X-d))(1-\exp(-(X-d)) \quad = \quad Fcos(\tilde{\omega}\tau)$$

where $A = \frac{\nu}{\omega_p}$, $B = \frac{2e\phi_0\alpha}{my_0\omega_p^2}$, $d = \frac{a}{y_0}$ and $F = \frac{f}{y_0\omega_p^2}$ are the dimensionless parameters. α is chosen to be $\frac{1}{y_0}$. As the above model is derived from the basic phenomenology, it does not exactly represent the experimental system at a microscopic level but this model is sufficient to explore the dynamical origin of observed experimental oscillations.

Eq. (4.3) is solved numerically using fourth order Runge-Kutta method with the initial conditions of $X = 0.1$ and $\dot{X} = 0.15$ at $\tau = 0$. The parameters A, B, d, and $\tilde{\omega}$ are assumed to have the following values, i.e., 0.2, 0.1, 0.1, and 0.8, respectively.

Figure 4.12 shows the simulated time series of X at different values of forcing strength (F) as mentioned in the caption of the figure. Figure 4.12(a) shows the limit cycle. It is observed that the number of periods increases with the increase in the forcing strength and finally system becomes chaotic at forcing strength $\sim$ 0.34.

Figure 4.13 shows the phase space plots for increasing control parameter F values. It clearly suggests that the dynamics of the system undergoes period doubling bifurcation with the increase of forcing strength (F).

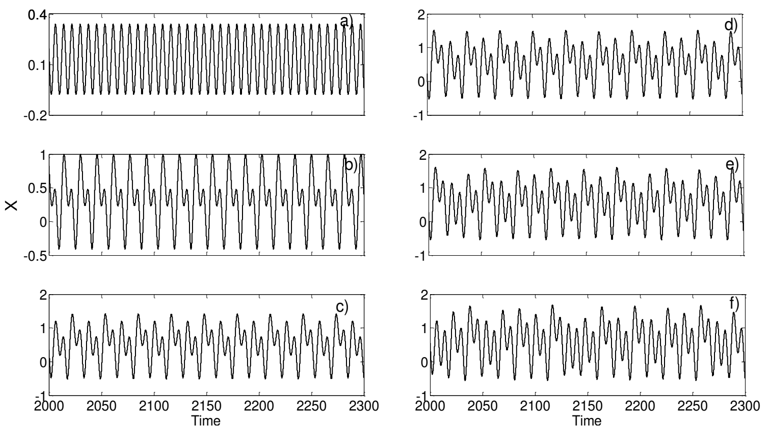

Figure 4.12: Numerically simulated time series data exhibiting period doubling bifurcation for control parameter F value: a) 0.1, b) 0.2, c) 0.3, d) 0.325, e) 0.350, and f) 0.375.

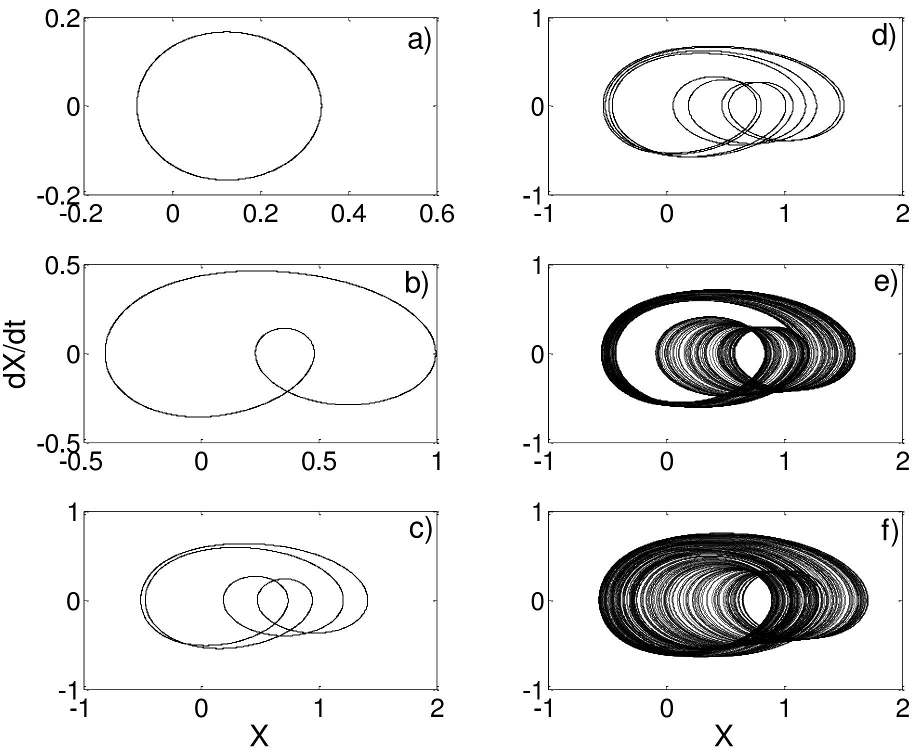

Figure 4.13: Phase space plots for control parameter F value: a) 0.1, b) 0.2, c) 0.3, d) 0.325, e) 0.350, and f) 0.375.

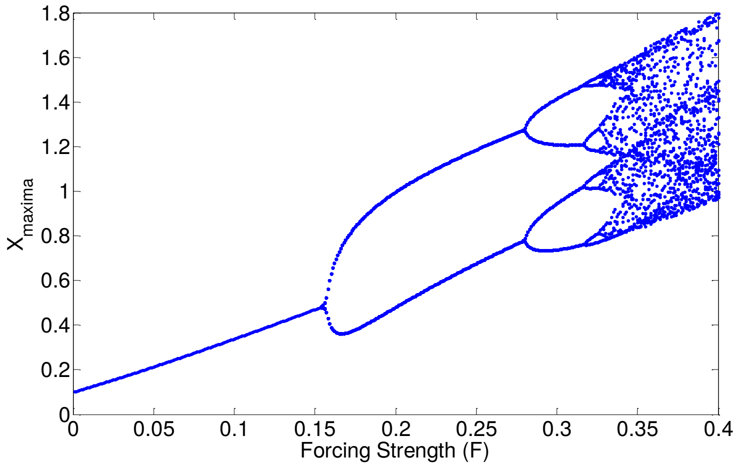

Figure 4.14: Bifurcation diagram: The maxima of X as a function of control parameter F.

The bifurcation diagram is shown in figure 4.14. It shows X_{maxima} in the range of control parameters $F \in (0, 4)$. This figure suggests that there is chaotic motion, which appears due to period doubling bifurcation.

4.5 Summary and Conclusions

Cathode glow, in the form of localized glow region, has been seen near the cathode surface in the presence of a bar magnet placed outside the cathode surface of a glow discharge plasma device. This localized region is due to the enhancement of the degree of ionization by electron confinement in dipole magnetic field and the negative potential cathode surface. Intensity of glow region increases with the strength of the magnetic field. An increase in the density in the glow region with the increase in the magnetic field is also observed. Periodic to chaotic oscillations via period doubling route has been observed in the presence of inhomogeneous magnetic field. Keeping the discharge voltage and neutral pressure constant, the dipole magnetic field strength was increased which led to change in the character of the oscillations from periodic to chaotic. System transits from periodic state to chaotic state accompanied by the appearance of a localized glow. Since this localized glow region may have different characteristics compared to the bulk plasma, the nonlinear interaction between the oscillations in the two regions is probably responsible for the observations of the period doubling route to chaos. Formation of potential structures with a minima are found [112] in plasmas in presence of a bar magnet. This has motivated development of a numerical model to study the ion dynamics under the influence of a potential well to understand the observed experimental results. The results obtained from the numerical simulation qualitatively (able to produce similar phenomena) agreeing with that of experiments. Thus it is quite likely that obtained fluctuations are due to the ion fluctuations trapped inside the localized glow region.

Since dipole magnetic fields are encountered in space plasma as well as in plasma devices used in applications such as magnetron sputtering device, more experimental and theoretical studies in dipole magnetic field need to be carried out in order to understand and explore the underlying physics related to the nonlinear behaviour of plasma in presence of a dipole magnetic field.

Chapter 5

Multifractal Nature of Floating Potential Fluctuations Obtained From a Glow Discharge Magnetized Plasma

In this chapter, an experimental study on the effect of an axial magnetic field on the plasma dynamics has been carried out. Phenomena like canard and MMOs, observed as a effect of the dipolar magnetic field on the plasma dynamics, require very fine tuning of the control parameter which is difficult to accommodate in the present configuration since variation of axial magnetic field in small increments is not possible. Application of axial magnetic field can give rise to various phenomena like order to chaos and vice versa depending on the parametric conditions like discharge voltage and pressure. Here our primary motivation was to investigate the multifractal behaviour exhibited by the plasma fluctuations that are found in chaotic regime.

5.1 Introduction

As of now, we have realized that the plasma fluctuations manifested in a dc glow discharge plasma and also in other plasma devices are mostly complex and multiscale in nature [119, 120]. The complexity and multiscale nature varies little from one condition of measurement to another. When a magnetic field is applied, the system dynamics, i.e. the fluctuations, becomes more complex due to generation of various magnetized plasma modes like cyclotron modes, $E \times B$ drift in addition to the unmagnetized plasma modes. These fluctuations also exhibit chaotic behavior and recognized to acquire self-similarity and also manifest strong fluctuations on all possible scales [13, 121, 122]. Since the fractality appears as a universal property of the complex systems, so, it is worthwhile to investigate the multifractal dynamics of the plasma which is also a complex system. The concept of multifractality is of great importance for space plasmas [123] because it allows us to look at intermittent turbulence in the solar wind [124]. It is also very important in the study of tokamak plasma turbulence [125]. Many attempts have been made to recover the observed scaling exponents, using multifractal phenomenological models of turbulence describing distribution of the energy flux between cascading eddies at various scales [126]. Multifractal dynamics for plasma edge electrostatic turbulence has been investigated using wavelet transform modulus maxima (WTMM) [127]. Here, multifractal detrended fluctuation analysis [128] (MF-DFA) technique is deployed to investigate the multifractal dynamics of floating potential fluctuations obtained from the glow discharge plasma device. MF-DFA method is based on the generalization of the detrended fluctuation analysis [129, 130, 131] (DFA), and is able to determine the multifractal scaling behaviour of a signal. MF-DFA is a fairly robust and powerful technique for the detection of the multifractality, has been applied successfully in diverse fields such as sunspot time series [54], traffic time series [132], stock market data [133], EEG signals [134], heart rate data [135], geophysical data [136], earthquake data [137] and many others [138, 139]. MF-DFA technique is also employed in the field of plasma to detect the multifractality in intermittent fluctuations of discharge plasma [140], tokamak edge plasma fluctuations [141], etc.

5.2 Multifractal Behaviour of Plasma Dynamics

Present experiment is carried out at constant pressure ~ 0.18 $mbar$ and DV ~ 316 V. An axial magnetic field is applied by passing a constant current through copper coil winding over the cylindrical chamber containing the cathode chamber. This arrangement is shown in the schematic diagram of the setup in the figure 2.1 in the chapter 2. Magnetic field strength (B) is considered as a control parameter. The system shows a sensitive dependence on magnetic field and its dynamics changes with the increase in the magnetic field.

Floating potential fluctuations with increasing applied magnetic field strength are shown in the figure 5.1. At the discharge voltage chosen for this experiment, before the application of magnetic field, a chaotic oscillation is observed [figure 5.1(a)]. Figure 5.1(b) shows that the frequencies of the oscillation remains almost same at $B \sim 15$ G as observed in the case of unmagnetized plasma. The oscillation becomes rapidly time varying compared to the unmagnetized case, with an increase in the magnetic field strength from ~ 45 G and onward as depicted in the figures 5.1(c)-5.1(f). It is also noted that amplitude of the oscillation increased by a factor

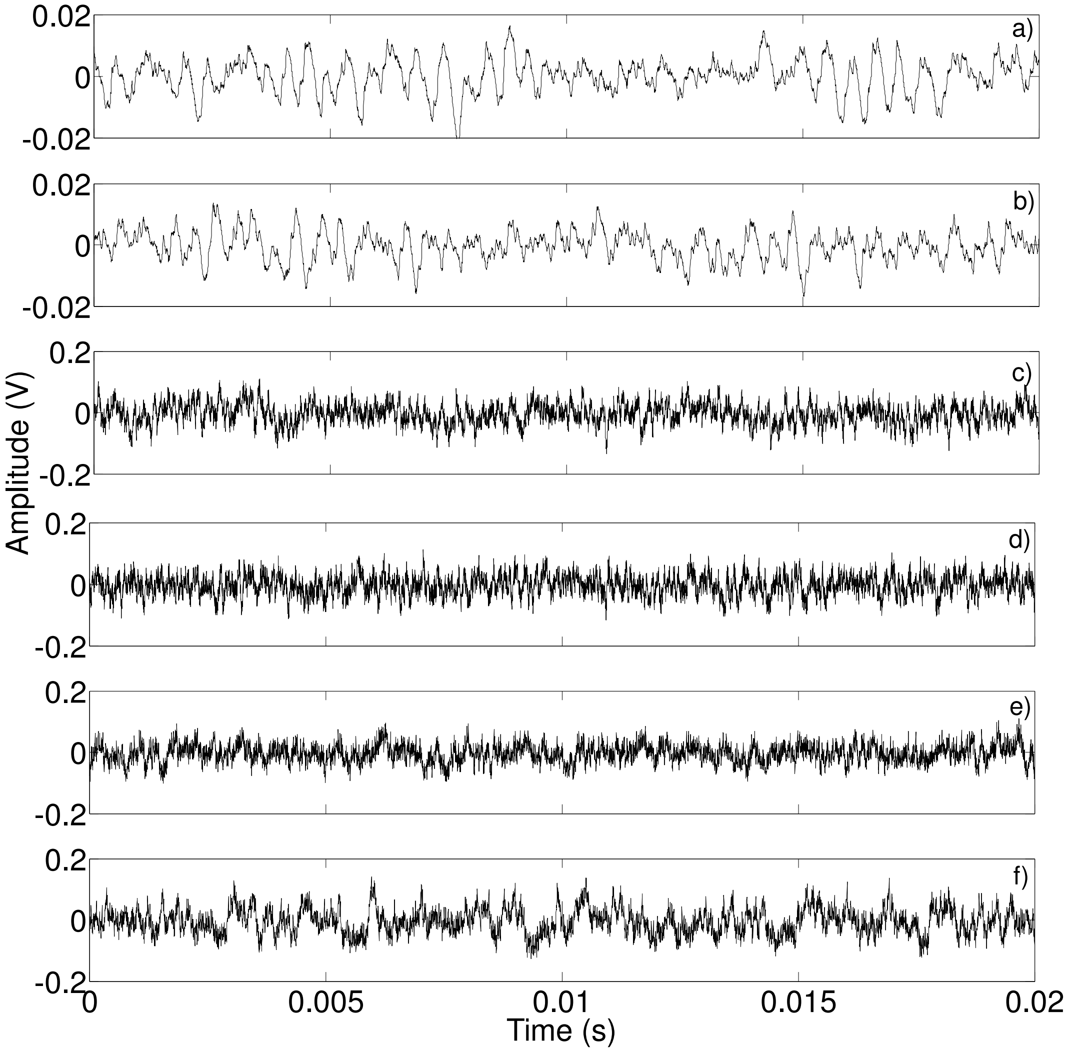

Figure 5.1: Time series of the floating potential fluctuations at DV $\sim 316\ V$ and pressure $\sim 0.18\ mbar$: a) 0 G, b) 15 G, c) 45 G, d) 75 G, e) 105 G, and f) 135 G.

~ 10 with the application of the magnetic field. Application of axial magnetic field reduces the losses of the charged particles which may be the probable reason for the amplitude enhancement. Since the Larmor radius of ions is greater than the system dimension at $B \sim 15\ G$ the ions remain unmagnetized under these conditions. Hence, the effect of magnetic field is not seen on the floating potential fluctuations at $B = 15\ G$.

The largest Lyapunov exponent(LLE), shown in figure 5.2, is calculated from

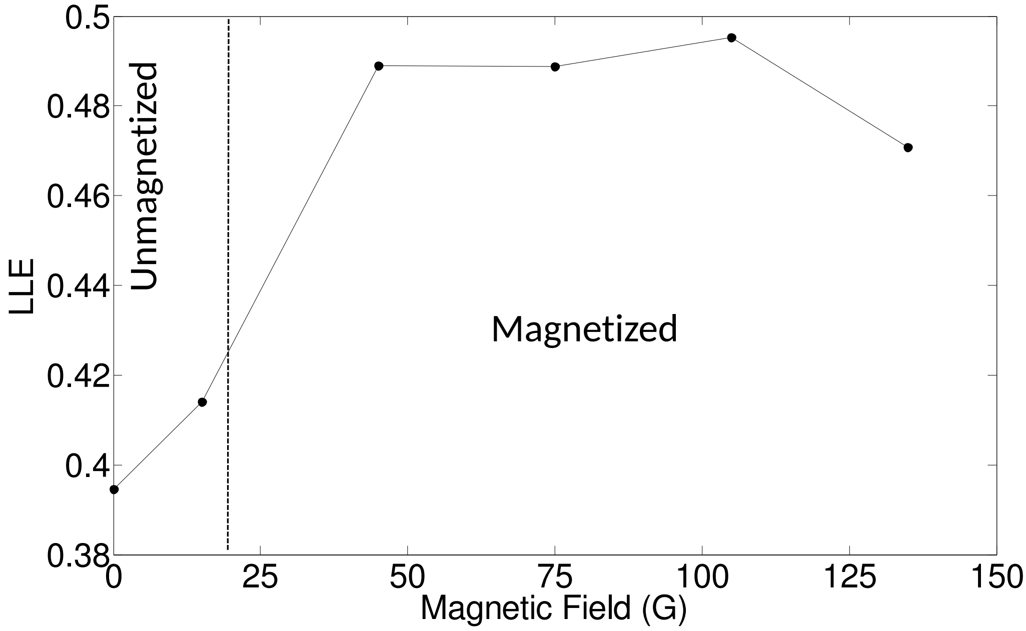

Figure 5.2: Variation of largest Lyapunov exponent (LLE) as a function of axial magnetic field strength. The error bar in the LLE is 2-4% from several estimates.

the experimental time series signal of the floating potential fluctuations by Rosenstein's technique [11] with the help of TISEAN software package [51] in order to characterize the chaotic behavior quantitatively. A detailed methodology to calculate the Lypunove exponet using the Rosenstein's technique is discussed in the section 2.3.3 of the chapter 2. The observation of positive LLE for the fluctuations suggests their chaotic nature. It is seen from figure 5.2 that the LLE shows a sudden jump from unmagnetized case to magnetized one and remains approximately constant for magnetised case. This observation indicates that maximum chaoticity in the system is observed for magnetised case.

The time series plots show that fluctuations have many time scales. These different time scales are introduced manly due to the simultaneous existence of many plasma modes. In these cases, the dynamics can be characterised by scaling laws which are valid over a wide range of time scales. Such dynamics are usually denoted as fractal or multifractal. This motivates us to carry out the multifractal analysis for above fluctuations using MF-DFA technique which has been discussed in detail in the section 2.3.4 of chapter 2.

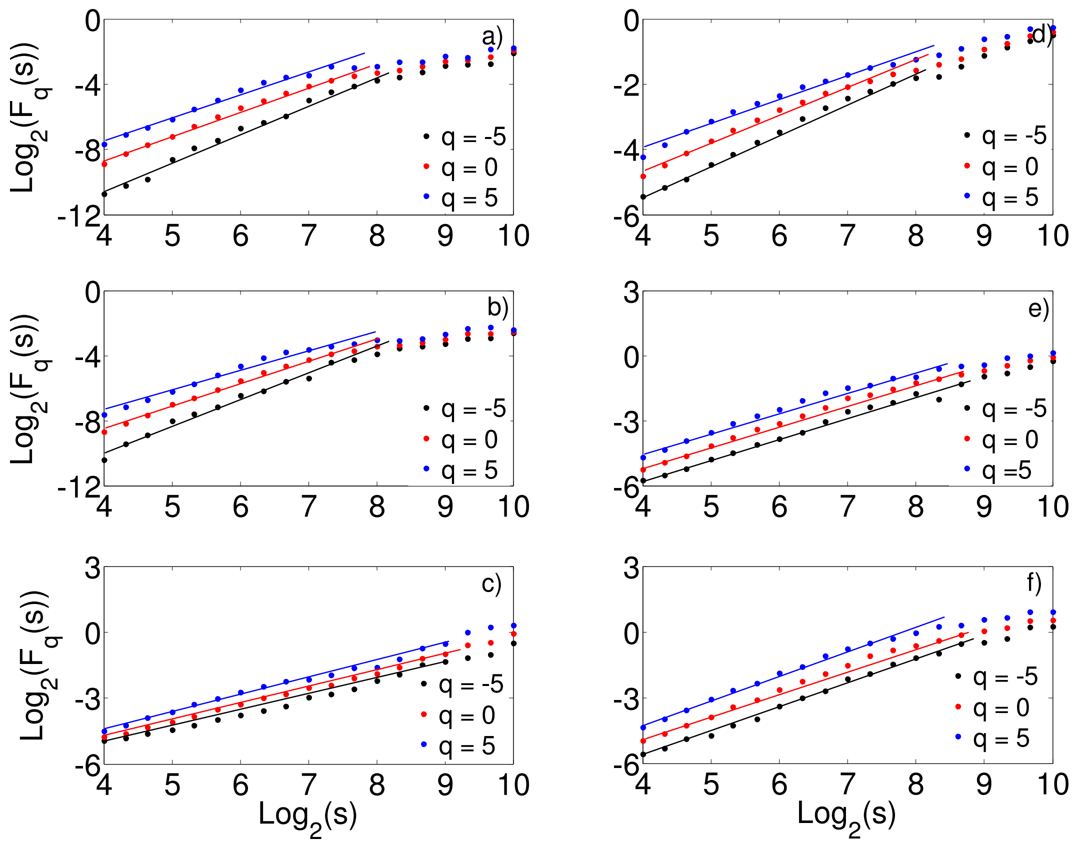

Figure 5.3: The MF-DFA fluctuation functions $F_q(s)$ versus the scale s in log-log plots for the time series shown in the figure 5.1: a) 0 G, b) 15 G, c) 45 G, d) 75 G, e) 105 G, and f) 135 G.

We calculated the fluctuation functions $F_q(s)$ using MF-DFA technique for $q \in$ [-5, 5] with a step of 1. Figure 5.3 shows the log-log plot of $F_q(s)$ versus s, for $q =$ -5, 0, +5 for the time series shown in the figure 5.1. The different slopes of the fluctuation curves indicate that small and large fluctuations scale differently.

The generalized Hurst exponent $h(q)$, estimated for $q =$ -5 to 5 using Eq. (2.14)

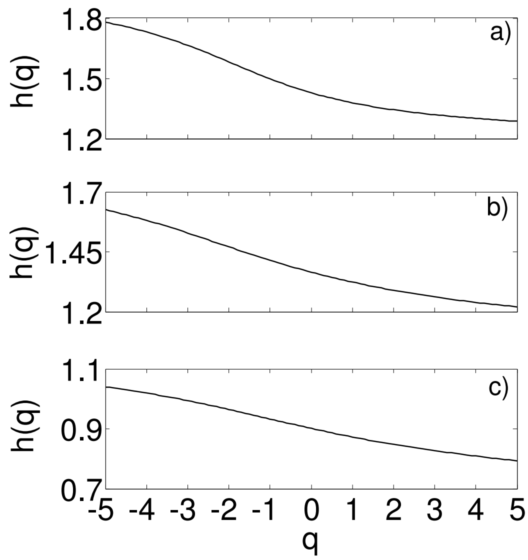

Figure 5.4: The q dependence of the generalized Hurst exponent $h(q)$ for the time series shown in the figure 5.1: a) 0 G, b) 15 G, c) 45 G, d) 75 G, e) 105 G, and f) 135 G.

of the chapter 2, is shown in figure 5.4. One can note that at all the fluctuations, the slopes $h(q)$ decrease nonlinearly as the moment q is increased from negative to positive values. Different values of $h(q)$ for different orders of q suggest that fluctuations exhibit multifractality. For the unmagnetized case, $h(q)$ lies in the range of 1.6 to 1.2 which indicates the slow variation of fluctuation. In the presence of magnetic field, i.e., for the magnetized case, range of $h(q)$ (1-0.7) reduced. These results are evidence of existence of long range correlation and also suggesting the multifractal nature of the fluctuations.

Rènyi exponent (τ(q)) is calculated using the Eq. (2.16) which provides another way to detect the multifractality behavior of the time series. The curve of the function τ(q) with respect to the variable q is shown in figure 5.5. The nonlinear shape of this curve reveals a multifractal behavior of the time-series data. The function $\tau(q)$ would be a linear function of q with constant slope for a monofractal time series.

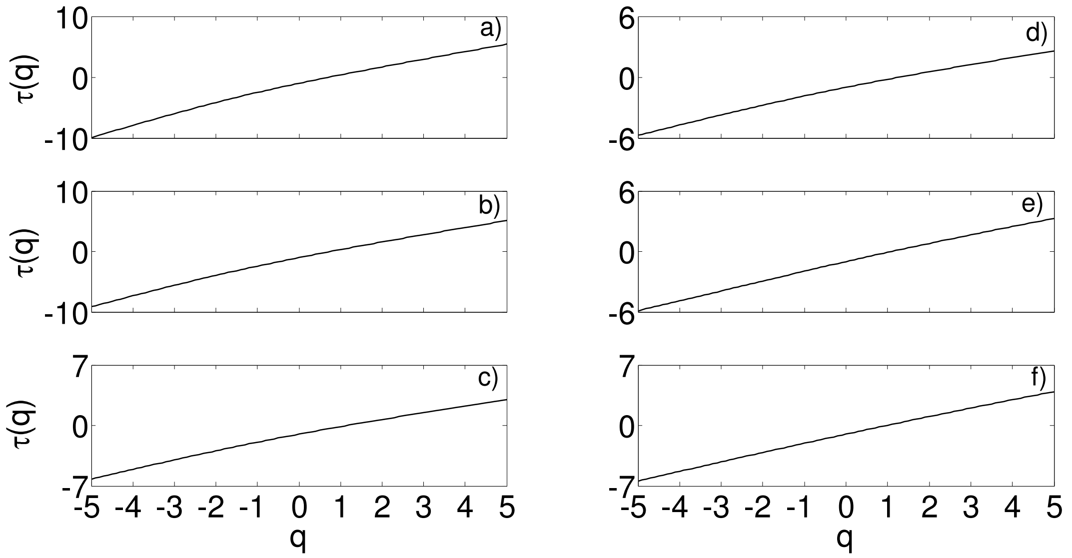

Figure 5.5: The q dependence of the Rényi exponent τ(q) corresponding to the time series shown in the figure 5.1: a) 0 G, b) 15 G, c) 45 G, d) 75 G, e) 105 G, and f) 135 G.

Multifractal nature of a time series is generally due to two reasons: 1) multifractality due to a broad probability distribution for the time series. In this case the multifractality cannot be removed by shuffling the series. 2) multifractality due to the presence of long range correlation of small and large fluctuation. The easiest way to clarify the type of multifractality is by analyzing the corresponding shuffled and surrogate time series. If the long range correlation contributes to multifractality, shuffled time series will exhibit a monofractal behavior as long range correlation are destroyed by shuffling. On the other hand, surrogate time series will have the same long range correlation but the probability function changes to the Gaussian distribution. If multifractality in the time series is due to a broad PDF, generalised Hurst exponent obtained by the surrogate method will be independent of q. If both types of multifractality are present, the shuffled and surrogate series will show weaker multifractality than the original one. In the shuffling procedure the values are put into random order [128], and thus all correlations are destroyed

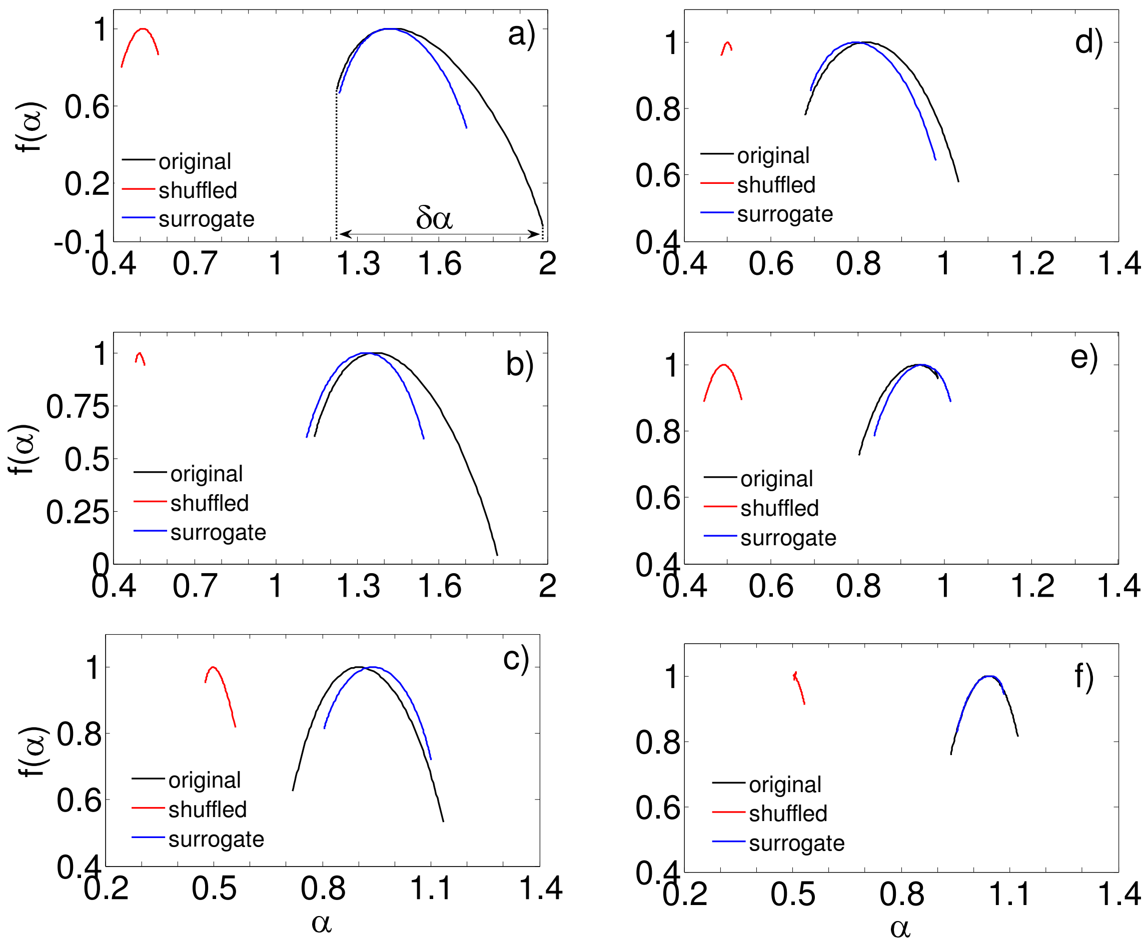

Figure 5.6: The singularity spectra $f(\alpha)$ for the time series shown in the figure 5.1 and corresponding shuffled and surrogate time series: a) 0 G, b) 15 G, c) 45 G, d) 75 G, e) 105 G, and f) 135 G.

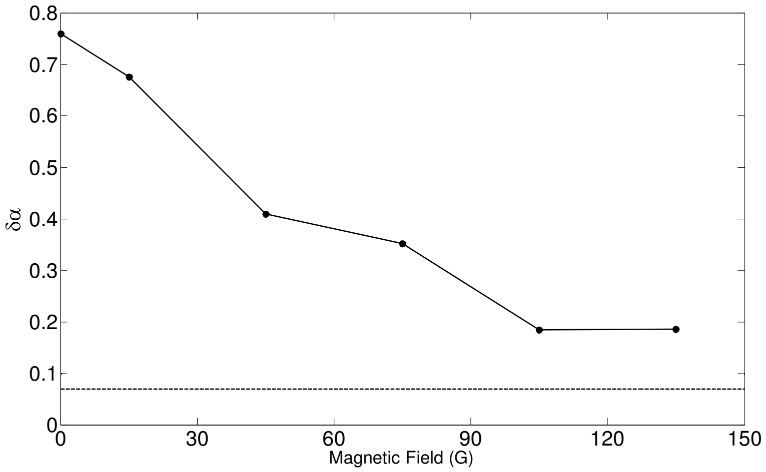

Figure 5.7: Dependency of multifractal spectrum width ($\delta\alpha$) on the magnetic field strength at constant DV $\sim$ 316 V and pressure $\sim$ 0.18 $mbar$. The broken line represents the values corresponding to the Brownian noise: a) 0 G, b) 15 G, c) 45 G, d) 75 G, e) 105 G, and f) 135 G.

but distribution remains intact. Surrogate data is obtained by the Fourier phase randomization of the original data [142].

The multifractal spectrums for the original time series [figure 5.1] and corresponding shuffled and surrogate time series are shown in figure 5.6. The multifractal spectrum width of the original time series significantly narrows after the series is shuffled, however, multifractal spectrum width of all the surrogate series is less narrow compared to shuffled one. This finding suggests that the multifractal characteristic of time series significantly reduces after shuffling. Therefore, the multifractal characteristics of the time series can be attributed to the significant existence of the long range correlation than the broadness of the probability density function.

We have estimated the Multifractal spectrum width ($\delta\alpha$), difference between the maximum and minimum singularity ($\alpha_{max} - \alpha_{min}$), from the multifractal spectrum. α_{max} and α_{min} are the highest value and the lowest value of α observed in multifractal spectrum respectively. The experimental signal spectrum width is wider than the monofractal Brownian noise, plotted as a broken line, statistically confirming their multifractal nature. The wider $\delta\alpha$ is corresponding to the richer and stronger multifractality of data. In order to compute the defined parameters for Brownian noise, we averaged the results obtained from 10 computed Brownian noise like time series having the same length as our experimental time series. Figure 5.7 shows the spectrum width for the original time series as a function of magnetic field strength. It is observed that the width of the spectrum shows a decreasing trend with the magnetic field strength indicating reduction in degree of multifractality. It also suggests that the system is going from multifractal dynamics to monofractal; since the Brownian noise is known to be monofractal. This result demonstrates that, in the presence high magnetic field, the dynamics evolves to correlated fluctuations that can be modeled as Brownian motion. In the time series plots, we have seen an appearance of high frequency oscillation for magnetized case whose interaction with existing low frequency oscillation probably destroyed the multifractal nature of the fluctuations. To verify this observation, we have carried out power spectrum analysis.

Figures 5.8(a)-5.8(f) show power spectrum plots corresponding to the floating potential fluctuations shown in the figures 5.1(a)-5.1(f) respectively. Broadband of frequencies within the range of 1 - 10 kHz is seen in the figure 5.8(a) and 5.8(b), i.e., for $B = 0$ G and $B = 15$ G. These frequency bands may be due to the domination of unmagnetized plasma modes, i.e., ion acoustic and ionization instabilities. A further increase in the magnetic field leads to a broadband nature in the $1-30$ kHz (increase by a factor of 3 compared to unmagnetized case) range of

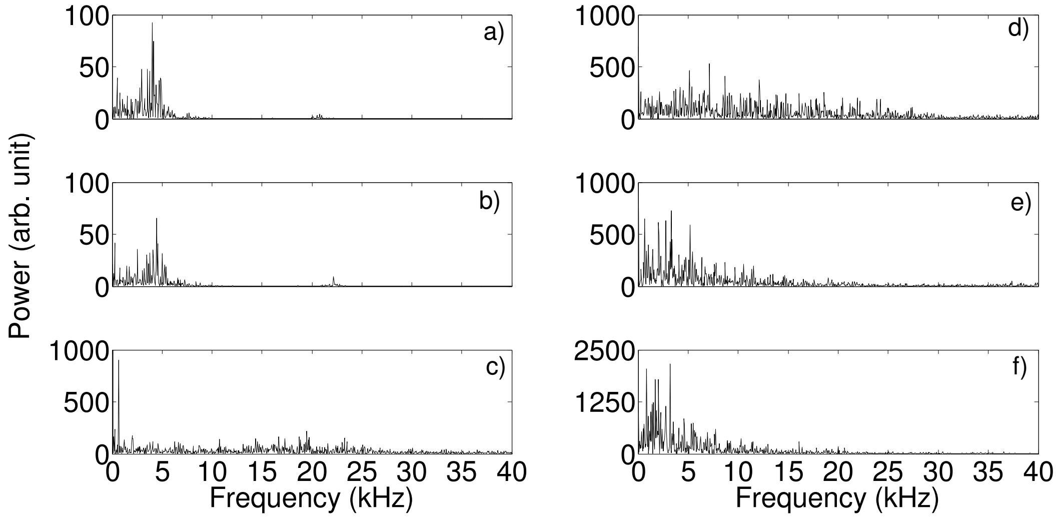

Figure 5.8: Power spectrum corresponding to the time series shown in the figure 5.1: a) 0 G, b) 15 G, c) 45 G, d) 75 G, e) 105 G, and f) 135 G.

the frequencies for values of magnetic field from 45 G and above. These observations clearly indicate the chaotic nature of the oscillations and also suggesting that higher frequencies appear due to the application of magnetic field. These observed frequency bands may be due to the domination of ion acoustic, ion cyclotron modes and interaction of magnetized (cyclotron modes, $E \times B$ effect, drift mode, etc.) and unmagnetized plasma modes. Hence, it is clear that system always show a broadband turbulence but the application of magnetic field further enhanced the broadband turbulence over a wide range of frequencies. Hence, with the enhancement in magnetic field strength, an evolution of the fluctuations towards Brownian type motion is taking place.

5.3 Summary and Conclusions

Phenomena like order to chaos and vice versa cap be obtained by applying axial magnetic field under satiable parametric conditions like discharge voltage and pressure [143]. However, mixed mode and canard oscillation, require small change in control parameters, are difficult to accommodate in present setup as only large increment in strength of axis magnetic field is possible. In this work, we are mainly interested in the multifractal behaviour of the chaotic fluctuations since this may have applications in toroidal fusion devices, and space plasma where the data is always chaotic and also observed to be multifractal in nature. An investigation on multifractal characteristics of floating potential fluctuations using multifractal detrended fluctuation analysis (MF-DFA) is carried out. The effect of axial magnetic field on the multifractal property and the amplitude of the fluctuation signal and the type of their correlation has been studied. It is seen that amplitude of the fluctuations increase in the presence of the magnetic field. The application of axial magnetic field can reduce the particle losses to the wall and hence the amplitude of the oscillation may increase. The presence of the magnetic field can lead to various characteristic frequencies into the system such as cyclotron frequencies, $\mathbf{E}\times\mathbf{B}$ drift and ∇B drift which can enrich the nature of the fluctuations. Observed frequencies lie in the range of ion acoustic frequency range, i.e., between 2.5 kHz to 10 kHz range, in the case of unmagnetized plasma, whereas for the case of magnetized plasma, broadband frequencies in range of 1 kHz to 30 kHz is seen. This broadband may be due to domination of ion acoustic, ion cyclotron modes and interaction of magnetized and unmagnetized plasma modes. The values of $h(q)$ are restricted between 1.6-1.1 and 1-0.7 for unmagnetized and magnetized case respectively. These results are evidence of the existence of long-range correlations in fluctuations. They also show the self similar nature of the floating potential fluctuations. Different values of generalised Hurst exponent for different q and nonlinear nature of Rènyi exponent curve strongly suggest the multifractal nature of the fluctuations. It is observed that multifractal spectrum width decreases and Degree of multifractality reduces with the increase in magnetic field strength.

We have produced the shuffled and surrogate time series from original data and deduced the singularity spectrum using the MF-DFA method. It is observed that the original time series has higher spectrum width compared with the shuffled and surrogate time series however the spectrum width of original and surrogate time series is comparable. This indicates that the shuffling and the surrogate techniques reduces all together the multifractality strength of the original time series and demonstrates that the long-range correlation makes a greater contribution to multifractality of the data than the broadness of the probability density function, i.e., fat-tail distribution. Results obtained in respect of these floating potential fluctuations in a glow discharge plasma in presence of a homogeneous magnetic field could also be important for the understanding of multifractal behaviour in the plasma dynamics of other magnetized plasma devices.

Chapter 6

Intrinsic Noise Induced Coherence Resonance in a Glow Discharge Plasma

In chapter 3, we investigated the effect of intrinsic noise on the plasma dynamics due to a magnetic field of a bar magnet. In this chapter, we will explore the effect of intrinsic noise without the magnetic field. Process behind the enhancement of intrinsic noise with DV is different with the process in the presence of a dipolar magnetic field discussed in chapter 3. Effect of intrinsic noise in the generation of coherence resonance phenomena is discussed and corroborated by numerical simulation. Coherence resonance is determined using normalized variance curve and also corroborated by Hurst exponent and power spectrum plots. FitzHugh-Nagumo like model derived in the chapter 3 is used to understand the excitable dynamics of glow discharge plasma in the presence of noise.

6.1 Introduction

Noise is omnipresent in all natural systems and plays a beneficial role in the dynamics of nonlinear systems yielding interesting results [144, 145]. There are many studies which have revealed that noise can play a constructive role like noise induced order in chaotic dynamics [146], synchronization of chaotic systems [147], stochastic [148, 149, 150, 151] and coherence resonances [152, 153, 154, 155, 156, 157, 158]. Noise can be divided into two categories: extrinsic and intrinsic. The extrinsic noise can originate from the environment [159] and an external noise generator in experimental systems, whereas intrinsic noise is generated due to an interplay between the components of the systems and could be of small amplitude. In the chapter 3, we have seen that application of dipolar magnetic field generates various plasma modes which nonlinear interact with other plasma modes resulting a broadband intrinsic noise. Of particular interest is the phenomenon of stochastic resonance [148, 151] (SR) in which the addition of random noise amplifies the pre existing subthreshold deterministic signal and has been observed in many systems such as physical [160], chemical [149, 161], electronics [162], biological [163]and numerical model like FitzHugh-Nagumo (FHN) [164]. Coherence resonance [155, 156, 157, 158] (CR), which is also called autonomous SR or internal signal SR, is an emergence of regularity in the dynamics under the influence of purely stochastic perturbations. In CR, the maximum regularity is achieved at an optimum noise amplitude which has been observed in many experimental systems: optical [165], electrochemical [156], chemical reactions [166], electronic monovibrator circuit [162] as well as in numerical simulation of the standard model like FitzHugh-Nagumo (FHN) model [157, 155] and a thermochemical system model [167]. The most important characteristic of CR is that the time scale of induced oscillations is determined by the intrinsic dynamics of the system.

In the chapter 1, we have studied that free energy sources like energetic electrons, density gradient, etc. in plasma dissipated by giving rise to several instabilities [30, 34, 35, 168, 169] that in turn interact to produce a background plasma noise of broadband nature ranging from low frequency ion acoustic modes to high frequency electron plasma oscillations. The common sources of intrinsic noise in experimental systems also include the plasma fluctuations [170], photons and fast neutrals in the system [171]. Though they are small, they are widely used in estimating the plasma temperature and other parameters. The aim of this chapter is to explore the effects of this kind of noise in generating coherent spikes when plasma is treated to be an excitable medium. There are several research works on the external noise induced dynamics in the plasma system [38] as well as reports on the observation of CR in glow discharge plasma under the influence of external noise perturbation [38] but we have observed the same phenomena without any application of external noise.

6.2 Coherence Resonance

In the present experiments, we started the system at a DV $\sim 478\ V$ and pressure $\sim 0.37\ mbar$ where it exhibited fixed point behavior, and then the DV was increased monotonically and floating potential fluctuations were recorded. Magnetic fields were absent during the experiment.

Figures 6.1(a)-6.1(l) show the time series of the floating potential fluctuation at different values of DV as mentioned in the caption of the figure. The dynamics of the time series show that the system behaves as an excitable one, presenting characteristic spiking for values of DV when it exceeds a threshold. It is also seen from the figures 6.1(a)-6.1(l) that the number of the spikes continuously increases with the increase in DV. Irregular bursts and higher amplitude spikes begin to appear in the fluctuation when DV exceeds 490 V. The approximate values of the rise and the fall time of the spikes are 0.12 $msec$ and 0.22 $msec$ respectively. These time scales are comparable with the ion transit time scale ($\tau = d/\sqrt{(\frac{k_B T_i}{m})}$ ~ 0.1 $msec$, where d, k_B, m and T_i are the electrode distance, Boltzmann constant, ion mass and ion temperature respectively.) between two electrodes. So probably these spikes correspond to bunches of ions excited from the anode.

The normalized variance (NV) was used to quantify the regularity in the spikes. From chapter 2, we came to know that the value of the computed NV will be lower for the more regular induced dynamics. For purely periodic dynamics, the NV will be zero. Figure 6.2 is the experimental NV curve as a function of DV. Higher value of NV at DV $\sim$ 479 V indicates the irregular nature of the spikes. It is seen that NV decreases with the increase in the DV indicating the enhancement in regularity and maximum regularity is achieved at DV $\sim$ 488 V. Further increase in DV leads to irregularity in the system. The minima in NV curve suggests that the phenomena is similar to coherence resonance. The observed minima is almost constant exhibiting features of constant coherence resonance (CCR) [83]. Generally, noise is responsible for the CR so we have estimated the intrinsic noise level with the help of Wiener filter [98, 172] subroutine in matlab. Figure 6.3 shows the intrinsic noise level as a function of DV depicting the enhancement in the intrinsic noise level with the increase in DV. As the intrinsic noise level

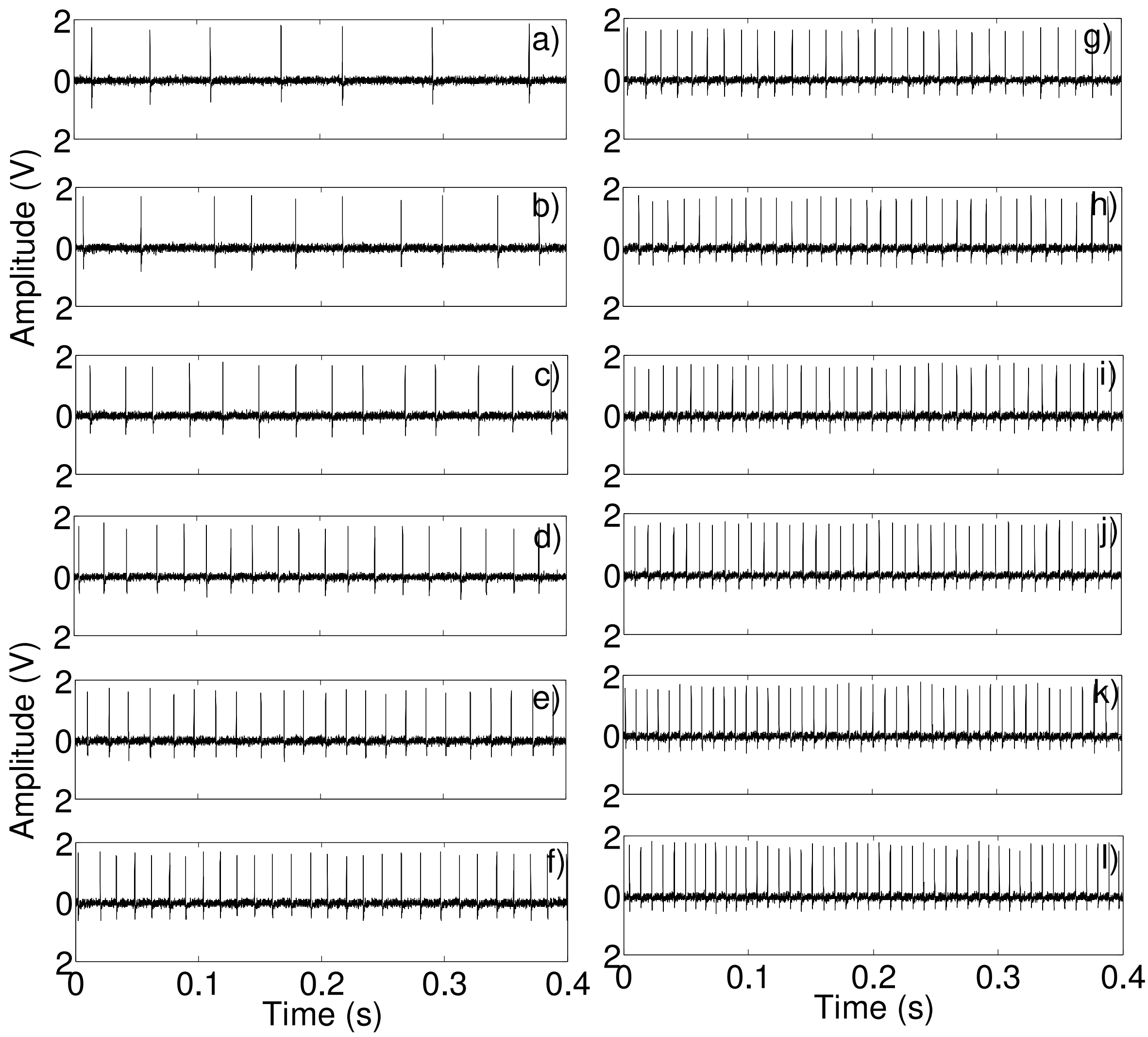

Figure 6.1: Time series of the floating potential fluctuation for different values of DV: a) 479 V, b) 480 V, c) 481 V, d) 482 V, e) 483 V, f) 484 V, g) 485 V, h) 486 V, i) 487 V, j) 488 V, k) 489 V, and l) 490 V. Magnetic field = 0 G, pressure $\sim$ 0.37 $mbar$.

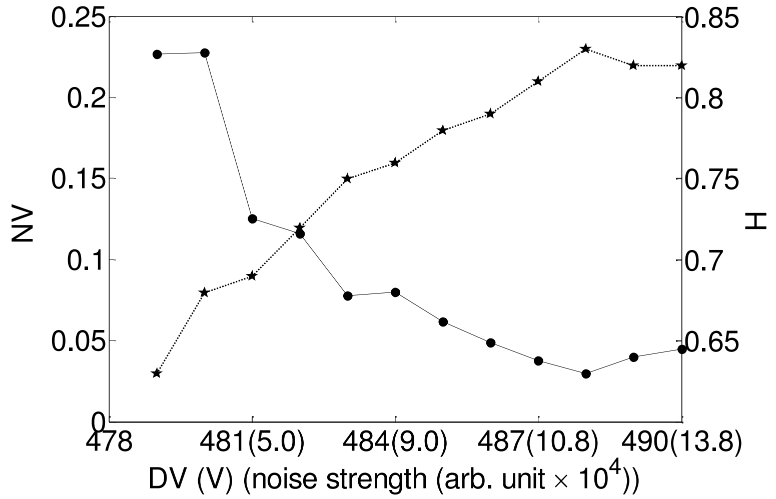

Figure 6.2: Plot of normalized variance (NV) (solid line) and the Hurst exponent (H) (dashed line) as a function of DV with its corresponding noise level given in the parenthesis.

increases with DV, it is clear that the regularity of the excitable spikes in the floating potential fluctuation increases with the increase in the noise level, upto an optimal value of the noise strength. The process behind the enhancement of intrinsic noise with DV is different with the process in the presence of dipolar magnetic field which we have discussed in chapter 3. Changing DV can accelerate the charged particle which can enhance the ionization and also create a situation conducive for the generation of various plasma instabilities that in turn interact to produce a background plasma noise.

The estimation of characteristic correlation time (τ) using normalized autocorrelation function has been shown as one of the measures of coherent behavior [155, 166]. The occurrence of a maxima in the τ vs noise amplitude curve at the point of maximum regularity has been reported for the coherence resonance phenomena [155]. It is well known that the Hurst exponent (H) can also be used as a measure of temporal correlation. Hence, to further characterize the coherence

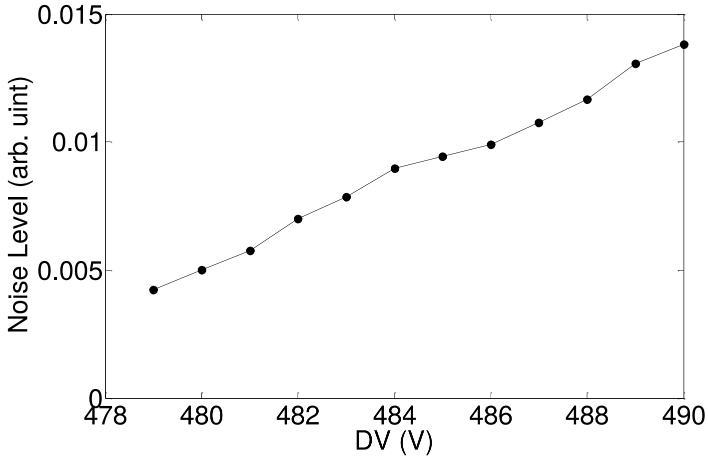

Figure 6.3: Intrinsic noise level as a function of DV.

resonance behaviour, we evaluated the Hurst exponent estimated using rescaled range analysis (R/S) method [63]. A detailed methodology of Hurst exponent is discussed in the chapter 2. The dependence of the Hurst exponent on the DV and noise strength is shown in figure 6.2. The nature of the H vs DV curve has an opposite trend with respect to NV vs DV curve. The plot clearly shows the coherence resonance maximum at DV $\sim 488\ V$ indicating the maximum temporal correlation at a particular discharge voltage and hence at a particular value of noise strength.

Power spectrum plot can also be used to compare the regularity of the signals [165]. For the regular time series signal, the power spectrum will show a narrow peak whereas for irregular time series signal it will show a broadband nature. Figures 6.4(a), 6.4(b) and 6.4(c) show the power spectra of the floating potential fluctuation for DV 487 V, 488 V and 489 V respectively. The power spectrum in the figure 6.4(b) exhibits a narrow and sharp band than the rest of two figures confirming the maximum regular behavior of the signal at 488 V. The power at DV 488 V, which is the point of coherence resonance, shows a higher power than

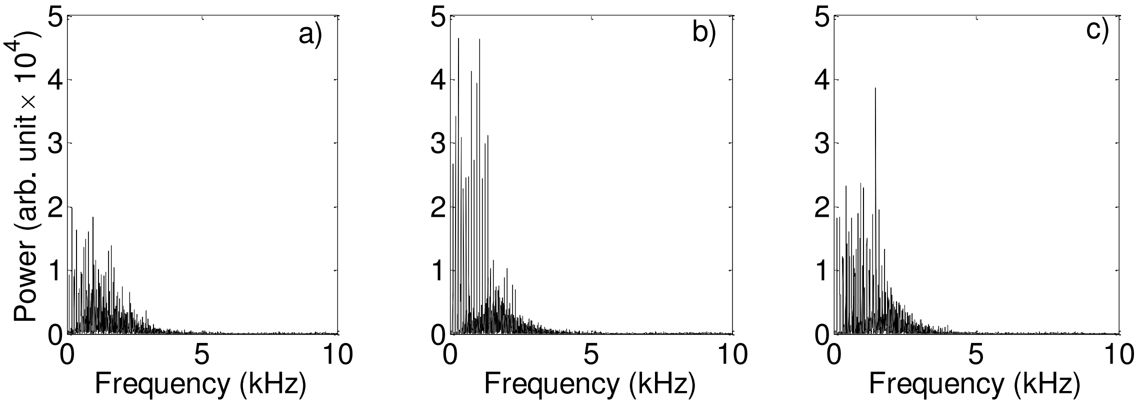

Figure 6.4: Power spectra for the floating potential fluctuation at DV: a) 487 V, b) 488 V, and c) 489 V.

the other values of DV. The average power of the frequency band $(0-1500\ Hz)$ in case figure 6.4(b) is approximately greater by a factor of 2.5 and 1.7 in comparison with figure 6.4(a) and figure 6.4(c) respectively.

The presence of a positive value of Lyapunov exponent is the reliable signature of chaos. The largest Lyapunov exponent(LLE), shown in figure 6.5, is calculated from the experimental time series signal of the floating potential fluctuations by Rosenstein's technique [11] discussed in section 2.3.3 of chapter 2. It is seen from figure 6.5 that the LLE is positive and approximately constant from $\sim 479\ V$ to $\sim 490\ V$. The positive value of the LLE indicates the chaotic nature of the observed signal.

6.3 Dynamical Model for Coherence Resonance

To understand the dynamical origin of the intrinsic noise induced CR in our experiments, we have carried out a numerical simulation using a FHN like model developed in chapter 3. The model represents an excitable system which is obtained by suitable transformation of anharmonic oscillator equation for plasma [19, 101]

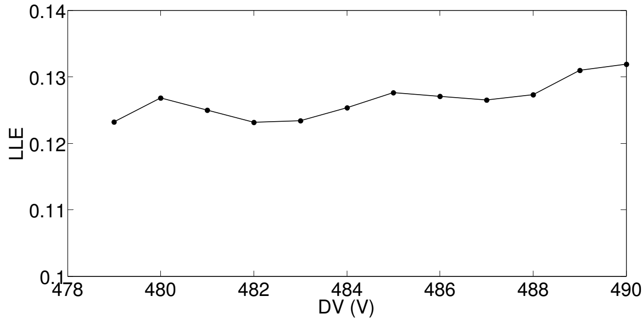

Figure 6.5: Plot of largest Lypunov exponent (LLE) as a function of DV. The error bar in the LLE is 2-4% from several estimates.

using the Liénard like co-ordinate system. The model is given by

$$\epsilon\dot{x} = (ax - \frac{bx^2}{2} - \frac{cx^3}{3}) - y \tag{6.1}$$

$$\dot{y} = x \tag{6.2}$$

where ϵ, a, b and c are $1/s, p/s, q/s$ and r/s respectively.

Although there is no explicit externally applied noise present in the experimental system, we consider the situation where noise is generated intrinsically. In order to investigate the behaviour of the nonlinear oscillations in the presence of an external discharge voltage, we include an additional biasing term k and a noise term $r * \xi$ on the right hand side of Eq. (6.2). ξ is a Gaussian noise term and r represent the strength of the noise.

$$\epsilon\dot{x} = (ax - \frac{bx^2}{2} - \frac{cx^3}{3}) - y \tag{6.3}$$

$$\dot{y} = x + k + r * \xi \tag{6.4}$$

This model does not exactly represent the experimental system at a microscopic level, but we expect to describe the excitable dynamics of glow discharge plasma as this model looks similar to FHN model. The above phenomena was observed in the small window of discharge voltage. Since the relative change in DV during the observation of CR phenomena was approximately 2.3% which is much smaller as compared to relative change in the noise level, we fixed the bias (k) at constant value such that the dynamics exhibit the excitable fixed point behavior and varied the noise strength. The above Eqs. (6.3) and (6.4) are solved numerically using fourth order Runge Kutta method with initial conditions and time step $x = 0$, $\dot{y} = 1$ at $\tau = 0$ and 0.01 respectively. The parameters ϵ, a, b, c and k are fixed at 0.01, 1, 0.95, 0.85 and 1.8 respectively.

Figure 6.6 shows the spiking oscillation at various values of the noise strength (r) as mentioned in the caption of the figure. It is observed that the number of spikes increases with noise strength.

Figure 6.7 shows the numerically computed NV curve. The value of computed NV is higher at lower noise strength indicating the irregularity in spikes and shows a minima at $r = 0.4$ corresponding to an optimum noise level where the maximum regularity of the generated spike sequence is observed. The numerically computed NV curve is consistent with the experimental results. The Hurst exponent is almost around 1 for all values of r probably because of the difference in the nature of the experimental and numerical time series data.

Power spectrum plot for noise strength (r) 0.35, 0.4 and 0.5 are shown in figure 6.8(a), 6.8(b) and 6.8(c) respectively. It is seen that the power is larger for the figure 6.8(b). Maximum power is observed for a particular noise level, which indicates the presence of coherence resonance phenomena. This result also shows a good qualitative agreement with the result obtained from the numerically computed NV curve.

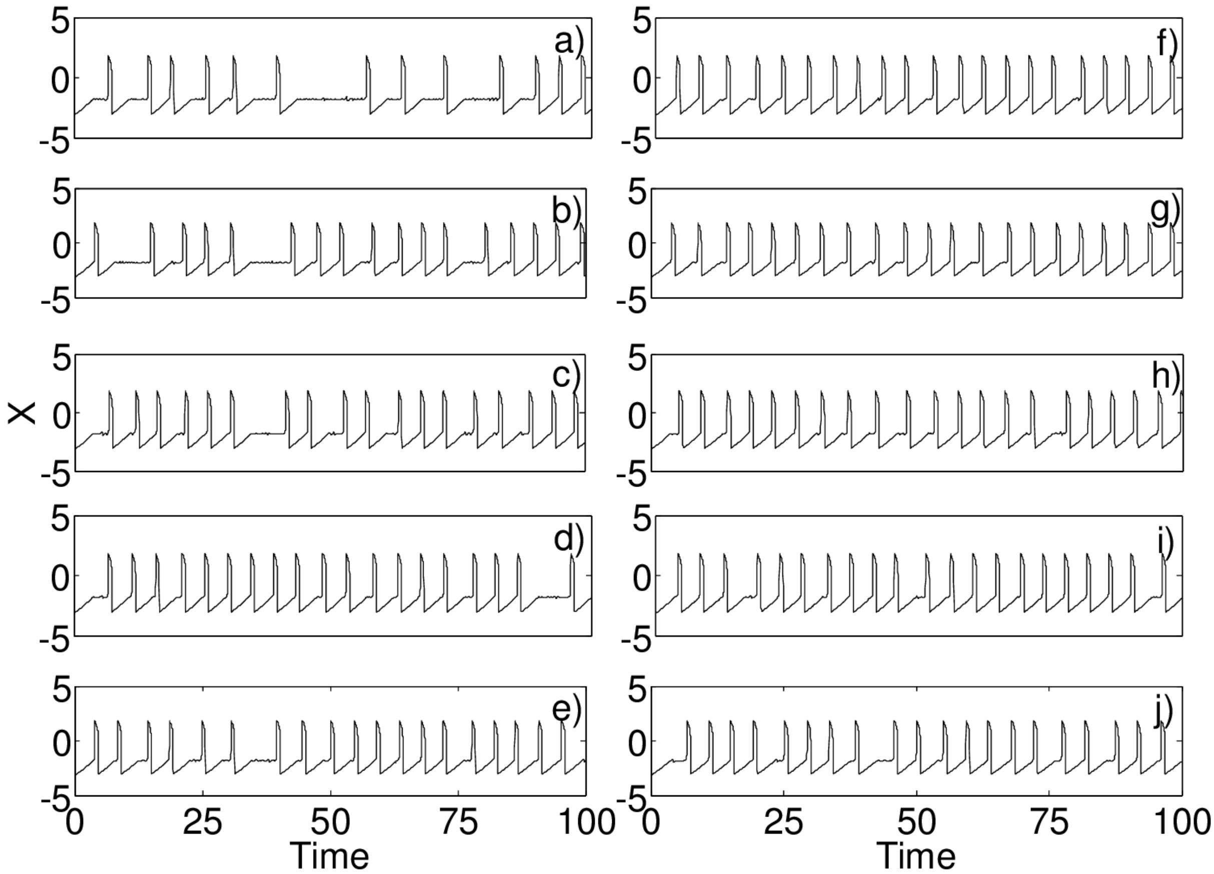

Figure 6.6: Solutions (x) of numerical model for various noise strength (r): a) 0.15, b) 0.20, c) 0.25, d) 0.30, e) 0.35, f) 0.40, g) 0.45, h) 0.50, i) 0.55, and j) 0.60.

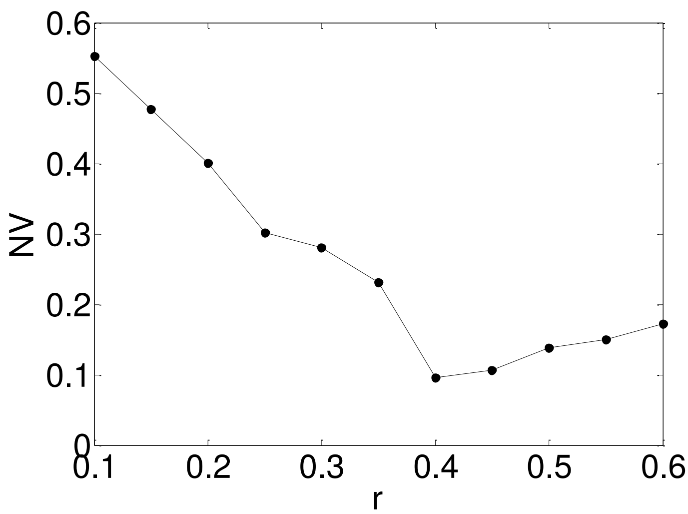

Figure 6.7: Normalized variance (NV) as a function of noise strength (r).

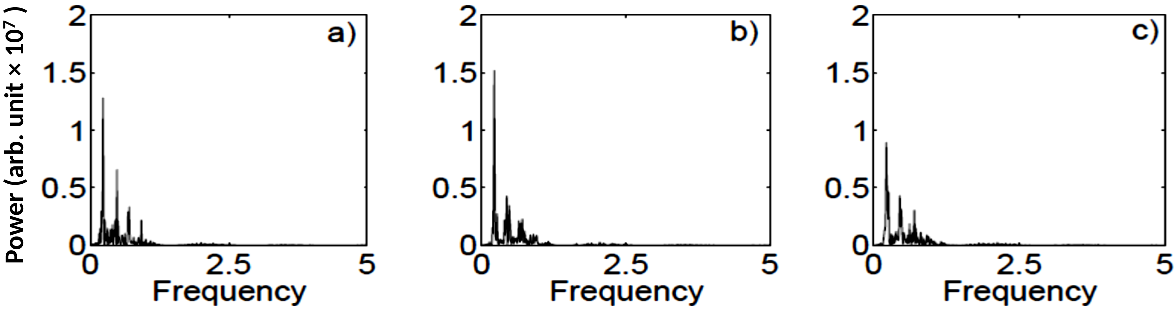

Figure 6.8: Power spectra of the numerical solution for noise strength (r): a) 0.35, b) 0.4, and c) 0.5.

6.4 Summary and Conclusions

Intrinsic noise induced coherence resonance has been observed in a glow discharge plasma. The amount of internal noise is dependent on the DV where an enhancement in noise level with discharge voltage has been observed. The resonance curve (NV curve) is used to quantify the regularity of the intrinsic noise induced oscillation and hence to verify the CR phenomena. It is shown that the floating potential fluctuations show maximum periodicity and maximum power in the power spectrum for a particular DV i.e. at a particular value of intrinsic noise. The utility of the Hurst exponent in the characterization of coherence resonance phenomena has been explored which suggests that Hurst exponent can be used a tool to identify the CR. In ref. [38] external noise induced CR have been reported for glow discharge. In contrast, in the present work we presented that intrinsic noise induced CR is also possible in a glow discharge plasma. We have also carried out a numerical simulation to understand the dynamics of such excitable system in the presence of noise. The results obtained from the numerical simulation are in good agreement with that of experiments. It is quite likely that noise induced spikes are related to the bunches of ions emanating from the anode and drift towards the cathode-anode gap. We hope our finding is helpful for studying the interaction of the intrinsic noise and plasma modes in plasma system and these results may be utilized to characterize various plasma based devices like plasma coating devices to improve their efficiency, plasma lasers to optimize the lasing output where intrinsic noise can play a beneficial role. Understanding the role of intrinsic noise therefore can be an important contribution to the study of excitable systems.

Chapter 7

Detection of Coherent Modes in the Chaotic Time Series Using Empirical Mode Decomposition and Discrete Wavelet Transform Analysis

Our studies reveal that experimentally observed plasma fluctuations are always contaminated with noise and any signal is composed of two parts: a coherent part and an incoherent noisy part. Realizing the need to separate out the coherent and incoherent part in a chaotic time series data, we have developed and applied an empirical mode decomposition based technique to different types of plasma fluctuation data. The results are compared with those from the well known wavelet based coherent mode detection technique. EMD based bicoherency technique is used to identify some of the mode-mode interactions.

7.1 Introduction

It was generally believed that turbulence is a random phenomena, but it has been observed that turbulent flows contain motion with a broadband of scales [173]. There are two different types of scales present in such a flow, one at which most energy resides and another at which energy dissipates. The energy containing scales exhibit the most evident structures that are usually referred to as coherent structures [173]. There are several definitions of coherent structures in literature [173, 174, 175, 176] but the most relevant one was given by Robinson et al. [176] "Coherent structure is defined as a region of flow over which at least one fundamental flow variable exhibits significant correlation with itself or with another variable over a range of space and/or time that is significantly larger than the smallest local scale of flow". With the advent of chaos theory, it is now recognized that both chaos and turbulence are closely related [177]. Chaos and turbulence differ in one aspect: chaos is produced by low-dimensional system whereas turbulence is produced by very large dimensional system. However, it is seen that weak turbulence displays all the symptoms of the chaos [177]. So, we can say a coherent structure is a mode which coexists in a turbulent or chaotic flow, retaining its form over many characteristic lengths or times and also shows a significant correlation with the original flow, and hence can have significant effects on the transport and mixing [178]. Coherent structures retain partially deterministic features of a turbulent flow field which have been experimentally observed using schlieren and shadowgraph pictures [179]. Incidentally, these structures which can also exist in a chain of mutually coupled oscillators [180] need not always be periodic or linear, and hence, for their detection, one has to resort to nonlinear techniques.

Turbulent or chaotic time series signals are some times highly fluctuating, non stationary and intermittent. They also have a broadband feature and may consist of a superposition of localized structures in time. Though there is no clear definition of coherent structure/mode present in a turbulent or chaotic time series data, Farge et al. [181] suggested that coherent modes are "not noise". Since any experimental time series is most likely to consist of noise side by side of any coherent feature, the remaining part of time series after denoising the time series can be considered as a coherent mode.

Currently, wavelet transform [62, 181, 182] and empirical mode decomposition [57, 58, 59, 183, 184, 185] (EMD), are two major time-frequency analysis tools that are commonly used for the processing of non-stationary and nonlinear signals. The wavelet transform decomposes a signal into different frequency bands and at different time points with the help of basis functions. The basis functions have the property of localization in time and frequency. The only difficulty in using the wavelet transforms, is that the choice of the basis functions influences the results [182]. EMD was introduced by N. E. Huang et al. [57] for the analysis of non stationary and nonlinear signals. It is widely deployed as non linear time series analysis tool in various disciplines, such as plasmas [59, 186, 187, 188], neuroscience [189], geophysics [190], earth science [191] and economy [192]. This method has been successfully used for analysis of turbulence [193] and nonlinear time series data [194]. It does not require any predefined basis functions as in Fourier or wavelet analysis. Fourier analysis can only be used to analyze stationary signals. As it decomposes a signal into globally uniform harmonic components, therefore, it needs many additional harmonic components to represent non-stationary data that are non-uniform globally. Fourier spectra needs additional harmonic components to simulate the deformed wave-profiles because it uses linear superposition of trigonometric functions. Although discrete wavelet transform (DWT) can be applied for the decomposition of non-stationary signals, EMD has certain advantages over the DWT. The levels/scales are fixed in DWT as a result of which the frequencies of the decomposed signals are predefined, whereas in EMD the frequencies of the decomposed signals are fixed according to the iteration. So EMD offers a better option in the extraction of the natural frequencies at which the signal oscillates [195]. Flandrin et al. [183] suggested EMD as a data-driven wavelet like expansion. The wavelet transform has been used extensively for denoising and detection of coherent modes of a time series data [62, 181, 182, 196]. In the reference [62, 182], a coherent mode has been identified as the mode with the highest energy concentration but it is possible to have more than one coherent mode. Since EMD has proved to be a data driven wavelet like expansion, it can be used as a tool for the detection of the coherent modes and in this chapter, we have identified the highest energy mode as well as those with comparable energy to the coherent modes. This allows us to not only identify but also study the interaction between the coherent modes leading to the chaotic behavior.

The detection of coherent structures in a plasma turbulence or chaos is important in view of their role in the transport of momentum and energy [197]. The aim of this chapter is to detect the coherent modes in the chaotic time series (CTS) data using EMD and discrete wavelet transform (DWT) analyses [62, 182]. The versatility of these techniques has been demonstrated by applying them to experimental time series data obtained from a glow discharge plasma. One can detect the periodic coherent modes using Fourier analysis, but the advantages of EMD and DWT are that as well as periodicity, they can also detect short timescale coherent modes.

7.2 Extraction of a Coherent Mode

There is not yet an universal definition of coherent mode in a chaotic or turbulent time series data, we prefer starting from more consensual statement about them, that coherent mode corresponds to significantly correlated and highest energy concentration mode of the original signal.

We propose a new method to extract coherent modes from chaotic time series data. In order to extract the coherent mode, we first decompose the signal into its intrinsic modes (IMFs) using EMD technique. Second, we will pick up the relevant IMFs by computing the correlation coefficient of IMFs with original signal and the rest of the modes are considered as redundant. Correlation coefficient (CC) of an IMF gives an idea about its contribution to the original signal and those IMFs which have a CC $> 0.1(10\%)$ are taken into consideration for the physically significant modes (relevant). The methodology for the decomposition of a signal using EMD and computation of cross correlation coefficient has been discussed in detail in the chapter 2. Information about the energy concentration of a mode can be obtained by estimating the variance of the modes. These two statistical estimates ensure that we can identify the coherent modes from the IMFs.

The energy based empirical variance of an IMF is given by the relation

$$V[k] = \frac{1}{N}\sum_{n=1}^{N}(IMF_k(n))^2, \tag{7.1}$$

where k and N are the mode index or IMF number and the data length of IMF respectively.

Since EMD can also be used as dyadic filter, the variance of the modes are related to the mode indices through the relation [183, 198]

$$V[k] \quad = \quad C2^{2(H-1)k}, \tag{7.2}$$

where C and H are constant and the Hurst exponent of the signal respectively.

It is clear from Eq. (7.2) that the plot of the log-variance of the IMFs vs mode indices is a straight line with gradient $2(H-1)$. $H = \frac{1}{2}$ is a special case which indicates the Gaussian noise. So the portion of the log-variance plot whose slope is -1, i.e., Hurst exponent (H) $\sim \frac{1}{2}$ indicates noise, while the maximum indicates the highest energy concentration at that IMF or at that time scale. If log-variance plot shows a maximum for a mode, which means an energy concentration, it often corresponds to a coherent mode.

Following steps are involved in the detection of the coherent modes:

1. Compute the IMFs of time series using EMD.

2. Compute the correlation coefficient and the variance and then plot the log-variance vs IMF number.

3. From the relevant IMFs, one with maximum log-variance is considered to be the coherent mode.

7.3 Test Data: Floating Potential Fluctuations

In this work, our objective was to investigate the coherent modes by applying DWT and EMD to different types of time series data. So, we analyzed three different

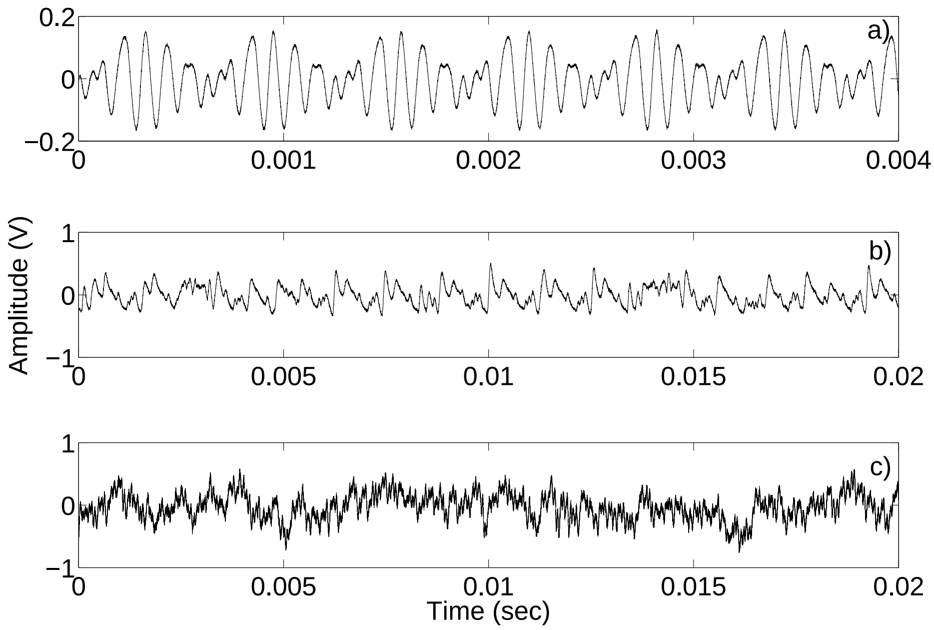

Figure 7.1: Plot of a) first experimental data, b) second experimental data, and c) third experimental data.

floating potential fluctuations in which the system was operated at a fixed pressure ~ 0.056 $mbar$ and three different discharge voltages ~ 426 V, 436 V and 440 V as shown in figures 7.1(a), 7.1(b) and 7.1(c) respectively. For the third case [figure 7.1(c)], we had applied an axial magnetic field of about 60 G. The power spectrum plots of the time series data are shown in figure 7.2. It is clearly seen from the time series and power spectra plots that the oscillatory behaviour is very different in the three signals. In order to have better resolution of the frequencies, we have used different sampling times for the first, the second and the third cases as .4 μsec, 2 μsec and .2 μsec respectively.

The measured electron temperature (T_e) and density (n) are ~ 2 eV and $\sim 10^9$ cm^{-3} respectively. The value of ion temperature, ion mass and charge state of the Ar was $\sim 0.1 - 0.2$ eV, $40M_p$ and 1 respectively, where M_p is the proton mass.

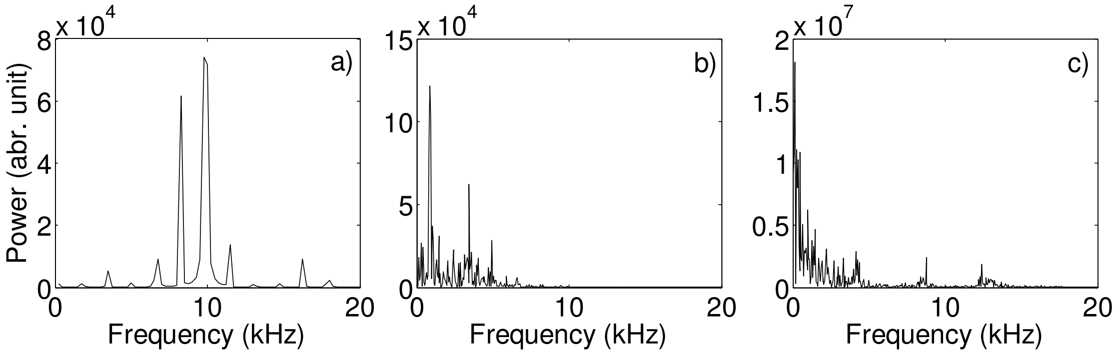

Figure 7.2: Power spectrum plot of a) first experimental data, b) second experimental data, and c) third experimental data.

So the typical values of the various frequencies, i.e., electron plasma, ion plasma, ion acoustic, ion drift, ion transit, and the ion cyclotron were ~ 284 MHz, ~ 1.05 MHz, $\sim 2.5-5$ kHz, ~ 21 kHz, ~ 11 kHz and ~ 2.3 kHz respectively.

7.3.1 First Experimental Time Series (Unmagnetized)

Figure 7.3 shows the first experimental time series of 10000 data points and its IMFs. The first four IMFs are the high frequency noise components of low amplitude. The higher IMFs from the sixth onwards exhibit a clear structure of lower frequency while the 11th IMF represents the trend. Hence EMD can also be considered to be a filter to separate various frequency components. Figures 7.4(a) and 7.4(b) show the CC and the log-variance vs IMF number respectively. The CC plot shows a peak at the fifth IMF and very small values for the others and it is seen that the CC of almost all the IMFs is $< 10\%$. The fifth IMF shows a peak in the CC while the others exhibit rapid fall. Correspondingly the log-variance also shows a maximum at the fifth IMF while the rest tend to exhibit a sharp fall. The log-variance plot also shows an initial slope of -1 for the higher frequency modes indicating that the first few high frequency modes are the contribution of

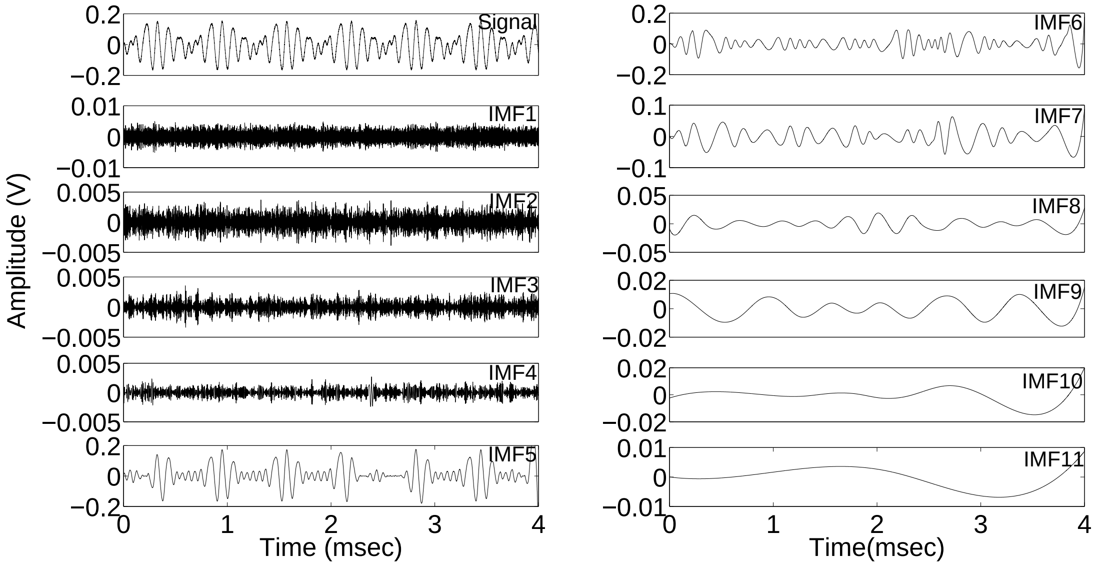

Figure 7.3: Plots for the first experimental time series (sampling time $.4\mu s$) and its IMFs.

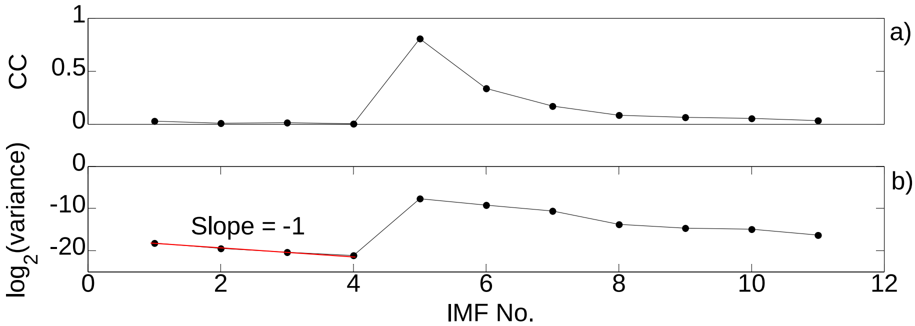

Figure 7.4: Plots for the a) correlation coefficient of IMFs, and b) $log_2(variance)$ of IMFs.

noise. Hence, we can consider the fifth IMF as the coherent mode which is shown in figure 7.6(b).

We estimated the log-variance of the wavelet coefficients of the time series at different levels using the db4 wavelet as depicted in the figure 7.5. The log-variance plot appears to be linear with gradient zero for the high frequency modes indicating noise like behaviour which is also observed in the EMD analysis. Figure 7.5 shows a peak at the 8th level which is shown in isolation in figure 7.6(c).

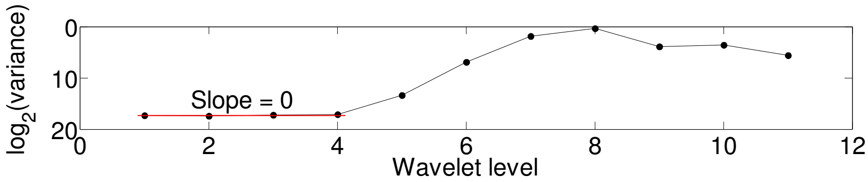

Figure 7.5: $log_2(variance)$ of wavelet coefficient vs wavelet level for first experimental chaotic time series.

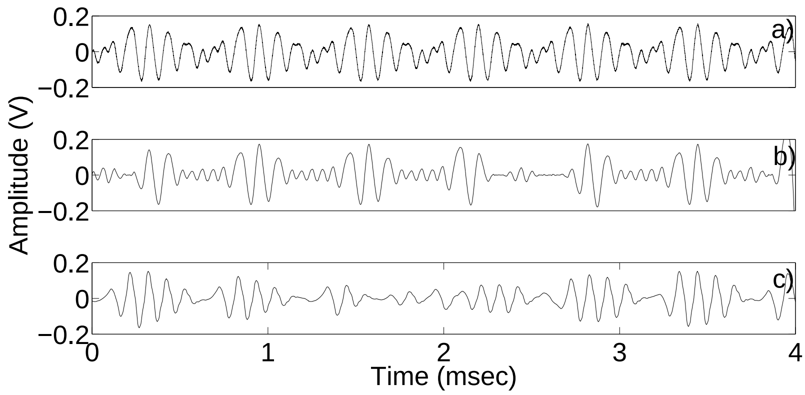

Figure 7.6: Plots for the a) time series signal, b) coherent mode obtained using EMD: 5th IMF, and c) coherent mode obtained using DWT: 8th wavelet level.

Both the EMD as well as DWT analysis show that only one coherent mode is present in this time series data [figure 7.6(a)] which are depicted in the figures 7.6(b) and 7.6(c) respectively.

7.3.2 Second Experimental Time Series (Unmagnetized)

Figures 7.7(a), 7.7(b) and 7.7(c) show the CTS of 10000 data points, the CC and the log-variance vs IMF number respectively. From figure 7.7(b), it is observed that the first four and the twelfth IMFs have a CC value $< 0.1(10\%)$. The log-variance plot shows a gradient of -1 for the higher frequency modes (i.e. 1st to 3rd modes) indicating that the first three modes could be the contribution of noise. There is a maxima in log-variance plot at the eighth IMF and hence from the above criteria this would have been considered as the coherent mode. If one looks

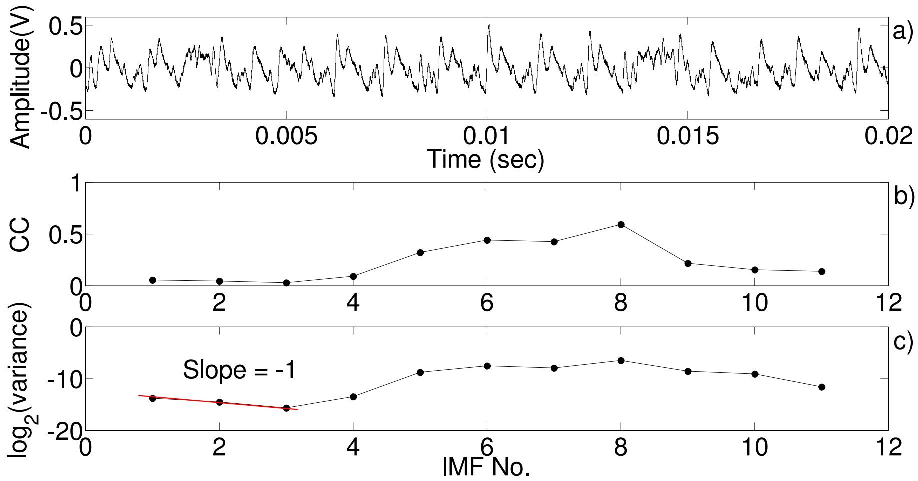

Figure 7.7: Plots for the second experimental data: a) chaotic time series (sampling time $2\mu s$), b) correlation coefficient of IMFs, and c) $log_2(variance)$ of IMFs.

at figure 7.7(c) more closely, it is also seen that the fifth to tenth IMFs exhibit nearly same high energy concentration and hence it may be necessary to consider these also as relevant coherent modes which are shown in figure 7.8.

The log-variance plot of the wavelet coefficient is shown in figure 7.9. Here also the initial gradient is close to zero, representing the noise like behaviour in the higher frequency modes which is also seen in EMD analysis. The log variance plot suggests that the 7th to 11th wavelet levels could correspond to the coherent modes in the CTS as seen in the figure 7.10.

The existence of multiple coherent modes is expected since the time series signal is chaotic in nature, with a broadband of frequencies and high energy concentration modes.

7.3.3 Third Experimental Time Series (Magnetized)

Figures 7.11(a), 7.11(b) and 7.11(c) show the CTS of 100000 data points, the CC and the log-variance vs IMF number respectively. From figure 7.11(b) it is

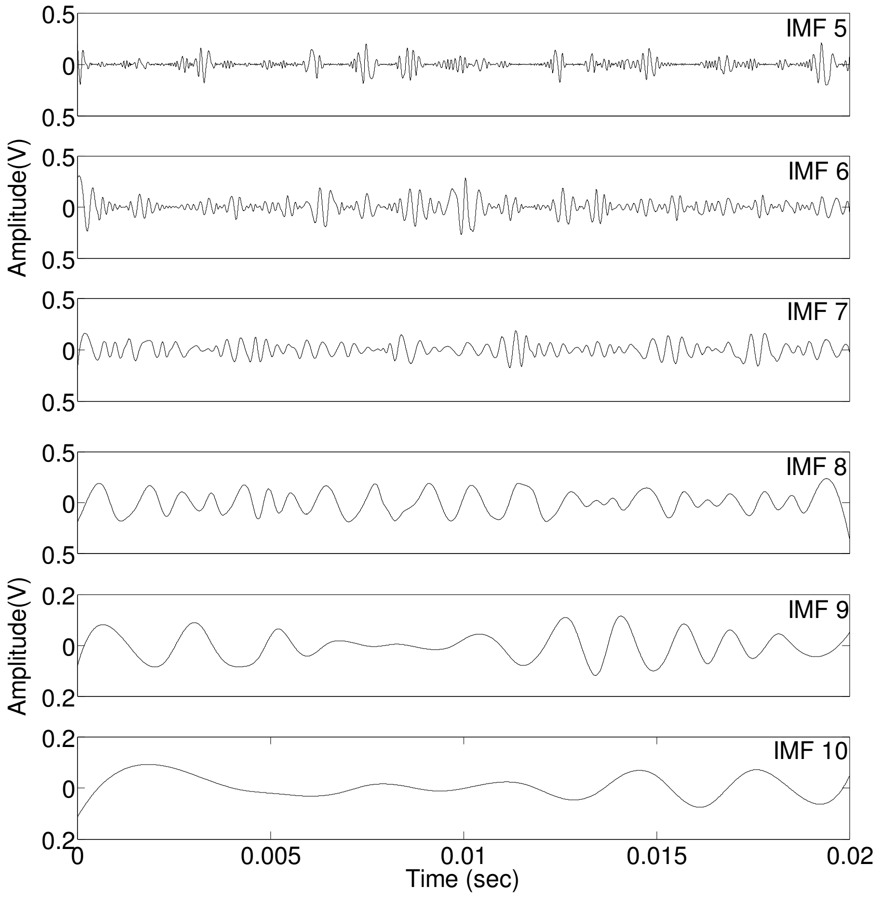

Figure 7.8: Coherent modes obtained using EMD for the second experimental time series data.

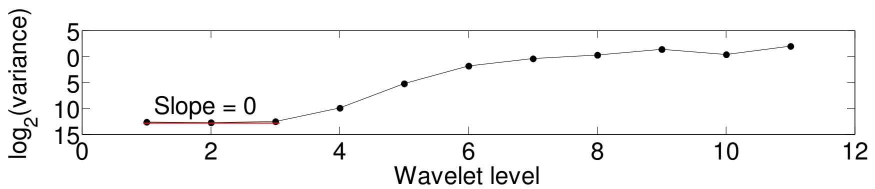

Figure 7.9: $log_2(variance)$ of wavelet coefficient vs wavelet level for second experimental time series.

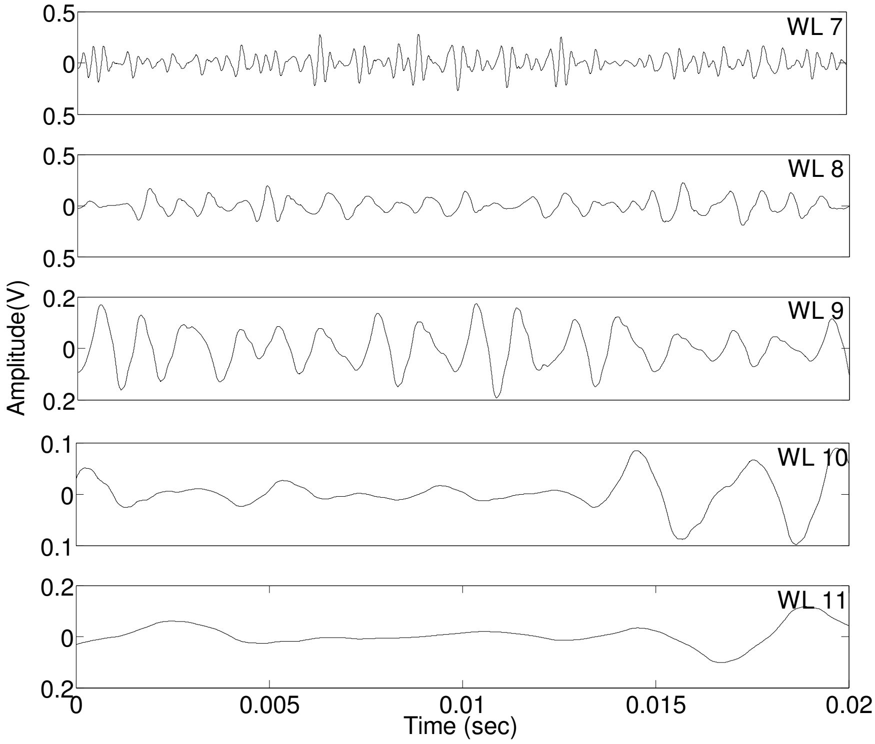

Figure 7.10: Coherent modes obtained using DWT for the second experimental time series data.

observed that the first six IMFs have a CC value $< 0.1(10\%)$. It is also seen that the CC values are more or less saturated after the 7th IMF compared to figures 7.4(a) and 7.7(b) where the CC values shows a sharp fall after reaching peak value. The corresponding log-variance also shows a similar saturated behaviour with a small peak at the 14th IMF. From the above criteria mentioned in section 7.2, 14th IMF only would have been considered as the coherent structure. Comparing the raw data of 7.6(a), 7.7(a) and 7.11(a) it can be said that 7.11(a) is most chaotic or may also be considered as the most turbulent signal which may be due to nonlinear interactions of several coherent modes with high energy concentration. If one looks at 7.11(c) it is seen that the eight to fifteen IMFs exhibit nearly same high energy concentration and hence it may be necessary to consider these also as

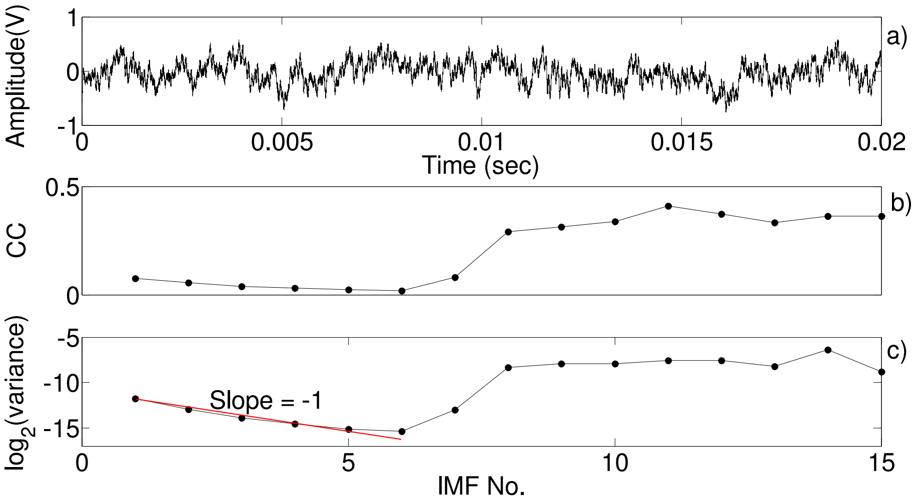

Figure 7.11: Plots for the third experimental data: a) chaotic time series (sampling time $.2\mu s$), b) correlation coefficient of IMFs, and c) $log_2(variance)$ of IMFs.

relevant coherent structures as depicted in figure 7.12. It is also likely that since a magnetic field is present, there is a possibility of different oscillations like ion acoustic, ion cyclotron and drift modes to interact and give rise to the complicated CTS.

The log-variance plot of the wavelet coefficients as a function of wavelet level is shown in figure 7.13. The initial gradient of the log-variance plot is close to zero suggesting a contribution from noise as in the earlier cases. Though there is a maximum at 14th wavelet level this time series could be dominated by more coherent modes since the 11th to 15th wavelet levels have a high energy concentration in the log variance plot. Figure 7.14 depicts the coherent modes obtained after DWT analysis.

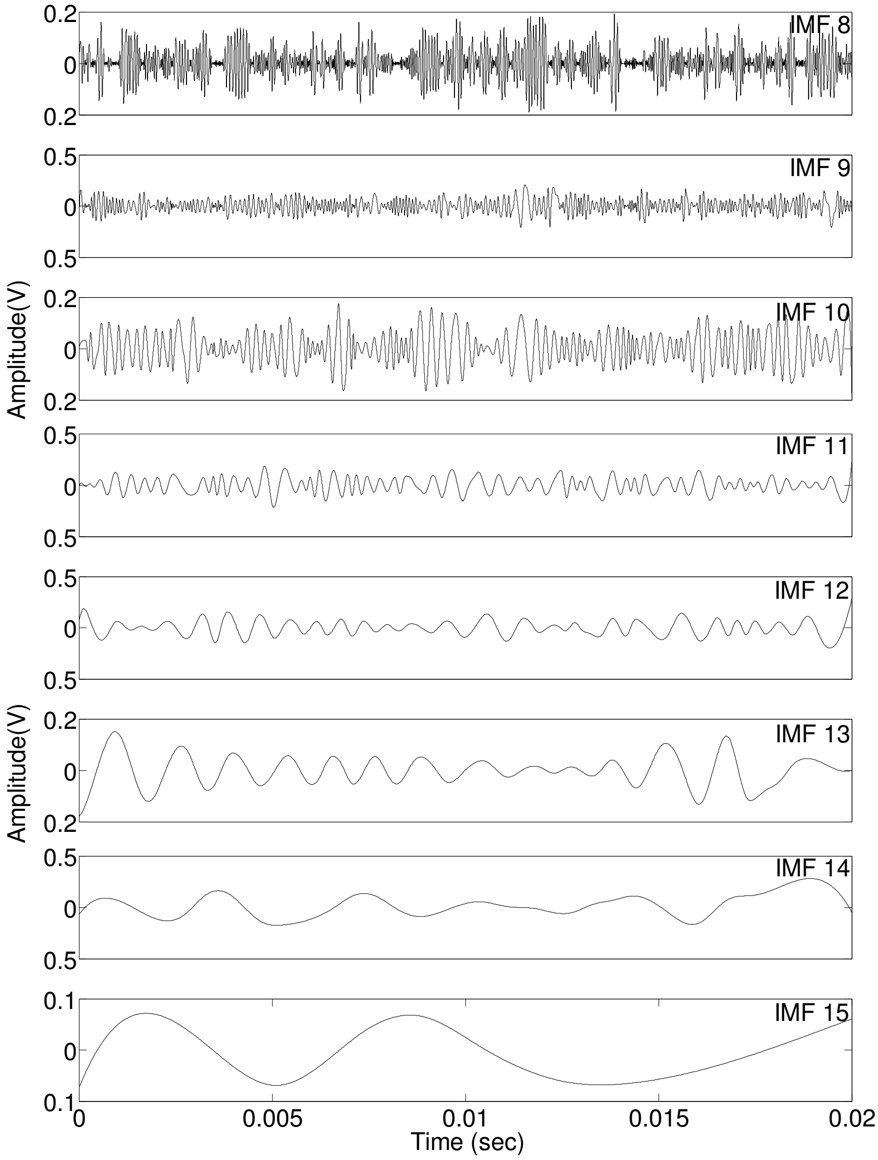

Figure 7.12: Coherent modes obtained using EMD for the third experimental time series data.

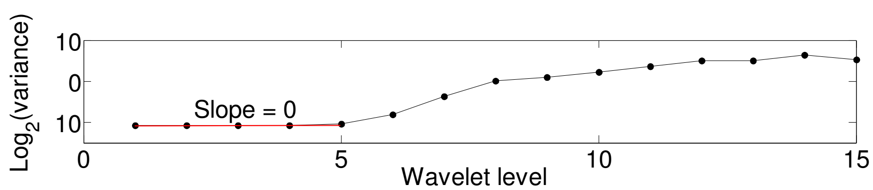

Figure 7.13: $log_2(variance)$ of wavelet coefficient vs wavelet level for third experimental time series data.

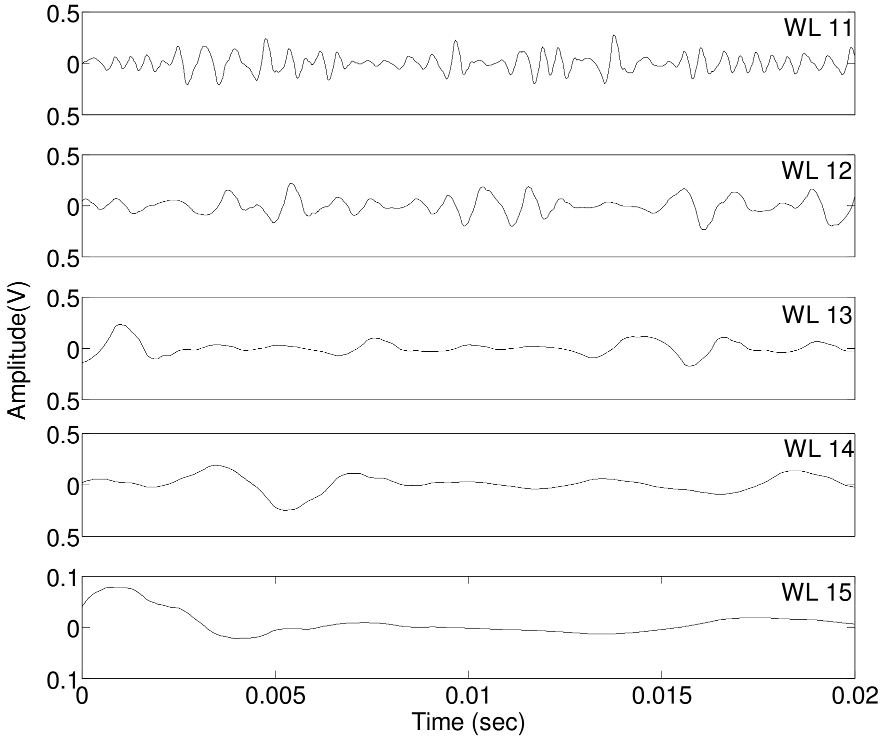

Figure 7.14: Coherent modes obtained using DWT for the third experimental time series data.

7.4 Estimation of the Frequencies and Comparison Between EMD and DWT

Each IMF is approximately a monocomponent in frequency [57, 199]. In the chapter 2, we have seen that by taking the Hilbert transform of an IMF, one can determine the phase angle $\phi(t)$ [57, 59] and the frequency $\omega = \frac{d\phi}{dt}$.

Figure 7.15 shows that the unwrapped phase angle of the IMFs increases approximately linearly with time from whose slope the instantaneous frequency can be estimated as $\omega = \frac{d\phi(t)}{dt}$. It is observed that the excursion of the instantaneous frequency is maximum for the highest frequency and decreases for lower frequencies. This technique gives instantaneous frequency of the IMF and the concept of

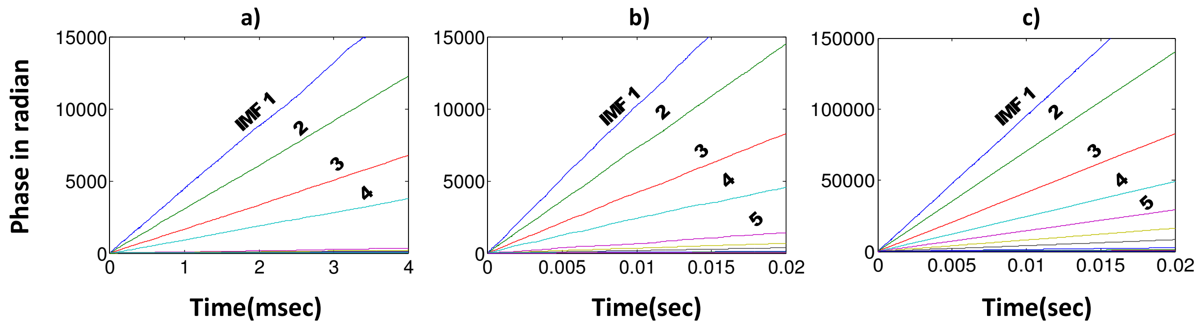

Figure 7.15: Unwrapped phases of IMFs of a) first experimental data, b) second experimental data, and c) third experimental data.

Table 7.1: Estimation of approximate frequencies of coherent modes (CMs)

Time series	Approx. freq. of CMs obtained using EMD (kHz)	Approx. freq. of CMs obtained using DWT (kHz)
First time series	12	7
Second time series	11, 5.2, 2.8, 1.1, 0.59 and 0.29	2.8, 1.4, 0.7, 0.35 and 0.18
Third time series	21, 10, 4.8, 2.5, 1.3, 0.7, 0.25 and 0.15	1.7, 0.87, 0.44, 0.22 and 0.11

frequency bandwidth is not applicable [200]. The time frequency spectrogram obtained by applying the Hilbert transform on the IMFs of the experimental signals is shown in figure 7.16. These plots gives the information of the instantaneous frequency whose amplitude can be noted from the corresponding colour bar. Figure 7.16(a) shows distinct instantaneous frequency whereas figure 7.16(b) and 7.16(c) show wide variations in amplitude and frequency indicating their chaotic nature.

Table 7.1 shows the estimated frequencies of the coherent modes using EMD and DWT. The frequencies are comparable with some of the plasma mode frequencies.

Figures 7.2(a), 7.2(b) and 7.2(c) show the power spectrum plots of the experimental time series shown in the figures 7.6(a), 7.7(a) and 7.11(a) respectively.

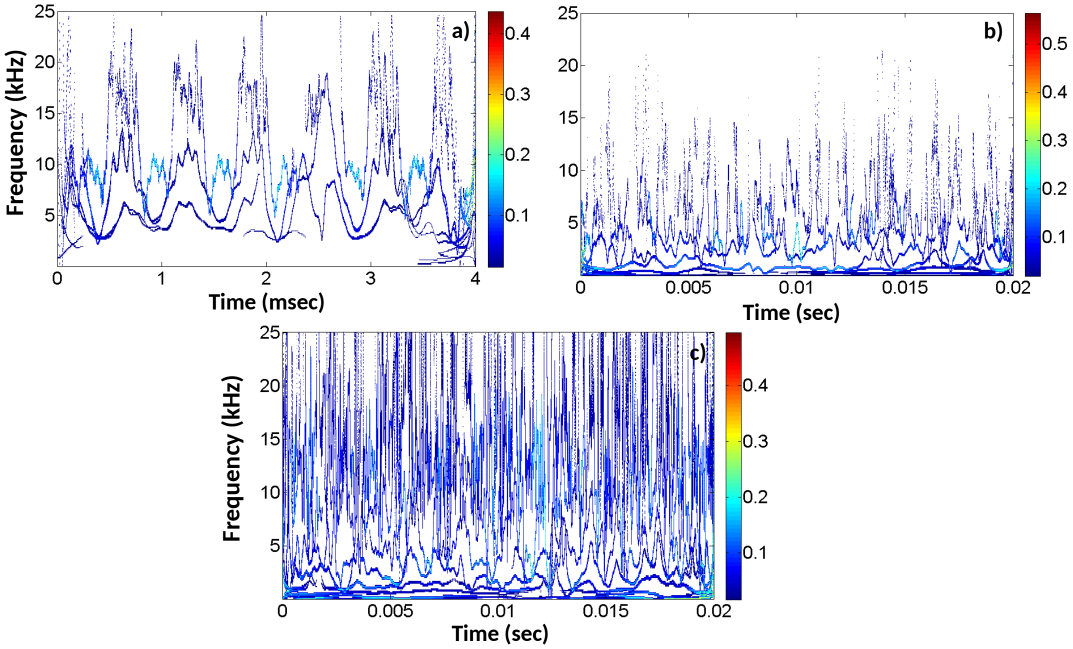

Figure 7.16: Time frequency spectrogram using Hilbert transform of a) first experimental data, b) second experimental data, and c) third experimental data.

Figure 7.2(a) clearly shows distinct peaks with dominant peak around $\sim 10\ kHz$ whereas a broadband nature is seen in the other two plots indicating chaotic nature of the time series. Such broadband time series signal is represented by the finite number of amplitude modulated single frequency modes (IMFs) using EMD.

Fourier transform of any fixed frequency amplitude modulated signal will show two uniform-amplitude components with different frequencies. On the other hand the Hilbert transform will yield a single frequency with modulated amplitude implying a monocomponent. A more detailed treatment of this subject can be found in reference [57, 199]. The dominant frequencies in the power spectrum plots are in good agreement with those obtained from EMD as compared to those using DWT.

It is seen from the table 7.1 that the frequencies of the coherent modes obtained using EMD have better agreement with the estimated plasma modes as well as power spectra in comparison with those obtained using DWT. This could be because the levels/scales are fixed in wavelet decomposition as a result of which the frequencies of the decomposed signals are predefined, whereas in EMD the frequencies of the decomposed signals are fixed according to the iteration. So EMD helps in the extraction of the natural frequencies at which the signal oscillates.

7.5 Bicoherency Factor and Study of Mode Interaction

Using bicoherency technique, we explored the possibility of the interactions between the various coherent modes obtained from EMD. Since, the IMFs can be represented in the form of $Z_i(t) = A_i(t)e^{j\phi_i(t)t}$ using Hilbert transform, the interaction amongst them can be studied by estimating the Bicoherency factor [59] discussed in the section 2.3.8 of chapter 2.

Figures 7.17(a), 7.17(b) and 7.17(c) show the bicoherency for the first, second and third time series respectively. The figure 7.17(a) shows that there is no interaction between the modes since there is only one dominant/coherent mode.

Figure 7.17(b) shows that the fourth and the fifth IMFs have a bicoherency factor higher than the error value. Hence it is possible that there are triplet interactions amongst the fourth to seventh IMFs corresponding to 36 kHz, 11 kHz, 5.2 kHz and 2.8 kHz respectively. But we observed from figure 7.8 that the fourth IMF is not a relevant coherent mode and hence can be discounted leaving us with the dominant modes corresponding to only fifth, sixth and seventh IMFs whose frequencies are 11 kHz, 5.2 kHz and 2.8 kHz respectively. Since they correspond to ion acoustic and ion transit range of frequencies, it is quite likely

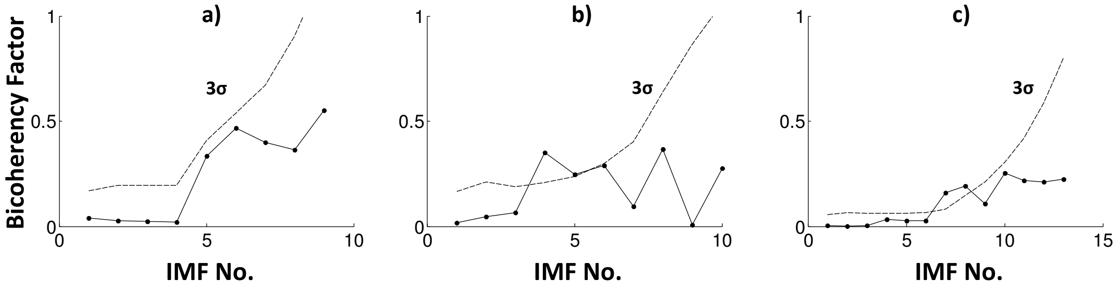

Figure 7.17: Bicoherency factor: a) first experimental data, b) second experimental data, and c) third experimental data. The dotted line indicates the error in bicoherency factor.

that the chaotic behaviour is due to interaction between these modes.

Following the same technique as above we see that from the figure 7.17(c) there could be a triplet interactions amongst the seventh to tenth IMFs corresponding to frequencies 65 kHz, 21 kHz, 10 kHz, and 4.8 kHz respectively. Since the seventh IMF does not fall in the relevant dominant mode, only eighth, ninth and tenth IMFs need to be considered for possible interaction implying frequencies 21 kHz, 10 kHz and 4.8 kHz respectively. Incidentally for a plasma with $T_e \sim 2\ eV$ and magnetic field 60 G, the 21 kHz, 10 kHz and 4.8 kHz fall in the ion drift, ion transit, ion acoustic and ion cyclotron range of frequencies respectively. Hence it is likely that there may be interaction between all these modes leading to the turbulent behaviour.

The frequency analysis only gives a tentative idea about the plasma modes. There may be other processes like ionization instability, nonlinear interaction between modes and nonlinear frequency shifts, etc. which can generate similar behaviour in the time series data.

We see that each of the IMFs has time localized structures suggesting the possible occurrence of some plasma instabilities at that instant of time which are not clearly visible in the original time series. In these structures, the oscillations seem to grow to a maximum amplitude before decaying. The estimation of the growth time scales of these localized structures give the tentative time scales of the instabilities. The typical growth time values are in the range of 2×10^{-4} s to 13×10^{-4} s corresponding to the lower frequency range, i.e. 700 Hz - 5 kHz, as observed in the power spectrum [figure 7.2].

7.6 Summary and Conclusions

We have shown the usefulness of empirical mode decomposition (EMD) in the extraction of coherent structures from a chaotic time series (CTS) of floating potential fluctuations and its effectiveness has been confirmed by comparing with the well known discrete wavelet transform (DWT) analysis. Since the experimental data also has some noisy components, and trends, EMD technique helps in filtering both of them leaving only the intrinsic mode functions (IMFs). From the IMFs also, it is necessary to delineate those that contribute to the coherent part. The IMFs that contribute to the coherent modes vary from case to case depending on the chaoticity of the signal. From the log-variance plots it was observed that the energy concentration was primarily in only one IMF in the first data, six IMFs in the second and eight IMFs in the third CTS data respectively.

In addition to the extraction of coherent modes from the CTS data, we have also been able to estimate the growth times of some of the time localized structures and the frequencies of the coherent structures. By applying the EMD based bicoherency technique on the IMFs, we have shown that the interaction between ion acoustic modes of different frequencies are possibly occurring in the unmagnetized plasma, whereas in the magnetized plasma it is quite likely that the interaction between the ion cyclotron and the ion acoustic modes is responsible for the chaotic behaviour in the time series.

On the evidence of our study of three time series, we feel that the EMD technique is a promising and appealing tool for the analysis of CTS. In addition, this is perhaps for the first time to our knowledge, we have applied EMD for the detection and investigation of possible interaction of the coherent structures in an experimental CTS, and we hope that these results will inspire a further use of EMD analysis for chaotic time series.

Chapter 8

Coherent Modes and Their Role in Intermittent Oscillations Using Empirical Mode Decomposition

In this chapter, applicability of the empirical mode decomposition based coherent mode detection technique, developed in previous chapter, has been shown by applying it on intermittent chaotic time series data. During the experiment, it is seen that these oscillations go to an ordered state from a chaotic state with increase in the discharge voltages through intermittence chaotic state. Role of coherent mode during this transition is given. The Hilbert Huang spectrum of the fluctuations confirm the presence of intermittency and the intermittent change in the frequency with time.

8.1 Introduction

In the chapter 7, we have developed a Empirical mode decomposition (EMD) based coherent mode detection technique. Efficiency of this method has been shown irrespective of the nature of data by applying it on three different kind of fluctuation data. Here, we will demonstrate the applicability and usefulness of this method by applying it on intermittent chaotic signal. All our previous chapters established that floating potential fluctuations occur at different scales and show a complex structure like chaos, mixed mode oscillation, multifractality, etc. In this chapter, we will focus on another complex structure known as intermittency. In any dynamical system, intermittency is considered as the irregular alternation of different phases like different forms of chaotic dynamics or periodic and chaotic dynamics [201]. In fluid dynamics, intermittency is usually referred to as a behaviour where long time intervals of regular behavior ("laminar phases") are interrupted by fast irregular bursts [202]. Intermittency is a frequently observed phenomena in many fields of science like electronics [203], plasma [211, 204, 205, 206], biology [207, 208], laser [209] and neurology [210]. As intermittent signals can be highly non stationary and nonlinear, EMD can give more acquaintance and better insight regarding the intermittent phenomena as compared to conventional techniques like Fourier transform and wavelet analysis [62]. EMD technique along with Hilbert transform can give temporal as well as frequency modulation information unlike the normal Fourier transform. All these facts motivated us to carry out the EMD analysis of intermittent signals which can be highly non linear and non stationary.

8.2 Intermittent Time Series and Their Analysis Using EMD

The experiment was performed in a cylindrical geometry dc glow discharge argon plasma by Ghosh et al. [211]. In this present experiment, pressure was kept at $\sim 0.028\ mbar$ and DV was varied in the range of 628 V to 674 V. The typical plasma density, electron temperature and ion temperature were around $\sim 10^7$ cm^{-3}, $\sim 1-3\ eV$ and $\sim 0.1\ eV$ respectively. The electron plasma frequency and ion plasma frequency were calculated to be $\sim 28\ MHz$ and $\sim 150\ kHz$ respectively while the ion acoustic frequency was found to be around $\sim 3-10\ kHz$. The floating potential fluctuations, consist of 8192 data points, recorded at a sampling rate of 10 μs. Details of the experiment can be found in Ghosh et al. [211] and for ease of comparison, the data from ref. [211] have been used in the present analysis.

Time series data of the floating potential fluctuations are shown in figures 8.1(a)-8.1(i) showing transition from the order (relaxation) state to the chaotic behaviour via type I intermittency [211]. Figure 8.2(a′), 8.2(b′) and 8.2(c′) show the expanded view of the time series shown in the figure 8.1(a), 8.1(d) and 8.1(i) respectively. From the figures, we have seen two different types of oscillations: relaxation oscillation (type A) and chaotic oscillation (type B). At lower discharge voltages, i.e., 628 V and below, relaxation oscillations of type A are seen, while type B oscillations appeared at and above DV 638 V. The occurrence of type A and type B oscillations are irregular and intermittent. Beyond 648 V, the frequency of occurrence of type B became higher compared to type A and finally the oscillations settled to type B from 674 V onwards.

As an example, we have shown in figure 8.3 the experimental time series (figure

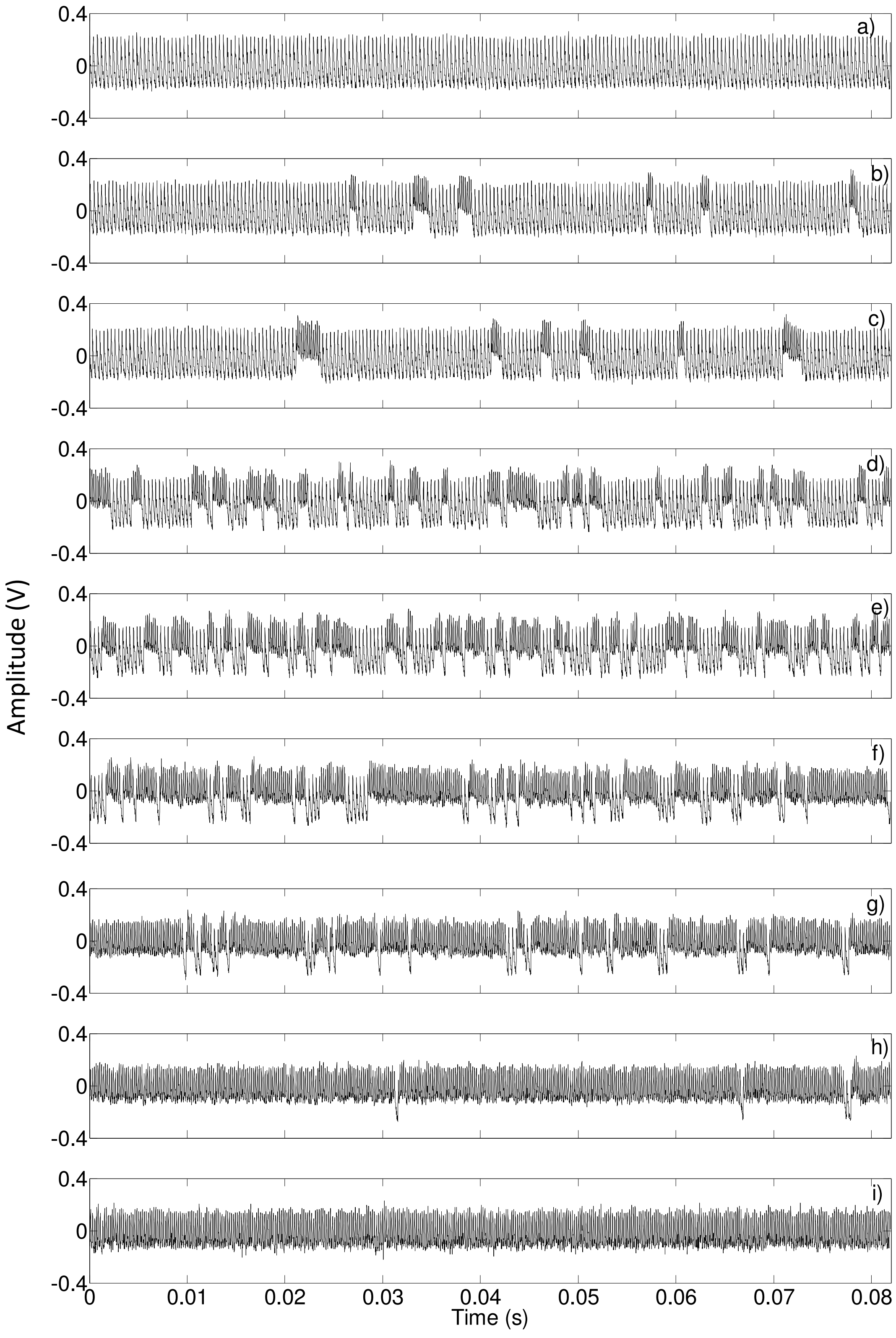

Figure 8.1: Time series of the floating potential fluctuation for different values of DV: a) 628 V, b) 638 V, c) 640 V, d) 645 V, e) 648 V, f) 655 V, g) 660 V, h) 670 V, and i) 674 V. Pressure is kept fixed at 0.028 $mbar$.

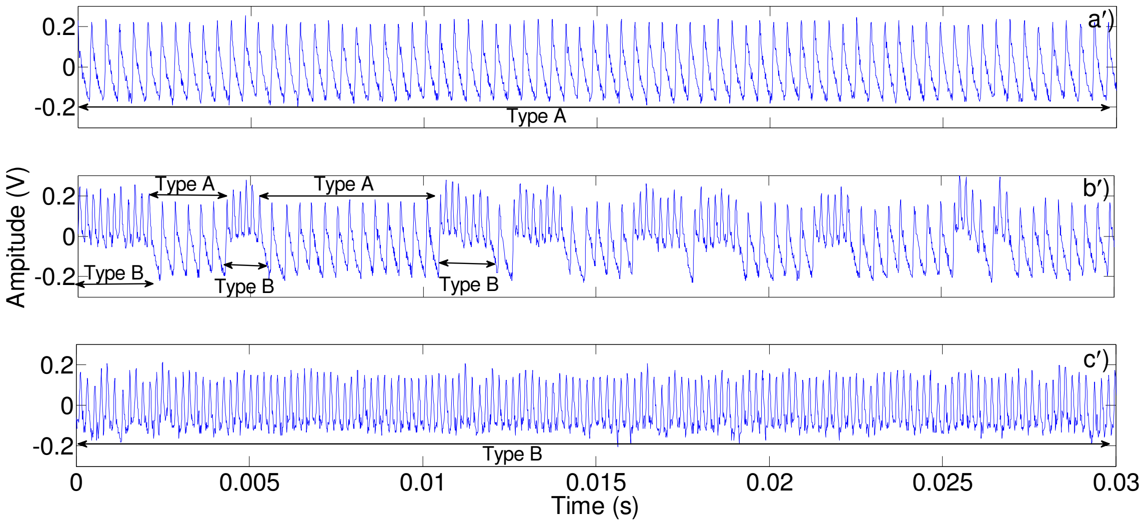

Figure 8.2: Expanded view of time series of the floating potential fluctuation at different values of DV: a′) 628 V, b′) 645 V, and c′) 674 V.

8.1(b)) and its IMFs decomposed by EMD technique. From the figure, it is clear that 1st IMF is related to high frequency low amplitude noise, 2nd-10th IMFs are associated with signal and 11th-13th IMFs are trend terms. This visual interpretation is verified by estimating the correlation of IMFs with the original signal [figure 8.4]. It is seen that the correlation coefficient of the IMFs contributing to the noise and trend turn out to be less than 10% and hence can be neglected for further analysis.

In the left and right panels of the figure 8.4, we have shown the correlation coefficient (CC) and the log-variance plots as a function of IMF number corresponding to the time series shown in the figure 8.1. For the first four time series data, the CC and log-variance plots show a maxima at 4th IMF indicating that the 4th IMF is the mostly correlated IMF with the original signal as well as possessing higher energy concentration. Thus, the 4th IMF can be considered as the coherent mode. Similarly for the last four time series data, 3rd IMF turns out to be the coherent mode. In the case of the fifth time series data, it is seen that the 3rd and the

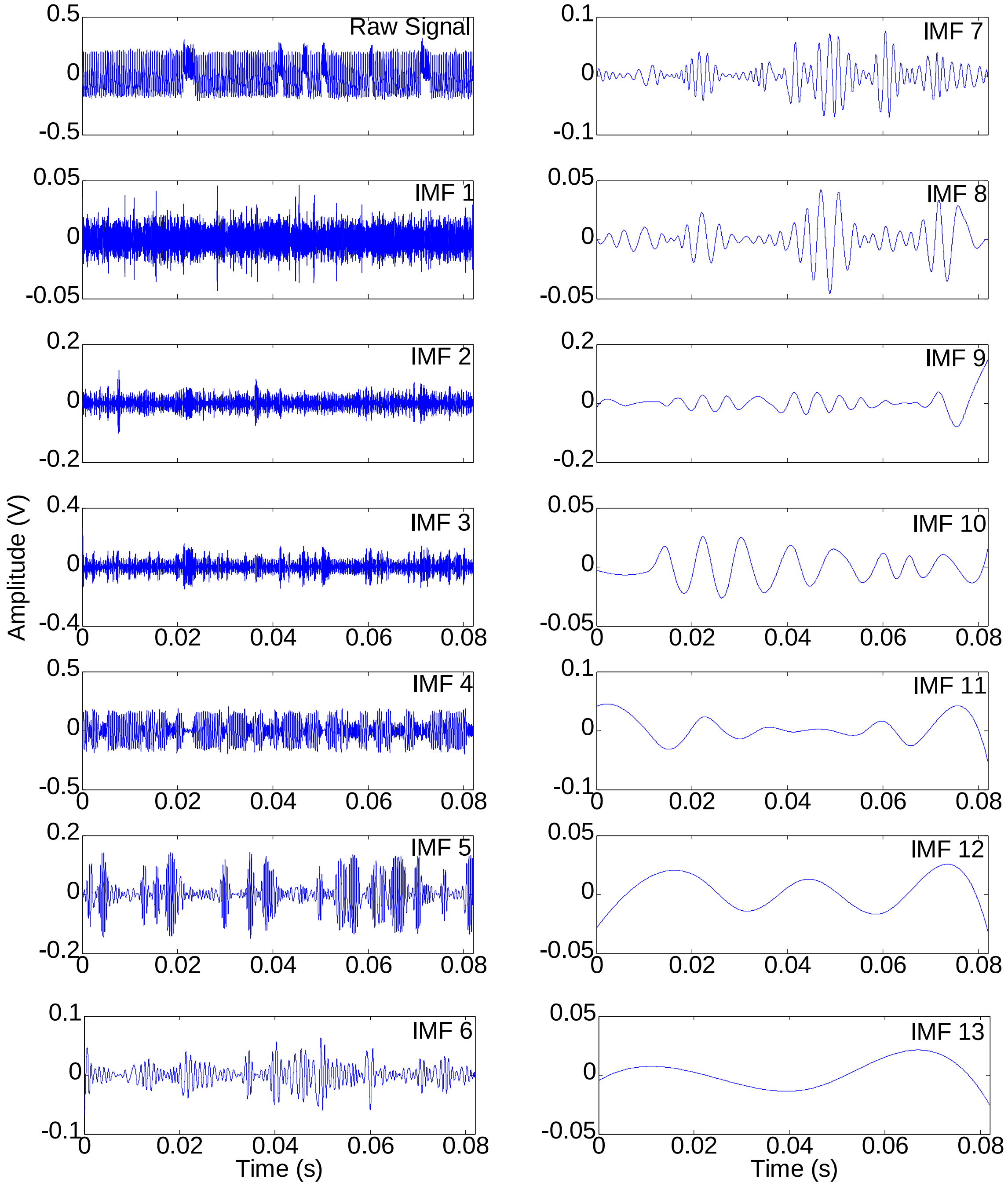

Figure 8.3: IMFs (excluding the residual) obtained using EMD for the experimental time series (figure 8.1(c)) at DV 640 V.

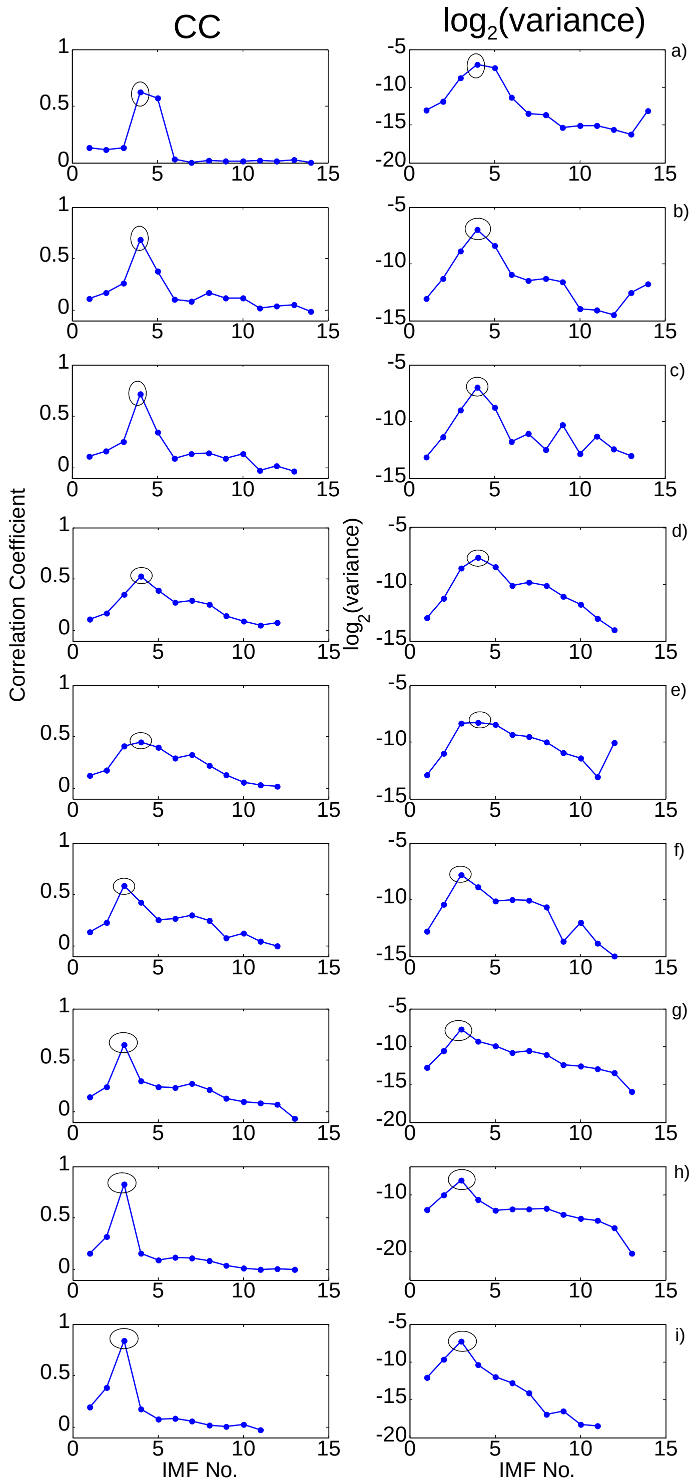

Figure 8.4: Plots for the correlation coefficient and log_2(variance) of IMFs obtained by decomposition of the time series shown in figure 8.1. Values of DV corresponding to plots are a) 628 V, b) 638 V, c) 640 V, d) 645 V, e) 648 V, f) 655 V, g) 660 V, h) 670 V, and i) 674 V respectively. Circle indicates the highest energy concentration mode which have higher correlation with the original signal.

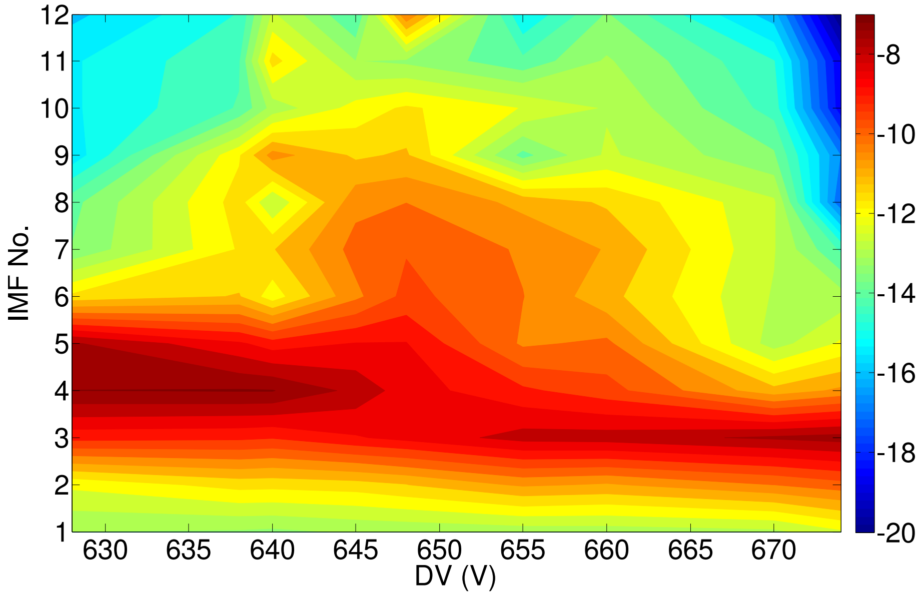

Figure 8.5: Representation of log-variance of IMFs of the fluctuations in an IMF no-DV space. Value of log-variance distributed according to colour axis.

4th IMFs exhibit the same energy concentration and hence it may be necessary to consider both the 4th as well as the 3rd IMF as the relevant coherent modes. This observation clearly indicates that energy is being transferred from one mode to another thus forcing the system to change intermittently from one oscillation to another.

As the plasma system is highly nonlinear, it is apparent from the analysis that there is an exchange of energy between the modes. The contour plot of figure 8.5 shows a clear visualization of the transfer of energy between the modes wherein the colour indicates the value of the log-variance (often energy). It is observed that initially the energy is concentrated around the 4th IMF, i.e., for DV below 648 V, and for the intermediate voltage (DV $\sim$ 650 V) the energy is distributed within 3rd to 6th IMFs. For the latter case i.e DV beyond $\sim$ 650 V, the energy is concentrated around the 3rd IMF.

In order to see the exchange of energy between the 4th and 3rd modes clearly,

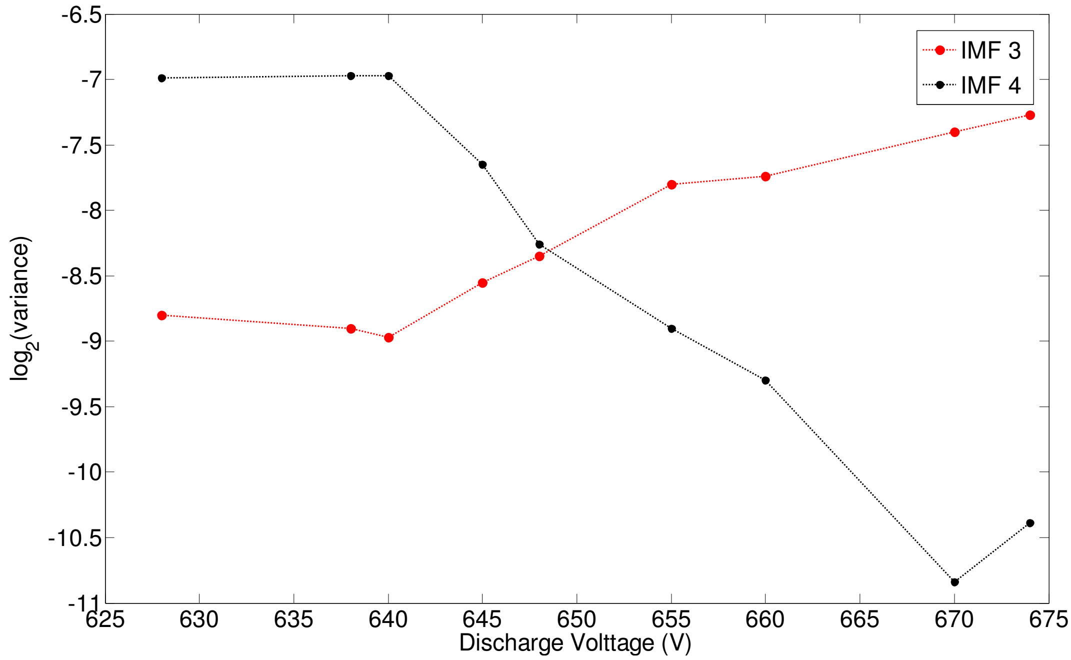

Figure 8.6: Comparison of energy concentration of 3rd and 4th IMFs of the time series signals: Plot of log variance as a function of DV.

we have plotted the log-variance of the 3rd IMF and the 4th IMF as a function of DV in the figure 8.6. It is seen from the figure that variance of the 4th IMF and the 3rd IMFs is decreasing and increasing respectively with the discharge voltage. Therefore, at lower discharge voltages (628-648 V) the highest energy mode, i.e., the 4th IMF, loses its energy with the increase in the discharge voltage and finally for DV > 648 V, 3rd IMF becomes highest energy mode. This gradual transfer of energy from the 4th to the 3rd IMF leads to the change in the coherent mode of system as a result of which one oscillation i.e relaxation oscillation changes to a chaotic one.

We have estimated the mean frequency of each IMF in order to better see how the decomposition is performing on the intermittent data. The relation between IMF no. and mean frequency is displayed in figure 8.7. The straight line in log-linear plot suggesting the following relation $\bar{f}(k) = f_0\rho^{-k}$, where f is the mean

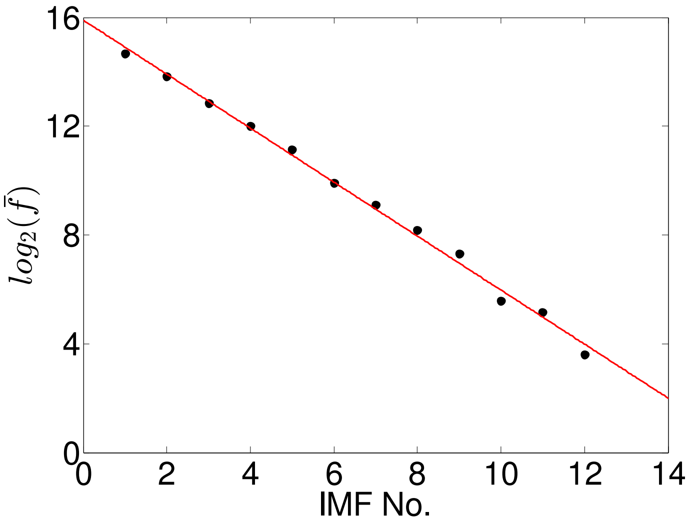

Figure 8.7: Mean frequency versus IMF number for the intermittent time series (DV $\sim$ 648 V). There is a power law with a slope very close to 1.

frequency, f_0 is a constant and $\rho \sim 2$. This indicates that EMD acts as a dyadic filter bank in the frequency domain.

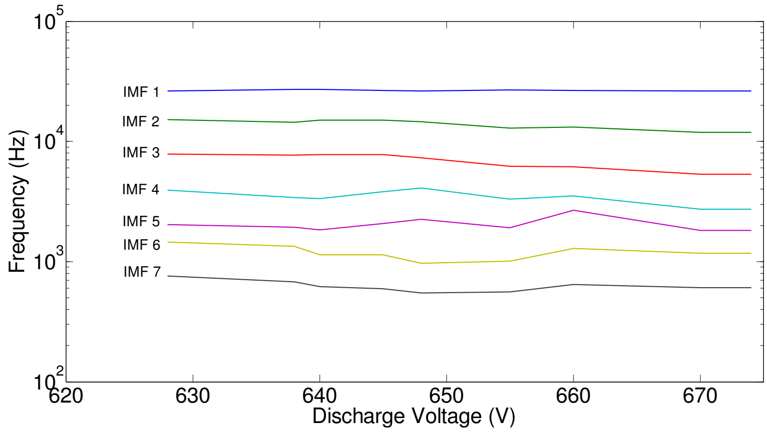

Figure 8.8: Mean frequency of IMFs as function of DV.

The mean frequencies of the first seven IMFs, having frequencies more than 500 Hz, as a function of DV is shown in the figure 8.8. It is seen that the time series data preserves the basic structure (in terms of frequency components) with the increase in the discharge voltage. Therefore, the IMFs have also preserved their respective mean frequencies throughout the DV as depicted in the figure

8.8. Information of the occurrence of the intermittent oscillations reflects as an increase in the amplitude of the IMF which corresponds to the frequency of the intermittently occurring mode. Different IMFs have different frequencies indicating that they are representing different modes. We observe that the system is mainly dominated by two distinct modes, i.e., 3rd and 4th IMFs. Initially the system is dominated by 4th IMF at low voltages, whereas it is dominated by 3rd IMF at high voltages.

The time frequency spectrograms obtained by applying Hilbert transform on the IMFs of the initial relaxation [figure 8.1(a)], the intermediate intermittent [figure 8.1(e)] and the final chaotic states [figure 8.1(i)] are shown in the figures 8.9(a), 8.9(b) and 8.9(c) respectively. The frequency band centred around ~ 2.5 kHz for type A oscillation is seen in the figure 8.9(a) whereas frequency band centred around ~ 5 kHz for type B oscillation as depicted in the figure 8.9(c). In the figure 8.9(b), a clear discontinuity in the contours as well as two frequency bands centered around ~ 2.5 kHz and ~ 5 kHz have been observed. The discontinuity in the contours and irregular switching of the contours between ~ 2.5 kHz band and ~ 5 kHz band indicates the presence of intermittency. The electron drift velocity for the range of DV $628-674$ V is $\sim 10^9$ cm/s which is ~ 13 times greater than the electron thermal velocity ($\sim 7\times10^7$ cm/s) for the 3 eV electron plasma and hence is conducive for the generation of ion acoustic instabilities which fall in the range of $3-10$ kHz. So, it is quite likely that observed frequencies are triggered by ion acoustic instabilities. Since the observed time series is of relaxation type in nature, its frequency changes from time to time within the oscillation thus implying the intrawave frequency modulation of the signal. As the frequency bands have time variation about the centre band frequency as depicted in figure 8.9, this indicates the frequency modulation.

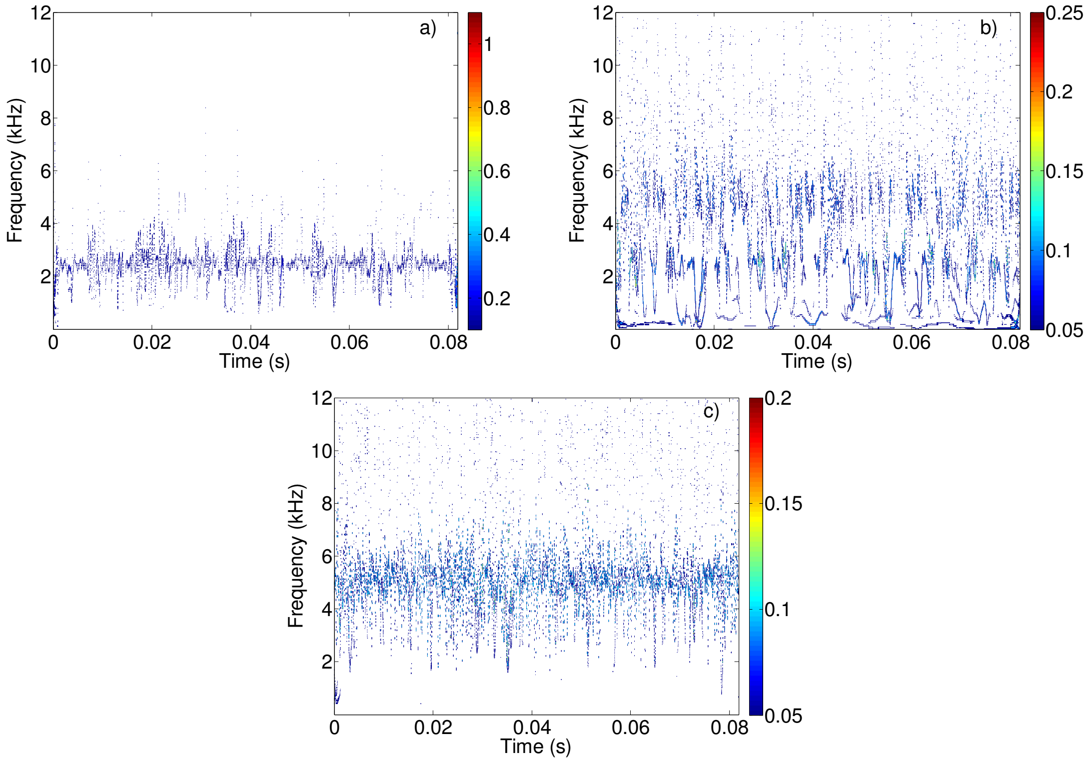

Figure 8.9: Time-frequency-energy representation, obtained using HHT, corresponding to the floating potential fluctuations shown in the figures 8.1(a), 8.1(e) and 8.1(i)

.

For the confirmation of the coherent modes obtained using EMD, we carried out R/S analysis [63] to detect the presence of coherent modes and also identify the respective frequencies [13]. Figures 8.10(a), 8.10(b) and 8.10(c) show the plot of $\log_{10}(R/S)$ versus $\log_{10}(m)$ for the time series shown in the figures 8.1(a), 8.1(e) and 8.1(i) respectively. In the R/S plot for type A oscillation [figure 8.10(a)], the presence of a single linear regime suggests the presence of one coherent mode whose frequency $\sim 2.1\ kHz$ is obtained from the bending in the curve. A similar observation has been made in the R/S plot, shown in the figure 8.10(c), for the

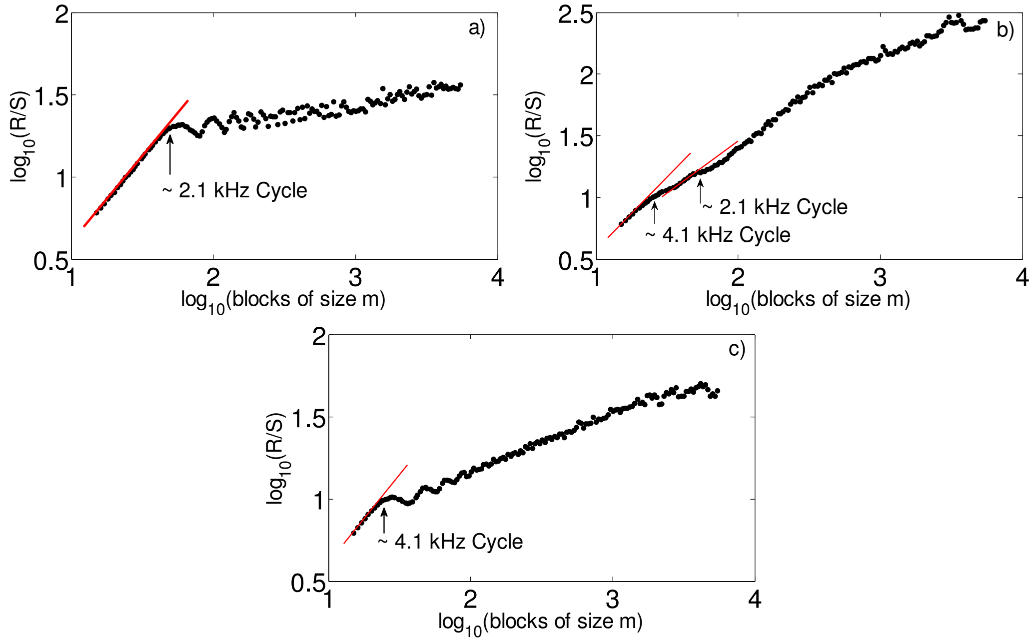

Figure 8.10: Plot of $log_{10}(R/S)$ versus $log_{10}(m)$ corresponding to the floating potential fluctuations shown in the figures 8.1(a), 8.1(e) and 8.1(i)

.

type B oscillation. The bending in the curve is due to the $\sim 4.2\ kHz$ cycle. However for the intermediate intermittent oscillation, the R/S curve shows the presence of two distinct linear regimes. These two distinct linear regimes suggest the coexistence of two coherent modes for the intermediate oscillation. These observations corroborate the observations made by EMD.

Figure 8.11 shows the reconstructed phase space plots for the time series shown in the figures 8.1(a), 8.1(e) and 8.1(i) respectively. A single centre of rotation is observed in the case of the non intermittent signals whereas two centres of rotation are observed for the intermediate intermittent oscillations. This is also revealed by the R/S curve where we have observed a single linear regime for the non intermittent signals and two linear regimes for the intermediate intermittent signals.

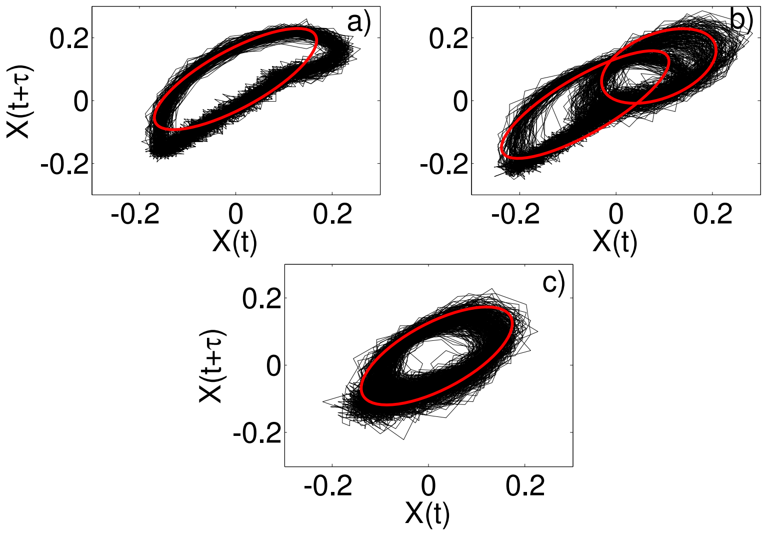

Figure 8.11: Reconstructed phase space plot corresponding to the floating potential fluctuations shown in the figures 8.1(a), 8.1(e) and 8.1(i). In these plots, the time delay, estimated using mutual information technique, $\tau = 20\ \mu s$ has been used. Solid red line indicates the mean trajectory.

8.3 Summary and Conclusions

We have applied here empirical mode decomposition technique to analyze the experimental intermittent time series data. After decomposition of the original time series data into several intrinsic modes, the coherent modes have been identified by estimating the correlation coefficient and the log variance. Comparing the log variance of the coherent modes, that signify the energy of the mode, we have observed that the associated coherent modes in the time series change while the system transits from one state to another i.e from relaxation to chaotic. At low discharge voltages ($< 650\ V$), there is an occurrence of type A oscillations dominated by one coherent mode represented by 4th IMF. At higher discharge voltages ($>$ 650 V), type B oscillations are present that are dominated by a different coherent mode represented by IMF 3. In the intermediate stage, at a discharge voltage of ~ 650 V, there is a crossover of energy from 4th IMF to 3rd IMF. The contour plot shows clearly the transfer of energy from 4th IMF to 3rd IMF. Presence of single linear regime in the R/S plot for initial and final states suggests the existence of a single coherent mode in each of these states whereas the presence of two linear regimes in the case of intermittent oscillations ($\sim 648\ V$) indicates the coexistence of two coherent modes. These observations corroborate the results obtained on the basis of EMD analysis. A single frequency band around 2.5 kHz and 5 kHz in HHT spectrum are seen in the initial and final non intermittent states respectively whereas for the intermittent case a clear discontinuity and irregular frequency switching between these frequency bands is observed. The observed frequencies which are probably due to ion acoustic instabilities are better represented by 4th IMF at low voltages, and by 3rd IMF at high voltages. These observed frequencies are triggered by ion acoustic instabilities. EMD along with HHT technique gives a clear confirmation about the presence of intermittency in the signal in contrast to the other traditional analysis techniques like phase space and Fourier transforms. The Power spectral analysis in Ghosh et al. [211] shows a broadband nature around the 2.6 kHz and 5.2 kHz but the temporal information about the occurrence of the intermittent frequencies was not present. This information has been clearly extracted using the EMD and the HHT analysis. Apart from that an important information about the intrawave frequency modulation is also extracted using the HHT analysis which cannot be done using power spectral analysis. So we feel that the method presented in this paper is a very powerful tool to analyze highly intermittent and non stationary data and may be very helpful to investigate data which are highly turbulent in nature.

Chapter 9

Summary and Future Scope

In this chapter, a quick recapitulation has been made on the works discussed in this thesis: "Investigation of nonlinear dynamics of a self-excited complex system like plasma". Some of the future scope regarding our works has also been discussed.

9.1 Summary

With the development of nonlinear dynamics, large scale simulations and large scale computations, scientists began to focus on research on complex systems to understand the various phenomena like long range correlations, self-organized behaviour, complex co-operative behaviour of some networks and so on. Plasma being a complex system, all these developments also caught the attention of plasma scientists and nonlinear dynamics turned out to be very useful to explain plasma instabilities, plasma transport, characterization of plasma turbulence etc. Various theoretical studies using nonlinear dynamical models have been carried out to explain plasma instabilities in late 60s while experimental observations like period pulling, period doubling have been effective in explaining the transition to turbulence. Nonlinear phenomena like period doubling, intermittency, mode locking, mixed mode oscillations, etc. have begun to emerge in the last few decades drawing the attention of plasma physicists into nonlinear dynamics. A conventional plasma physicist would be interested in oscillations from a spectral point of view like identification of frequencies and dispersion relations to explain various plasma phenomena. However a nonlinear dynamist would tend to explore the dynamics of plasma fluctuations and their dynamical origin to explain the plasma processes like plasma transport, control of chaos, etc. In the present day scenario, nonlinear dynamics has become an inseparable tool to understand various plasma phenomena.

Glow discharge plasmas, very common and versatile in plasma technology, provide an excellent platform to study and understand various nonlinear phenomena ranging from complex space charge configurations to chaotic dynamical processes.

Owing to the various dynamical processes that are taking place in a plasma such as ionization and recombination mechanisms, and due to the free energy sources provided by the space charge configurations, plasma is easily susceptible to the excitation of waves and instabilities. The potential configurations themselves are also in a dynamical state, often undergoing makes and breaks. This in turns forms the driving engine for more nonlinear dynamical processes that are observed in the bulk of the plasma. For the very many reasons stated above, the glow discharge plasma device has given way to numerous experimental observations such as deterministic chaos, hysteresis, homoclinic bifurcation and mixed mode oscillations, etc. Inspite of the numerous experimental studies in glow discharge plasma under various conditions, the role of magnetic field and intrinsic noise have not yet been explored much. "Both these features are close companions of a plasma, while the former is used extensively in plasma confinement, the latter is always present in a plasma due to thermal fluctuations". Thus, for the understanding of nonlinear dynamical behaviour of the plasma under the influence of external dipolar as well as axial magnetic fields and intrinsic plasma noise, we have carried out several experiments in an argon dc glow discharge plasma device. A brief summary of the results and discussions of the studies made in this thesis on these topics is drawn here.

9.1.1 The Glow Discharge Plasma Device, Plasma Diagnostics and Fluctuations Analysis Tools

Within the scope of the present thesis, a glow discharge plasma device was used and put into operational condition with the specific intention of studying nonlinear dynamical behaviour of plasma fluctuations. The device consists of $\sim$20 cm long cylindrical stainless steel cathode chamber with $\sim$10 cm diameter and a central wire anode of length $\sim$ 3 cm and diameter $\sim$ 3 mm. The base pressure $\sim$ 0.01 $mbar$ is obtained using a rotary pump of speed 250 l/min. With argon as the filling gas, plasma is produced by applying a high voltage power supply ($0-1000$ V) between the electrodes.

A Langmuir probe (LP) was used for the measurement of plasma density (n), electron temperature (T_e) and floating potential fluctuations which were recorded using an oscilloscope (DPO 4034). The range of the various plasma parameters like plasma density (n), electron temperature and ion temperature is $\sim 10^7 - 10^9$ cm^3, $T_e \sim 1-4$ eV and $T_i \sim 0.1$ eV respectively.

For analysis of the plasma fluctuations, various linear and nonlinear time series analysis tools along with statistical analysis tools have been used. These are the following tools: Fourier transform, discrete wavelet transform, phase space reconstruction, Lyapunov exponent, multifractal detrended fluctuation analysis, Hurst exponent, empirical mode decomposition, Hilbert Huang transformation, bicoherency, correlation coefficient, normalized variance etc.

9.1.2 Experiments in the Presence of Dipolar Magnetic Field

To begin with, keeping a fixed value of neutral pressure at $\sim$ 0.36 $mbar$, a discharge was initiated at $\sim$ 286 V, the voltage was latter set at $\sim$ 401 V for the system to exhibit the excitable fixed point behaviour. Then an inhomogeneous magnetic field was applied by placing a bar magnet near the cathode surface. Quasiperiodic oscillation was observed at $\sim$ 2 G and with increase in magnetic field strength the large, but bounded periodic limit cycle oscillations appeared between the small quasiperiodic oscillations, confirming the occurrence of canard orbit. In the range of magnetic field strength $\sim$ 6-20 G, irregular mixed mode oscillations (MMOs) were seen and they became regular mixed mode for the magnetic field strength $>$ 25 G. The frequency of the quasiperiod oscillations was lies in the ion acoustic range whereas for regular mixed mode it was around ion cyclotron frequency. The occurrence of canard and irregular MMOs has been attributed to the effects of intrinsic noise, i.e, a stochastic process, whereas the regular MMOs are attributed to the domination of the ion cyclotron mode. As the application of dipolar magnetic field generates ion cyclotron mode with different frequencies and polarization characteristics which can interact with the unmagnetized plasma mode as well as among themselves leading to a broad band intrinsic noise. A numerical simulation has been carried out using a FitzHugh-Nagumo (FHN) like model to understand the dynamical origin of the canards and MMOs. The model represents an excitable system which is obtained by a suitable transformation using the Liénard like co-ordinate system of anharmonic oscillator equation used to explain the plasma instabilities. Obtained results from the numerical simulation agrees with the experimental results.

In addition to the generation of intrinsic noise, dipolar magnetic field also gives rise to the formation of a localized glow or cathode spot near the cathode surface. The secondary electrons produced from the cathode surface travel along the dipolar field lines (shown in the figure 3.5) and get reflected at cathode surface. These electrons ionize neutrals, and produce a dense plasma compared to the bulk plasma near the cathode surface. The intensity of the glow and the density of the plasma are seen to increase with the increase in the strength of the magnetic field. When the system dynamics settles into an oscillatory state at DV $\sim$ 597 V and pressure $\sim$ 0.130 $mbar$ instead of an excitable state, nonlinear dynamical features associated with the localized glow were observed. Plasma fluctuations showed that the emergence of such a localized structure leads the system towards highly nonlinear dynamical regimes. Transition from order to chaos via period doubling bifurcation is seen with increase in the magnetic field strength which were analyzed using bifurcation diagram, phase space plots, power spectrum plots, Hilbert Huang transform and by estimating the largest Lyapunov exponent. It was seen that system became chaotic after the appearance of the localized glow (for magnetic field > 2 G). Appearance of this structure near the cathode surface modified the monotonic potential profile into a potential structure with minima. As a result of which ions are trapped in this potential structure and oscillate within it. Thus, it is quite possible that the observed result of period doubling in the bulk plasma is a consequence of these ion oscillations. We have carried out a numerical simulation of ion oscillations within a potential structure with minima under external forcing. With the change in the external forcing strength, period doubling bifurcation is observed agreeing with experimental observations.

9.1.3 Experiment in the Presence of Axial Magnetic Field

Here, we studied the effect of an axial magnetic field on the plasma dynamics. Phenomena like order to chaos could be observed. However finer structures like canards and mixed mode oscillations, observed in the case of the dipolar magnetic field effect on plasma, were not observed in this experiment probably due to the constraint of last step variation in the magnetic field strength. We started with the normal oscillatory state of plasma dynamics at DV $\sim 316\ V$ and pressure $\sim 0.18\ mbar$. Chaotic fluctuation were observed at the chosen experimental parameters which exhibited multifractal behaviour. Multifractal detrended fluctuation analysis was used to analyse the dynamics, which showed a clear suggestion that the degree of multifractality decreases with an increase in the strength of the axial magnetic field. We also found that the generalized Hurst exponent lies in the range of $\sim$ 1-1.6 suggesting a long range correlated dynamics. We also showed that long-range correlation makes a greater contribution to multifractality of the data than the broadness of the probability density function, i.e., fat-tail distribution.

9.1.4 Experiment in Unmagnetized Plasma

It is known that change in magnetic field and DV can lead to effects like changing the system dynamics and enhancement in the intrinsic noise. However, the dynamical process is different in the two cases. In the case of magnetic field, the effects are mainly due to the generation of new plasma modes and interaction between them as discussed in chapter 3-4. In the case of DV, the effects are due to acceleration of charge particles which can enhance ionization, and also create a situation conducive for the generation of plasma instabilities. Here, we tried to explore the effect of intrinsic noise on plasma dynamics by changing DV. As the noise effect is prominent in the case of excitable dynamics, the system was operated at neutral pressures $\sim 0.37\ mbar$ and DV $\sim 478\ V$ at which an excitable fixed point dynamics was observed. With the increase in DV, large amplitude spikes were observed. The rising and falling time scales were comparable with the ion transit time scale between two electrodes. It was noted that the intrinsic noise increases with increase in DV. It was seen that these excitable spikes achieved maximum regularity for a particular DV, i.e., at a particular value of intrinsic noise suggesting the occurrence of coherence resonance phenomena. Since model used in the chapter 3 is valid for any excitable dynamics, we have used same numerical model to understand the dynamics of the observed experimental results here. This model also confirmed the occurrence of coherence resonance phenomena.

9.1.5 Empirical Mode Decomposition Based Coherent Mode Detection

In all the above experiments, we have seen that experimental time series are generally contaminated with noise/incoherent part. In the chapter 7, we have developed a method for separating out coherent and incoherent parts of a time series data. For the first time, we proposed empirical mode decomposition (EMD) based method for detection of coherent mode of a chaotic or turbulent time series. The correlation coefficient and variance estimation are helpful to identify the coherent modes from the intrinsic mode functions obtained by decomposing the time series signal using EMD. We have established this method by comparing it with well established wavelet based coherent mode detection technique. The efficiency of this method is shown by applying it on three chaotic time series data obtained from the glow discharge plasma. EMD based bicoherency analysis is also carried out which suggested that chaotic/turbulent feature is due to nonlinear interactions of various physical plasma modes.

Applicability and the usefulness of this method was demonstrated by using it for the analysis of intermittent chaotic fluctuations from the glow discharge plasma. Data showing a transition from periodic state to chaotic state via intermittent chaos with the increase in the DV was used. EMD along with Hilbert Huang transform clearly confirmed the intermittent nature and provided the temporal information about the signal. Using the coherent mode detection technique, it has been clearly shown that the system is well represented by one coherent mode in case of periodic and chaotic states whereas it is well represented by two coherent modes in the case of intermittent data. An exchange of energy between two modes was seen during the transition. Transfer of energy from one mode to another mode led to transition from periodic to chaotic state. For the intermittent case, the modes seem to have same energy. So we feel that the developed method is a very powerful tool to analyze highly chaotic, intermittent and non stationary data.

9.2 Scope for Future Works

In this thesis, certain nonlinear dynamical phenomena of plasma have been investigated and efforts have been made to give possible explanations. The studies have led to many interesting questions which need to be addressed in future works for a better understanding of the plasma phenomena.

Here in the following I try to share some of the questions that have evolved out of the investigations:

- We have used a single bar magnet placed outside the cathode surface while investigating plasma dynamics in the presence of an inhomogeneous magnetic field. It would be very interesting to see the plasma dynamics by placing two bar magnets on the same line with same pole facing each other because it will create an inhomogeneous magnetic field everywhere with a magnetic field null region in the center of the cathode chamber.

- In the experiments, bar magnet was placed outside the chamber. One can put a bar magnet inside the plasma chamber and study the confinement of plasma in a dipole magnetic field. This will be helpful to understand the plasma confinement around planets because planets also have dipole type magnetic fields.

- Due to constraint in the variation of the axial magnetic field, It is quite possible that we have missed out many dynamical features. So, by eliminating this constraint one can look for nonlinear features under axial magnetic field which will be helpful to understand nonlinear dynamical phenomena in other magnetized plasma devices.

- We have tried to give possible physical as well as dynamical explanations of the observation of such complex nonlinear features associated with the plasma dynamics. However, further experimental studies like measurement of density fluctuations and dispersion relations will help to correlate these studies with those of conventional plasma physics.

- The models developed in this thesis are able to explain the dynamical processes behind the origin of the observed phenomena but these models are not one to one related with the microscopic plasma phenomena. As in the case of MMO, we have not used the direct magnetic field term in the model which seen to be important parameter in the generation of the regular MMO. So, development of numerical model starting from basic plasma features are needed to establish the direct link between the plasma and numerical model.

- In plasma based nanoparticle or thin film growth, articles have been reported showing that the plasma fluctuations are highly correlated with the fluctuations in the nanoparticle growth. Thus, it will be worthwhile to investigate and correlate structural surface characteristics of nanoparticle growth under different types of nonlinear plasma fluctuations.

- The method we have developed for the detection of coherent modes is applicable for scalar data (1D), i.e, for a time series data. This method can be extended to 2D with the help of 2D EMD which will be helpful to extract the coherent structure from a flow data.

Finally, we sincerely hope that the works presented in this thesis can help us to understand the complex and nonlinear behaviour of plasma and enlighten our way to proceed furthermore in this direction.

Bibliography

[1] Bar-Yam, *Dynamics of complex systems*, Addison-Wesley, Reeding, Massachusetts, (1997).

[2] I. Newton, Mathematical Principles of Natural Philosophy (A. Stranhan, London), (1802).

[3] D. T. Whiteside, *The Mathemetical Papers of Isaac Newton*, Cambridge University Press, Cambridge, U. K., (2008).

[4] D. Aubin, and A. D. Dalmedici, Historia Mathematica **29** , 273 (2002).

[5] Steven H. Strogatz, *Nonlinear dynamics and Chaos, with application to physics, biology, chemistry, and Engineering*, Perseus Books, Reading, Massachusetts, (1994).

[6] E. N. Lorenz, Journal of the atmospheric sciences **20**, 130 (1963).

[7] D. Ruelle, and F. Takens, Commun. Math. Phys. **20**, 167 (1971).

[8] M. Feigenbaum, J. Stat. Phys. **19**, 25 (1978).

[9] A. Wolf, J. B. Swift, H. L. Swinney, and J. A. Vastano, Physica D **16**, 285 (1985).

[10] P. Grassberger, and I. Procaccia, Phys. Rev. Lett. **50**, 346 (1983).

[11] M. T. Rosenstein, J. J. Collins, and C. J. De Luca, Phys. D **65**, 117 (1993).

[12] B. T. Milne, Ecosystems **1**, 449 (1998).

[13] B. A. Carreras, B. P. Van Milligen, M. A. Pedrosa, R. Balbín, C. Hidalgo, D. E. Newman, E. Sánchez, M. Frances, I. Garca-Corts, and J. Bleuel, Physics of Plasmas **5**, 3632 (1998).

[14] E. Scholl, and H. G. Schuster, *Handbook of Chaos Control*, WILEY-VCH Verlag GmbH and CO., Germany, (2008).

[15] E. Ott, C. Grebogi, and J. A. Yorke, Phys. Rev. Lett. **64**, 1196 (1990)

[16] A. Pikovsky, M. Rosenblum, and J. Kurths, *Synchronization: A universal concept in Nonlinear Sciences*, Cambridge University Press, (2001).

[17] C. W. Wu, and L. O. Chua, Int. J. Bif. and Chaos **3**, 1619 (1993).

[18] R. Roy, K. Thornburg, and J. Scoot, Phys. Rev. Lett. **72**, 2009 (1994).

[19] B. E. Keen, and W. H. Fletcher, J. Phys. D: Appl. Phys. **3**, 1868 (1970).

[20] I. Langmuir, *Oscillations in ionized gases*, Proceedings of the National Academy of Sciences **14**, 627 (1928).

[21] F. F. Chen, *Introduction to plasma physics and controlled fusion*, Plenum Press, New York, (1984).

[22] L. Tonks, and I. Langmuir, Physical Review **33**, 195 (1929).

[23] N. A. Krall, and A. W. Trivelpiece, *Principles of Plasma Physics*, McGraw-Hill Book Company, New York, (1973).

[24] T. H. Stix, *Waves in Plasmas*, AIP, New York, (1992).

[25] D. G. Swanson, *Plasma Waves*, Academic Press, San Diego, (1989).

[26] R. H. Abrams, E. J. Yadlowsky, and H. Lashinsky, Phys. Rev. Lett. **22**, 275 (1969).

[27] R. W. Boswell, Plasma Physics and Controlled Fusion **27**, 405 (1985).

[28] P. Y. Cheung, and A. Y. Wong, Phys. Rev. Lett. **59**, 551 (1987).

[29] T. Braun, J. A. Lisboa, R. E. Francke, and J. A. C. Gallas, Phys. Rev. Lett. **59**, 613 (1987).

[30] Md. Nurujjaman, R. Narayanan, and A. N. Sekar Iyengar, Chaos **17**, 043121 (2007).

[31] Jiang Yong, Wang Haida, and Yu Chagxuan, Chinese Phys. Lett. **5**, 489 (1988).

[32] B. K. Sharma, A. Buragohain, and J. Chutia, Inter. J. Bifur. and Chaos **3**, 455 (1993).

[33] T. Braun, J. A. Lisboa, and J. A. C. Gallas, Phys. Rev. Lett. **68**, 2770 (1992).

[34] T. Klinger, F. Greiner, A. Rohde, A. Piel, and M. E. Koepke, Phys. Rev. E **52**, 4316 (1995).

[35] T. Klinger, F. Greiner, A. Rohde, and A. Piel, Physics of Plasmas **2**, 1822 (1995).

[36] S. Ghorui, S. N. Sahasrabudhe, P. S. S. Murthy, A. K. Das, and N. Venkatramani, IEEE Trans. Plasma Sci. **28**, 253 (2000).

[37] S. Ghorui, S. N. Sahasrabudhe, P. S. S. Murthy, A. K. Das, and N. Venkatramani, IEEE Trans. Plasma Sci. **28**, 2179 (2000).

[38] Md. Nurujjaman, A. N. Sekar Iyengar, and P. Parmananda, Phys. Rev. E **78**, 026406 (2008).

[39] I. Lin, and Jeng-Mei Liu, Phys. Rev. Lett. **74**, 3161 (1995).

[40] A. Dinklage, C. Wilke, and T. Klinger, Phys. Plasmas **6**, 2968 (1999).

[41] M. Mikikian, M. Cavarroc, L. Couëdel, Y. Tessier, and L. Boufendi, Phys. Rev. Lett. **100**, 225005 (2008).

[42] P. P. Tsai, L. C. Wadsworth, and J. R. Roth, Textile Research Journal **67**, 359 (1997).

[43] E. Pugliese, R. Meucci, S. Euzzor, J. G. Freire, and J. A. C. Gallas, Scientific Reports **5**, article 8447 (2015).

[44] P. Alex, S. Arumugam, K. Jayaprakash, and K. S. Suraj, Results in Physics **5**, 235 (2015).

[45] R. H. Huddlestone, and S. L. Leonard, *Plasma Diagnostic techniques*, Academic Press, New York, (1965).

[46] I. H. Hutchinson, *Principles of Plasma Diagnostics*, Cambridge University Press, Cambridge, (2002).

[47] O. Auciello, and D. L. Flamm, *Plasma Diagnostics*, Academic Press, Inc., San Diego, CA, (1989).

[48] F. Takens, *Detecting strange attractor in turbulance, Lecture notes in mathematics*, Vol. 898, Springer, Berlin, (1981).

[49] M. B. Kennel, R. Brown, and H. D. I. Abarbanel, Phys. Rev. A **45**, 3403 (1992).

[50] A. M. Fraser, and H. L. Swinney, Phys. Rev. A **33**, 1134 (1986).

[51] The TISEAN software package is publicly available at http://www.mpipks-dresden.mpg.de/~tisean.

[52] http://www.matjazperc.com/ejp/time.html.

[53] Stane Kodba, Matjaž Perc, and Marko Marhl, Eur. J. Phys. **26**, 205 (2005).

[54] M. S. Movahed, G. R. Jafari, F. Ghasemi, S. Rahvar, and M. R. Tabar, J. Stat. Mech. Theory Exp. **2006**, P02003 (2006).

[55] C. K. Peng, S. V. Buldyrev, S. Havlin, M. Simons, H. E. Stanley, and A. L. Goldberger, Phys. Rev. E **49**, 1685 (1994).

[56] A. L. Barabási, and T. Vicsek, Phys. Rev. A **44**, 2730 (1991).

[57] N. E. Huang, Z. Shen, S. R. Long, M. C. Wu, H. H. Shih, Q. Zheng, N. C. Yen, C. C. Tung, and H. H. Liu, Proc. R. Soc. Lond. A **454**, 903 (1998).

[58] G. Rilling, P. Flandrin, and P. Gonzalves, IEEE-EURASIP Workshop on Nonlinear Signal and Image Processing **3**, 8 (2003).

[59] R. Jha, D. Raju, and A. Sen, Physics of Plasmas **13**, 082507 (2006).

[60] I. Daubechies, *Ten Lectures on Wavelets*, Philadelphia: SIAM, PA, (1992).

[61] C. K. Chui, *An Introduction to Wavelets*, Academic Press, San Diego, (1995).

[62] W. J. Staszewski, and K. Worden, International Journal of Bifurcation and Chaos **9**, 455 (1999).

[63] B. B. Mandelbrot, and J. R. Wallis, Water Resources Research **5**, 321 (1969).

[64] B. B. Mandelbrot, and J. R. Wallis, Water Resources Research **5**, 967 (1969).

[65] H. E. Hurst, Trans. Am. Soc. Civ. Eng. **116**, 770 (1951).

[66] V. Suyal, A. Prasad, and H. P. Singh, Solar Phys **260**, 441 (2009).

[67] F. Marino, G. Catalán, P. Sánchez, S. Balle, and O. Piro, Phys. Rev. Lett. **92**, 073901 (2004).

[68] F. Marino, M. De Rosa, and F. Marin, Phys. Rev. E **73**, 026217 (2006).

[69] M. A. Kramer, R. D. Traub, and N. J. Kopell, Phys. Rev. Lett. **101**, 068103 (2008).

[70] V. A. Makarov, V. I. Nekorkin, and M. G. Velarde, Phys. Rev. Lett. **86**, 3431 (2001).

[71] E. I. Volkov, E. Ullner, A. A. Zaikin, and J. Kurths, Phys. Rev. E **68**, 026214 (2003).

[72] F. Marino, and F. Marin, Phys. Rev. E **87**, 052906 (2013).

[73] F. Marino, M. Ciszak, S. F. Abdalah, K. Al-Naimee, R. Meucci, and F. T. Arecchi, Phys. Rev. E **84**, 047201 (2011).

[74] T. Rao, T. Xiao, and Z. Hou, J. Chem. Phys. **134**, 214112 (2011).

[75] M. D. McDonnell, and L. M. Ward, Nat. Rev. Neurosci. **12**, 415 (2011).

[76] K. Wiesenfeld, and F. Moss, Nature **373**, 33 (1995).

[77] Z. Gingl, L. B. Kiss, and F. Moss, Europhys. Lett. **29**, 191 (1995).

[78] T. Kondo, and T. Munakata, Phys. Rev. E **79**, 061121 (2009).

[79] M. Wechselberger, Scholarpedia **2**, 1356 (2007).

[80] P. Borowski, R. Kuske, Y.-X. Li, and J. L. Cabrera, Chaos **20**, 043117 (2010).

[81] V. Petrov, S. K. Scott, and K. Showalter, J. Chem. Phys. **97**, 6191 (1992).

[82] M. Koper, Physica D **80**, 72 (1995).

[83] Md. Nurujjaman, Phys. Rev. E **81**, 036203, (2010).

[84] M. Nurujjaman, P. S. Bhattacharya, A. N. S. Iyengar, and S. Sarkar, Phys. Rev. E **8**0, 015201 (2009).

[85] M. Nurujjaman, and A. N. S. Iyengar, Phys. Rev. E **82**, 056210 (2010).

[86] X. Li, J. Wang, and W. Hu, Phys. Rev. E **76**, 041902 (2007).

[87] M. Desroches, B. Krauskopf, and H. M. Osinga, Chaos **18**, 015107 (2008).

[88] M. Brøns, T. J. Kaper, and H. G. Rotstein, Chaos **18**, 015101 (2008).

[89] T. Vo, R. Bertram, J. Tabak, and M. Wechselberger, J. Comput. Neurosci. **28**, 443 (2010).

[90] N. Berglund, and D. Landon, Nonlinearity **25**, 2303 (2012).

[91] C. B. Muratov, and E. Vanden-Eijnden, Chaos **18**, 015111 (2008).

[92] J. Touboul, M. Krupa, and M. Desroches, *Noise-induced canard and mixed-mode oscillations in large stochastic networks with multiple timescales*, arXiv preprint arXiv:1302.7159, (2013).

[93] M. Desroches, J. Guckenheimer, B. Krauskopf, C. Kuehn, H. Osinga, and M. Wechselberger, SIAM Rev. **54**, 211 (2012).

[94] D. Simpson, and R. Kuske, Physica D **240**, 1189 (2011).

[95] W. Wang, J. Foster, A. E. Wendt, J. H. Booske, T. Onuoha, P. W. Sandstrom, H. Liu, S. S. Gearhart, and N. Hershkowitz, Appl. Phys. Lett. **71**, 1622 (1997).

[96] K. Leung, G. Taylor, J. Barrick, S. Paul, and R. Kribel, Phys. Lett. A **57**, 145 (1976).

[97] D. G. Lominadze, *Cyclotron Waves in Plasma*, Pergamon Press, (1981).

[98] N. Wiener, *Extrapolation, Interpolation, and Smoothing of Stationary Time Series*, MA:MIT press Cambridge, (1949).

[99] R. G. Brown, and P. Y. Hwang, *Introduction to Random Signals and Applied Kalman Filtering*, Wiley, New York, (1997).

[100] N. Singh, Physics of Plasmas **18**, 122105 (2011).

[101] B. E. Keen, and W. H. W. Fletcher, Phys. Rev. L **23**, 760 (1969).

[102] C. T. Teodorescu-Soare, D. G. Dimitriu, C. Ionita, and R. W. Schrittwieser, Physica Scripta **91**, 034002 (2016).

[103] R. L. Stenzel, C. Ionita, and R. Schrittwieser, Plasma Sources Science and Technology **17**, 035006 (2008).

[104] M. Agop, D. G. Dimitriu, O. Niculescu, E. Poll, and V Radu, Physica Scripta **87**, 045501 (2013).

[105] M. Megalingam, B. Sarma, N. H. Prakash, and A. Sarma, Physics of Plasmas **23**, 072102 (2016).

[106] A. Scipioni, P. Rischette, G. Bonhomme, and P. Devynck, Physics of Plasmas **15**, 112303 (2008).

[107] A. Biancalani, and F. Pegoraro, Journal of Geophysical Research: Space Physics **115**, A09330 (2010).

[108] V. A. Petržilka, F. Leuterer, F. X. Söldner, L. Giannone, and R. Schubert, Nuclear fusion **31**, 1758 (1991).

[109] E. Gravier, X. Caron, G. Bonhomme, T. Pierre, and J. L. Briancon, The European Physical Journal D **8**, 451 (2000).

[110] S. F. Masoudi, and S. M. Salehkoutahi, The European Physical Journal D **57**, 71 (2010).

[111] Z. Yoshida, H. Saitoh, Y. Yano, H. Mikami, N. Kasaoka, W. Sakamoto, J. Morikawa, M. Furukawa, and S. M. Mahajan, Plasma Physics and Controlled Fusion **55**, 014018 (2012).

[112] X. Wang, M. Horányi, and S. Robertson, Journal of Geophysical Research: Space Physics **117**, A06226 (2012).

[113] J. W. Dungey, Phys. Rev. Lett. **6**, 47 (1961).

[114] A. Rizk, S. B. Youssef, and S. K. Habib, Vacuum **38**, 93 (1988).

[115] G. K. Sabavath, P. K. Shaw, A. N. S. Iyengar, I. Banerjee, and S. K. Mahapatra, Physics of Plasmas **22**, 082121 (2015).

[116] E. Martines, M. Zuin, M. Marcante, R. Cavazzana, A. Fassina, and M. Spolaore, Physics of Plasmas **23**, 053511 (2016).

[117] H. G. Enjieu Kadji, B. R. Nana Nbendjo, J. B. Chabi Orou, and P. K. Talla, Physics of Plasmas **15**, 032308 (2008).

[118] A. M. Wharton, A. N. S. Iyengar, and M. S. Janaki, Physics of Plasmas **20**, 022301 (2013).

[119] U. Deka, A. Rao, and M. Nurujjaman, Physica Scripta **90**, 125602 (2015).

[120] C. Hidalgo, M. A. Pedrosa, C. Silva, D. Carralero, E. Ascasibar, B. A. Carreras, T. Estrada, F. Tabars, D. Tafalla, J. Guasp, and M. Liniers, Europhys. Lett. **87**, 55002 (2009).

[121] B. A. Carreras, B. P. van Milligen, M. A. Pedrosa, R. Balbín, C. Hidalgo, D. E. Newman, E. Sánchez, R. Bravenec, G. McKee, I. Garca-Corts, and J. Bleuel, Physics of Plasmas **6**, 1885 (1999).

[122] M. Nurujjaman, and A. S. Iyengar, Phys. Lett. A **360**, 717 (2007).

[123] W. M. Macek, Nonlinear Processes Geophys. **14**, 695 (2007).

[124] E. Marsch, and C.-Y. Tu, Nonlinear Process. Geophys. **4**, 101 (1997).

[125] B. A. Carreras, V. E. Lynch, D. E. Newman, R. Balbín, J. Bleuel, M. A. Pedrosa, M. Endler, B. van Milligen, E. Sánchez, and C. Hidalgo, Physisc of Plasmas **7**, 3278 (2000).

[126] V. Carbone, Phys. Rev. Lett. **7**1, 1546 (1993).

[127] C. R. Neto, Z. O. Guimares-Filho, I. L. Caldas, I. C. Nascimento, and Y. K. Kuznetsov, Phys. Plasmas **15**, 082311 (2008).

[128] J. W. Kantelhardt, S. A. Zschiegner, E. Koscielny-Bunde, S. Havlin, A. Bunde, and H. E. Stanley, Physica A **316**, 87 (2002).

[129] K. Hu, P. C. Ivanov, Z. Chen, P. Carpena, and H. E. Stanley, Phys. Rev. E **64**, 011114 (2001).

[130] Z. Chen, P. C. Ivanov, K. Hu, and H. E. Stanley, Phys. Rev. E **65**, 041107 (2002).

[131] D. Horvatic, H. E. Stanley, and B. Podobnik, Europhys. Lett. **94**, 18007 (2011).

[132] P. Shang, Y. Lu, and S. Kamae, Chaos, Solitons & Fractals **36**, 82 (2008).

[133] Y. Yuan, X. T. Zhuang, and X. Jin, Physica A **388**, 2189 (2009).

[134] T. Zorick, and M. A. Mandelkern, PLoS One **8**, e68360 (2013).

[135] R. Galaska, D. Makowiec, A. Dudkowska, A. Koprowski, K. Chlebus, J. Wdowczyk-Szulc, and A. Rynkiewicz, Ann. Noninvasive Electrocardiol. **13**, 155 (2008).

[136] D. Subhakar, and E. Chandrasekhar, Physica A **445**, 57 (2016).

[137] L. Telesca, and L. Toth, Physica A **448**, 21 (2016).

[138] R. G. Kavasseri, and R. Nagarajan, Chaos, Solitons & Fractals **24**, 165 (2005).

[139] L. Telesca, V. Lapenna, and M. Macchiato, New J. Phys. **7**, 214 (2005).

[140] C. R. Stan, C. P. Cristescu, and D. G. Dimitriu, Rom. J. Phys. **56**, 79 (2011).

[141] M. Lafouti, M. Ghoranneviss, S. Meshkani and A. S. Elahi, J. Plasma Phys. **80**, 43 (2014).

[142] J. Theiler, S. Eubank, A. Longtin, B. Galdrikian, and J. D. Farmer, Physica D **58**, 77 (1992).

[143] B. Sarma, S. S. Chauhan, A. M. Wharton, and A. N. S. Iyengar, Physica Scripta **88**, 065005 (2013).

[144] M. A. Lopes, K. E. Lee, A. V. Goltsev, and J. F. F. Mendes, Phys. Rev. E **90**, 052709 (2014).

[145] B. Lindner, J. García-Ojalvo, A. Neiman, and L. Schimansky-Geier, Physics Reports **392**, 321 (2004).

[146] K. Matsumoto, and I. Tsuda, J. Stat. Phys. **31**, 757 (1983).

[147] R. Toral, C. R. Mirasso, E. Hernández-García, and Oreste Piro, Chaos **11**, 665 (2011).

[148] R. Benzi, A. Sutera, and A. Vulpiani, J. Phys. A **14**, 453 (1981).

[149] S. Dey, D. Das, and P. Parmananda, Chaos **21**, 033124 (2011).

[150] Yang Tang, H. Gao, W. Zou, and J. Kurths, Phys. Rev. E **87**, 062920 (2013).

[151] B. J. Gluckman, T. I. Netoff, E. J. Neel, W. L. Ditto, M. L. Spano, and S. J. Schiff, Phys. Rev. Lett. **77**, 4098 (1996).

[152] C. Zhou, and J. Kurths, Chaos **13**, 401 (2003).

[153] I. Z. Kiss, Y. Zhai, J. L. Hudson, C. Zhou, and J. Kurths, Chaos **13**, 267 (2003).

[154] A. Simon, and A. Libchaber, Phys. Rev. Lett. **68**, 3375 (1992).

[155] A. S. Pikovsky, and J. Kurths, Phys. Rev. Lett. **78**, 775 (1997).

[156] I. Z. Kiss and J. L. Hudson, G. J. E. Santos, and P. Parmananda, Phys. Rev. E **67**, 035201 (2003).

[157] Gerardo J. Escalera Santos, M. Rivera, and P. Parmananda, Phys. Rev. E **92**, 230601 (2004).

[158] O. V. Ushakov, H.-J. Wünsche, F. Henneberger, I. A. Khovanov, L. Schimansky-Geier, and M. A. Zaks, Phys. Rev. Lett. **95**, 123903 (2005).

[159] L. A. da Silva, E. H. Colombo, and C. Anteneodo, Phys. Rev. E **90**, 012813 (2014).

[160] F. Moss, A. Bulsara, and M. F. Shlesinger, J. Stat. Phys. **70**, 1 (1993).

[161] A. Guderian, G. Dechert, K. P. Zeyer, and F. W. Schneider, J. Phys. Chem. **100**, 4437 (1996).

[162] D. E. Postnov, S. K. Han, T. G. Yim, and O. V. Sosnovtseva, Phys. Rev. E **59**, R3791 (1999).

[163] F. Moss, D. Pierson, and D. O'Gorman, Int. J. Bifurcation Chaos Appl. Sci. Eng. **4**, 1383 (1994).

[164] Yang Gao, and Jianjun Wang, Phys. Rev. E **86**, 051914 (2012).

[165] G. Giacomelli, M. Giudici, S. Balle, and Jorge R. Tredicce, Phys. Rev. Lett. **84**, 3298 (2000).

[166] K. Miyakawa, and H. Isikawa, Phys. Rev. E **66**, 046204 (2002).

[167] A. Lemarchand, J. Gorecki, A. Gorecki, and B. Nowakowski, Phys. Rev. E **89**, 022916 (2014).

[168] Robert L. Merlino, and Nicola D'Angelo, Physics of Plasmas **12**, 054504 (2005).

[169] Md. Nurujjaman, R. Narayanan, and A. N. S. Iyengar, Physics of Plasmas **16**, 102307 (2009).

[170] P. J. Fimognari, D. R. Demers, X. Chen, and P. M. Schoch, Rev. Sci. Instrum. **85**, 11D849 (2014).

[171] S. A. McLuckey, G. L. Glish, K. G. Asano, and B. C. Grant, Analytical Chemistry **60**, 2220 (1988).

[172] J. Chen, J. Benesty, Y. Huang, and S. Doclo, IEEE Transactions on Audio, Speech, and Language Processing **14**, 1218 (2006).

[173] P. Holmes, J. L. Lumley, and G. Berkooz, *Turbulance, Coherent Structures, Dynamical Systems and Symmetry*, Cambridge University Press, (1996).

[174] A. K. M. F. Hussain, J. Fluid Mech. **173**, 303 (1986).

[175] M. Farge, Annual Review of Fluid Mechanics **24**, 395 (1992).

[176] S. K. Robinson, Annual Review of Fluid Mechanics **23**, 601 (1991).

[177] J. Argyris, G. Faust, and M. Haase, Philosophical Transactions: Physical Sciences and Engineering **344**, 207 (1993).

[178] P. E. Dimotakis, R. C. Maike-Lye, and D. N. Papantoniou, Physics of Fluids **26**, 3185 (1983).

[179] A. Roshko, AIAA journal **14**, 1349 (1976).

[180] G. V. Osipov, and M. M. Sushchik, Phys. Lett. A **201**, 205 (1995).

[181] M. Farge, K. Schneider, and P. Devynck, Physics of Plasmas **13**, 042304 (2006).

[182] J. S. Murguía, and E. Campos-Cantón, Revista Mexicana De Física **52**, 155 (2006).

[183] P. Flandrin, and P. Goncalves, International Journal of Wavelets, Multiresolution and Information Processing **2**, 477 (2004).

[184] H. G. Li and G. Meng, Chaos, Solitons & Fractals **30**, 930 (2006).

[185] K. Guhathakurta, I Mukherjee, and A. R. Chowdhury, Chaos, Solitons & Fractals **37**, 1214 (2008).

[186] A. Sarma, S. Gopi, and D. Saha, Physica Scripta **T161**, 014064 (2014).

[187] E. U. Nathaniel, N. J. George, and S. E. Etuk, Atmospheric and Climate Sciences **3**, 576 (2013).

[188] J. Kurzyna, S. Mazouffre, A. Lazurenko, L. Albaréde, G. Bonhomme, K. Makowski, M. Dudeck, and Z. Peradzyński, Physics of Plasmas **12**, 123506 (2005).

[189] C. M. Sweeney-Reed, and S. J. Nasuto, Journal of Computational Neuroscience **23**, 79 (2007).

[190] P. De. Michelis, G. Consolini, and R. Tozzi, Nonlin. Processes Geophys. **19**, 667 (2012).

[191] B. M. Battista , C. Knapp, T. McGee, and V. Goebel, Geophysics **72**, H29 (2007).

[192] C. S. Lina, S. H. Chiub, and T. Y. Linb, Economic Modelling **29**, 2583 (2012).

[193] Y. X. Huang, F. G. Schmitt, Z. M. Lu, and Y. L. Liu, EPL (Europhysics Letters) **84**, 40010 (2008).

[194] Y. X. Huang, F. G. Schmitt, J.-P. Hermand, Y. Gagne, Z. M. Lu, and Y. L. Liu, Phys. Rev. E **84**, 016208 (2011).

[195] P. Flandrin, and P. Goncalves, International Journal of Wavelets, Multiresolution and Information Processing **2**, 477 (2004).

[196] R. Narasimha, Sadhana **32**, 29 (2007).

[197] R. G. Kleva, Phys. Fluids B **3**, 3312 (1991).

[198] G. Rilling, P. Flandrin, and P. Goncalves, *Empirical mode decomposition, fractional Gaussian noise and Hurst exponent estimation*, International Conference on Acoustics, Speech, and Signal Processing **4**, IEEE, Philadelphia, Pennsylvania, USA, (2005).

[199] David Looney, Apit Hemakom, and Danilo P. Mandic, Proc. R. Soc. Lond. A **471**, 2173 (2015).

[200] L. Cohen, Proc. IEEE **77**, 941 (1989).

[201] P. Manneville, and Y. Pomeau, Phys. Lett. A **75**, 1 (1979).

[202] D. J. Tritton, *Physical Fluid Dynamics*, Oxford University Press Inc., New York, (1988).

[203] P.W. Hammer, N. Platt, S. M. Hammel, J. F. Heagy and B. D. Lee, Phys. Rev. Lett. **73**, 1095 (1994).

[204] D. L. Feng, C. X. Yu, J. L. Xie, and W. X. Ding, Phys. Rev. E **58**, 3678 (1998).

[205] S. Chiriac, D. G. Dimitriu, and M. Sanduloviciu, Physics of Plasmas **14**, 072309 (2007).

[206] S. K. Saha, and S. Chowdhury, Physics of Plasmas **15**, 012305 (2008).

[207] R. Balocchi, D. Menicucci, E. Santarcangelo, L. Sebastiani, A. Gemignani, B. Ghelarducci, and M. Varanini, Chaos, Solitons & Fractals **20**, 171 (2004).

[208] S. Rybalko, S. Larionov, M. Poptsova, and A. Loskutov, Phys. Rev. E **84**, 042902 (2011).

[209] A. Campos-Mejía, A. N. Pisarchik, and D. A. Arroyo-Almanza, Chaos, Solitons & Fractals **54**, 96 (2013).

[210] J. L. Cabrera, and J. G. Milton, Phys. Rev. Lett. **89**, 158702 (2002).

[211] S. Ghosh, P. K. Shaw, A. N. S. Iyengar, M. S. Janaki, D. Saha, A. M. Wharton and V. Mitra, Physics of Plasmas **21**, 032303 (2014).